Doctoral Dissertation (Shinshu University)

Design and fabrication of antibacterial nanocoatings on cotton and silk fibers through supramolecular self-assembly technology

September 2016

SIJUN XU

Table of Contents

List of Figures

List of Tables

List of Schemes

Chapter 1
Introduction

Chapter 1 Introduction

1.1 Biological fibers

Biological fibers can be divided into three categories as follows: natural biological fibers, regenerated biological fibers, and synthetic biological fibers. Natural biological fibers consist of animal and plant fibers. Cotton, wool, hemp, and silk fibers are four typical natural biological fibers, which has been used for textiles in the last several millennia. The earliest evidence for humans using fibers can be traced back to 36,000 BP in the Republic of Georgia [1, 2].

With the development of biological science and technology, regenerated biological fibers have caused the extensive concern in recent decades. Nowadays, various kinds of regenerated biological fibers have been fabricated such as bamboo pulp fibers, regenerated cellulose and silk fibers, calcium alginate fibers, and chitosan fibers [3-5]. Synthetic biological fibers are recently developed chemical fibers that are made of synthetic biopolymers.

Biological fibers have broad potential applications because of their intrinsic properties including biodegradability, biocompatibility, biological safety, and in some case specific functions. Biological fibers have more classically been used in the textile industry. Natural fibers are amongst the most best-selling commodities around the word because of their ease to obtain, excellent mechanical properties, and good hygroscopicity and warmth retention. Several regenerated biological fibers with special performances find their applications in medical and adsorbent materials. For examples, calcium alginate and chitosan fibers now have been widely used in medical dressings,

because of their unique gel-forming ability or antibacterial activity [6, 7]. Carbon fibers made from cotton and viscose fibers are efficient and recyclable sorbents for oils, organic solvents, and solid particulates in the air [8]. Furthermore, unlike most synthetic polymers, many biological macromolecules such as cotton cellulose and silk protein are capable of forming into well-defined structures across multiple levels of order because of intrinsic built-in sequences of chemical moieties. By re-construction of their supramolecular structure, biological fibers find their potential in three dimensional (3D) biological scaffolds [9].

1.2 Antibacterial biological fibers

Nowadays, ongoing efforts in generating biological fibers have been extended to recreate the structural and functional character present in biological fibers or integrate functional nanomaterials such as carbon nanomaterials and inorganic nanomaterials into the fiber structure to increase the mechanical properties of biological fibers or impart advanced functions to them by altering the fabrication process or embedding or coating of functional materials to biological fibers. When forming these structure, the biological fibers in either random or aligned configurations can be endowed with advanced functions for different applications. Compared with moderate growth of conventional textiles, functional textiles show over proportional market growth [10]. Such functional textiles provide the textile industry with new opportunities and challenges, which has significantly changed our way of life.

In recent years, with the improvement of human living, control of harmful effects of microorganism become necessary [5]. Nowadays, the antimicrobial function has become very important in apparel and protective, decorative, and technical textile

products [11].

Biological textiles can provide a comfortable environment such as appropriate humidity and temperature to grow microorganisms. Imparting the antimicrobial function of textiles can protect consumers from pathogenic or odor-generating microorganisms that can cause medical and hygienic problems. Because of this, a large number of antimicrobial agents suitable for textile application on the market have increased dramatically [11]. These antimicrobial agents can be generally divided into two categories-organic antimicrobial agents and inorganic agents. Organic antibacterial agents are commonly used antibacterial agents. However, recent researches show that many organic antibacterial agents have harmful or toxic effects on the human body and are found to lose their potency over time because of the development of drug resistance [12]. Recently using inorganic nanomaterials has become popular for the antibacterial treatment of textiles owing to their low bacterial resistance, broad antibacterial activity, and good biosafety because of their special antibacterial mechanism and simple chemical structure. Among them, nano-silver is the most powerful antibacterial agent, which has drawn extensive attention.

1.3 Molecule-functionalised nanomaterials

Polymer-functionalised inorganic nanomaterials consist of an inorganic core, made up of atoms with the number ranging from a few hundreds to a few thousands, and an organic outer layer of molecules.

The interest in using nanomaterials, and especially nanoparticles (NPs), as a basic building block in advanced materials mainly owe to their unique size-dependent physical, optical, electronic, and chemical properties [13]. The nano-size results in an

obvious quantum-confinement effect, defined by an increasing bandgap accompanied by the quantization of the energy levels to discrete values [14]. NPs also possess ultra-high surface-to-volume ratios and nontrivial surface areas. For example, when the NP size is less than 20 nm (about 2.5×10^5 atoms), the atom ratio of surface/volume is around 10%. When the diameter further decreases to 2 nm, the surface atoms can comprise 80% of the total. The typical quantum confined properties include the size-dependent photoluminescence of nanocrystalline semiconductor quantum dots, the plasmonic resonances of metal NPs, the electrical properties of carbon nanomaterials, and the paramagnetism and catalytic properties of certain inorganic NPs. For examples, ZnO nanoparticles (ZnONPs) and titanium dioxide nanoparticles (TiO_2NPs) commonly generate green emission when excited by the ultraviolet (UV) light [15]. Recently, nanocrystals of cesium lead halide perovskites, a new comer optoelectronic material, were also found to have high photoluminescence performances with readily tunable bandgap energies and emission spectra over the entire visible spectral region of 410-700 nm and related wide color gamut [16]. Besides, for many metal NPs, when the NP size is smaller than the wavelength of light, the free electrons can be displaced from the lattice of positive ions and collectively oscillate in resonance with the light, known as a localized surface plasmon resonance (LSPR). Gold nanoparticles (AuNPs) and silver nanoparticles (AgNPs) are two important candidates in supporting surface plasmons because of their high surface plasmonic resonances in the visible wavelength range [17]. The main applications of plasmonic nanomaterials include LSPR sensing and detection, enhancement or manipulation of the optical response of surrounding molecules, and manipulation of light with plasmonic circuitry [18]. Another direct evidence for the quantum Hall effect of nanomaterials is the electrical properties of graphene. Graphene

exhibits extremely high carrier mobility (over 15,000 $cm^2/V \cdot s$) and lower electrical resistivity (10^{-6} $\Omega \cdot cm$) compared with Ag and Cu because of the quantum effect of the one-atom-thick sheet of sp^2-hybridized carbon [19]. Different from other nanomaterials, magnetic NPs such as iron oxide NPs possess unique nano-properties namely superparamagnetism, which now have been extensively investigated for their biomedical applications such as magnetic resonance imaging (MRI), drug delivery, and therapy [20]. The tremendous application potential in catalysis owes to the high specific surface area and surface chemical activity of nanomaterials [21]. AuNPs are one of the important nanocatalysts and have been widely used in many catalytic reactions such as hydrogen purification for fuel cells, chemical synthesis, control of environmental pollution, and electro catalysis [22]. Recently research showed that supported AuNPs also showed high catalytic efficiency on CO oxidation [22].

Inorganic NPs allow for attachment of molecules on their surfaces, which should be contributed to their high surface chemical activity and high surface-to-volume ratio. The reason for functionalization of molecules are as follows:

(1) Improvement of solution stability of inorganic NPs.

Core-shell structured inorganic NPs can be stabilized against aggregation through coating outer layers of organic molecules. The molecules on the surface of NPs can provide electrostatic, steric, or electrosteric repulsion among NPs, imparting them with good solution stability [23]. For example, long-chain alkyl surfactants such as oleic acid and oleyalmine can provide steric shielding for NPs to avoid agglomeration. Note that the good water stability of inorganic NPs is very important for the applications in biomedicine, pollution treatment, and functional textiles.

(2) Adjustment of the surface charges of inorganic NPs.

The surface charges of inorganic NPs are tunable by surface modification with cationic or anionic molecules. For their application in biomedicine, the surface charge of molecule-capped NPs is in favour of their interaction with molecules on the cell surface and therefore improves their cellular uptake. Studies point out that positively charged NPs seem to exhibit higher internalization into cells compared with the neutral and negatively charged NPs [23]. Another application for charged inorganic NPs is heavy metal or dye molecules adsorption. For example, molecule-functionalised magnetic NPs can be used for the wastewater treatment. Fresnais *et al*. reported negatively-charged poly(acrylic acid)-functionalised magnetic NPs with adsorption capacity of methylene blue molecules up to 803 mg/g [24].

(3) Imparting multi-functions to inorganic NPs.

The most important purpose for surface functionalization of inorganic NPs with molecules is imparting new functions to NPs. Today, molecule-functionalised inorganic NPs have been one of most popular research in nanoscience and technology. Molecule-functionalised inorganic NPs can be used with three opposite functional goals. One focuses on utilizing the inherent structural, special recognition, or catalytic properties of capping molecules to assemble composite nanomaterials with advanced functions. One typical case is using DNA as programmable and sequence-specific "glues" to design precisely space-controlled advanced materials [25, 26]. Zhang *et al*. reported a general strategy for the creation of heterogeneous nanoparticle superlattices using DNA and carboxylic based conjugation. This study showed that all major types of functionality including plasmonic (Au), magnetic (Fe_2O_3), catalytic (palladium), and

luminescent (CdSe/Te@ZnS and CdSe@ZnS) can be integrated into binary systems in a rational manner [27]. The second is utilizing the nano-properties of inorganic NPs. For example, citric acid-capped AgNPs exhibit strong antibacterial activity because of their antibacterial Ag core. The functions of capping molecules are the prevention of AgNPs from agglomeration and chlorination/oxidation. The third is that both inorganic core and organic shell play important roles in the functions of composite NPs. For example, molecule-functionalised paramagnetic NPs can be applied in biomedical and pharmaceutical applications such as drug delivery, hyperthermia, biosensing, and biochemical separation because the magnetic core possesses an ability of magnetic accumulation of the NPs at the target site, whereas their functional shell is designed to serve as a molecular probe, a drug carrier able to release the drug, or an adsorbent for ions and specific molecules through ingenious design of the chemical structure of the capping molecules [28].

1.3.1 Molecule-functionalised silver nanoparticles

Since ancient times, metallic Ag has been very known to mankind for its antimicrobial properties [29]. With the booming development of nanotechnology and an increased risk of bacterial resistance compared to existing organic antimicrobial agents, a new form of Ag, i.e. AgNPs, have become a popular subject due to their superiority compared to bulk Ag and organic antibiotics including robust and broad-spectrum antimicrobial activity, low bacterial resistance, and good biosafety [12]. Studies indicate that AgNPs can inhibit over 650 disease-causing organisms in the body at very low concentration [12].

Although exact antimicrobial mechanism is still subject to debate, researchers are

inclined to believe that the antimicrobial ability of AgNPs mainly derives from the interaction of Ag ions that are released from NP surfaces with important proteins and enzymes and the oxygen stress caused by peroxides such as O_2^- and OH^- that are formed on surfaces of AgNPs [30]. Owing to the excellent antimicrobial activity and unique antimicrobial mechanism, AgNPs have been widely used in food preservation, water disinfection, and medical devices.

Surface functionalization of NPs with molecules provides long-term chemical stability and protection of them against photo- or chemical degradation since chemically synthesized AgNPs are prone to chlorination or oxidation when they are directly exposed to air. Besides, capping molecules also provide sufficient electrostatic or steric repulsion for AgNPs imparting good water stability and preventing NP from agglomeration. These characteristics are very important for antibacterial functionalization of biological fibers because fast oxidation of metallic AgNPs leads to the short quality guarantee period. Besides, a stable coating solution able to generate uniform nanocoatings is the precondition of the finishing of fibers or textiles [31]. Finally, molecules capping the surface of AgNPs should be biocompatible and biodegradable to assure their biosafety.

Until now, various molecules are used to protect AgNPs against aggregation and oxidation including small molecules, polymers, and surfactants. Small molecules include carboxylic acid and its derivatives, amines, and amide derivatives, and organophosphorus. Citrate is the most common carboxylic acid used as a capping agent. Besides, carboxylic acids and amines with alkyl chains and organophosphorus such as oleic acid (OA), octadecylamine (ODA), and tri-n-octylphosphine oxide (TOPO) are

generic protectants for inorganic NPs. For examples, OA can be used for synthesis of metal NPs such as AuNPs [32] and AgNPs [33] and inorganic oxide NPs such as ZnO NPs [34], TiO_2 NPs [35], Fe_3O_4 NPs [36], and PbS NPs [37]. However, the main problems of these small molecules are that most of them show poor biocompatibility, lack solubility in water or strong binding affinity towards biological substrates, or have a low protection ability to prevent NPs from corrosion. Therefore, above molecule-capped AgNPs are rarely used in antibacterial AgNPs. Likewise, surfactants face similar problems for their applications in antibacterial textiles. Therefore, the most widely used capping molecules are polymers.

Compared with small molecules, polymeric protection agents have several advantages. First, polymers are capable of serving as multiple binding sites or nanoreactors to control the size and size distribution of AgNPs. Second, polymers can provide effective electrostatic repulsion and steric hindrance to prevent NPs from aggregation [38]. Third, polymers can form a thick coating on the surface of AgNPs, endowing NPs with good chemical stability. Fourth, polymers possess many functional groups, capable of imparting NPs with additional functions. Various types of polymers have been used as capping agents for AgNPs including linear polymers, hyperbranched polymers, and dendrimers. Linear polymers are cheap and effective modifiers. Polysaccharides are common protection agents including compounds like gum arabic (GA), sophorolipids, and other sugars [30]. Recently, biological macromolecules such as silk fibroin, starch, and chitosan are very popular for the protection of AgNPs because of their biocompatibility and biodegradability [39, 40]. Besides, a synthetic linear polymer like poly(vinyl pyrrolidone) (PVP), polyvinyl acetate (PVA), polyethylene glycol (PEG), and polyacrylic acid (PAA) are also used [41, 42]. However,

owing to linear chain entanglement, above synthetic NPs usually show broad size distribution, lower stability, and less surface functional groups compared with hyperbranched polymers and dendrimers. Li Zhang et al. have compared the conventional capping agents including PEG, PVA, and PAA with hyperbranched polymers in the synthesis of various nanocrystals. It was shown that PEG-, PVA-, and PAA-capped nanocrystals showed bigger size, wider polydispersity, or poor stability in water compared with hyperbrached polyglycerol [38].

Although plentiful polymers can protect AgNPs, the design of multifunctional AgNPs specific to biological fibers is still a great challenge. Nowadays, most studies mainly focus on their antibacterial core. The design of functions of the polymer core is still under-explored.

One of most desired functions for antibacterial treatment of biological textiles is high binding affinity of AgNPs towards biological substrates. This property can increase the treatment efficiency, reduce the cost, precisely control the Ag content, and decrease or even eliminate Ag-containing wastewater and related environmental risks. Because of poor compatibility of metallic AgNPs to biomolecules, to obtain such functions, a capping polymer with a high binding ability or a recognition ability to biological molecules is necessary.

Although same biological molecules such as DNA and special protein macromolecules can serve as programmable and sequence-specific “glues”, they are costly for practical applications. Conversely, dendrimers and hyperbranched polymers seem to be alternative functional polymers. Nowadays, dendrimers and hyperbranched polymers are popular research objects which have attracted a broad and long term

interest for academic researchers due to their unique three-dimensional (3D) hyperbranched morphological structure, multi-functionalities, programmable chemical and physical properties, and potential applications in catalysts, nanomaterials, and biomedicine [43-46]. A dendrimer consists of dendritic units and terminal units with perfectly branched structure. Hyperbranched polymers possess similar properties to their dendrimer analogues but the structure is much more irregular than dendrimers. The advantage of hyperbranched polymers is that they can be synthesized by "one-step" reaction while dendrimers need several reaction steps. Therefore, hyperbranched polymers is a much cheaper protectant. Furthermore, hyperbranched polymers possess non/low entanglement, good solubility, quasi-spherical structure, and abundant functional end groups, which is also suitable for functionalization of NPs [45]. In addition, their nano-cavity structure and terminate functional groups make hyperbranched polymers suitable to serve as nano-carriers. Many guest molecules can be embedded into above nanocarrier systems, including drugs, dyes, imaging agents, catalysts, metal NPs, and enzymes [45]. Finally, by choosing appropriate functional end groups or binding/grafting special functional molecules to their terminated groups, hyperbranched polymers can be endowed with an ability of specific molecular recognition and combination [47]. One of our research purposes is to design polymer-functionalised AgNPs with a strong binding ability to biological molecules such as silk macromolecules and cotton cellulose. Such functional NPs can spontaneously and nearly completely assemble onto biological substrates through strong supramolecular interactions, making environmental-friendly fabrication of antibacterial AgNP coatings possible.

1.4 Nanofabrication technology

In this section, we focus on the nanocoating technology that is applicable for textiles. The methodology for coating AgNPs on textiles is vital to the antibacterial function of the final product. For example, the aggregation state of AgNP coatings can affect the antibacterial activities by affecting the specific surface areas of AgNPs that are dispersed on the fiber surface. In addition, AgNPs clusters are prone to precipitate to the sediment when they re-dissolve in the aqueous solution [48]. Therefore, AgNPs should be mono-dispersed on the fiber surface.

With widespread application of AgNPs in functional textiles, the mass production of AgNPs in textile industry will inevitably increases health and ecosystem risks. Though the long historical use of Ag has not shown obvious negative effects, there is a great concern about the potential risks of AgNPs in the natural environment [49]. Indeed, recent studies have shown that AgNPs have toxic effects on various organisms including aquatic and terrestrial plants, algae, vertebrates, invertebrates, microorganisms, and human cells [30]. Thus, the coating process should avoid producing large quantities of AgNP-containing wastewater. Besides, the complete uptaking of AgNPs by biological substrates is also necessary for quality control and cost-saving.

In summary, an ideal coating technology for textiles should achieve a uniform coating and nearly complete uptaking of AgNPs by fibers through a simple and inexpensive coating strategy.

1.4.1 Traditional nanofabrication technology

Various coating strategies have been developed or are under development to impart an antimicrobial function to biological fibers. Most of the common coating strategies can be categorized to the top-down nanocoating technology. The pad-dry-cure processes

are one classical strategy for antibacterial coating on textiles. Spraying, sputtering, and evaporation are also used for coating. However, these physical coating technologies have similar disadvantages.

(1) Since AgNPs are physically assembled onto the fiber surface, their binding forces are dominated by weak Van der Waals' forces, leading to poor antibacterial durability.

(2) Because of the poor binding affinity of AgNPs to biological molecules, AgNP-containing wastewater is inevitable during the treatment.

(3) The physical coating cannot achieve the precise control of density, uniformity, and thick of AgNP coatings, resulting in unstable product quality.

Except physical coating strategies, chemical coating strategies including in-situ deposition and the sol-gel process become popular in recent studies. In-situ deposition technology involves in-situ generation of inorganic NPs under pre-determined reaction conditions and their subsequent deposition on fiber surface or first attachment of inorganic precursors on the fiber surface followed by subsequent in-situ generation of inorganic NPs [50, 51].

The sol-gel technology involves preparation of nanosol by hydrolysis of inorganic precursors, coating nanosol on textiles, and drying [10]. Like in-situ deposition, this technology allows fabrication of various inorganic nanocoatings on biological substrates.

Although chemical coating strategies are simpler and more inexpensive, they still face same shortcomings to physical coating strategies. Besides, all these technologies

only achieve a spatial arrangement of AgNPs on the fiber surface at a macro level. The precise spatial arrangement of AgNPs on a molecular or even a nanoscale level is still unreachable.

1.4.2 Self-assembly technology

Self-assembly refers to the process by which discrete components such molecules and NPs spontaneously organize due to direct specific interactions and/or indirect interactions, through their environment [52]. Notably, the organization of independent building blocks into ordered macroscopic structures need direct interactions or indirect interactions [52]. In this section, we mainly discuss molecule-driven self-assembly because it shows highest application possibility for nanocoating technology. Supramolecular molecular self-assembly can simply be divided into three classes, which is expounded as follows:

(1) Molecular-molecular self-assembly. There are many molecular-molecular self-assembly phenomena in the natural word. For examples, the formation and evolution of biological cells, the synthesis of the protein in biological cells, the storage and transfer of genetic information among DNA molecules are all realized through intermolecular self-assembly. Hydrogen-bond interactions play an important role in molecular-molecular self-assembly. Two important discoveries can evidence the significance of hydrogen bonding in biological structure: the α-helix and β-pleated sheet structures of protein architecture and the Watson-Crick base-pairing in the DNA double helix [53]. Hydrogen bonds are weak attractions, with a binding strength less than one-tenth that of a normal covalent bond [53]. The weakness of an individual bond is such that is often not sufficient to provide a necessary driving force for self-assembly

system. However, this can overcome by construction of multi-hydrogen bonding interactions. Therefore, the design and engineering of the hydrogen-bond structure are very important. Except DNA and protein, the self-assembly of amphiphilic hyperbranched polymers also attracted increasing interesting. For example, Yan et al. prepared honeycomb-like microporous films by self-assembly of amphiphilic hyperbranched polymers through slow evaporation of a chloroform solution of the precursors in a humid atmosphere [45].

(2) Nanoparticle-nanoparticle self-assembly. Nanoparticle-nanoparticle self-assembly is often guided by molecules. One of the interesting subjects is DNA-guided self-assembly of NPs. For examples, Pal et al. developed a robust strategy for the assembly of AgNPs into well-defined nano-architectures [54]. The demonstrated strategies showed a potential application in photonic structures enabled by the precise spatial control of AgNP structures. Nykypanchuk et al. reported the formation of 3D crystalline assemblies of Au NPs mediated by supramolecular interactions between complementary DNA molecules attached to the nanoparticles' surface [55]. However, DNA-guided self-assembly strategy is too costly. In spite of this, such cooperative self-assembly concept inspires us to design complementary molecules to achieve similar cooperative self-assembly (see chapter 3 and 4).

(3) Self-assembly of nanoparticles on macroscale materials. Undoubtedly, most researches focus on self-assembly of NPs on a two dimensional (2D) surface such as glass, silicon, or biological substrates. For examples, Yap et al. prepared ordered arrays of uniform clusters on flat silicon and glass chips, by electrostatic self-assembly of citrate-capped Au NPs onto polyelectrolyte templates [56]. Conversely, self-assembly

of NPs on 3D biological fibers is still a great challenge because of their complex surface and relatively weak surface chemical activity. Unlike above substrates, biological fibers should maintain their physico-chemical construction and related crystal structure. In other words, any obvious damages to biological fibers are not encouraged in the functional treatment.

In summary, the supramolecular self-assembly technology is a spontaneous spatial arrangement process. Their spontaneous molecular-level spatial arrangement of NPs make a simple, environmental-friendly, and precisely controlled coating of NPs on biological fibers possible.

1.5 The purpose of this study

In brief, the purposes of this study are to develop different supramolecular self-assembly strategies to environmentally-friendly and controllably coat polymer-functionalised AgNPs onto biological fibers.

The aim to choose AgNPs as function materials is to impart an excellent antibacterial function to biological fibers. Supramolecular self-assembly technologies were developed to avoid the environment pollution and control spatial distribution of AgNPs on the fiber surface by employing intermolecular interactions including electrostatic and hydrogen bonding interactions and realize nearly complete adsorption of AgNPs by biological fibers.

1.6 Composition of this study

In this study, three supramolecular self-assembly strategies were developed to controllably and environmental-friendly coat AgNPs on the surface of biological fibers.

In Chapter 2, AgNPs with a high binding affinity towards biological molecules were designed and synthesized through functionalization of AgNPs with hyperbranched poly(amide-amine) (HBPAA). As a cationic polymer, HBPAA possesses a positive charge and high density of amino end groups. Therefore, the strong intermolecular forces between the HBPAA and biomacromolecules can guide AgNPs onto the fiber surface.

Next, an environmental-friendly approach was developed for the preparation of AgNP-coated biological fibers by HBPAA-guided self-assembly of AgNPs on the surface of biological fibers (cotton, silk, and calcium alginate fibers) in aqueous solution. The self-assembly of HBPAA-functionalised AgNPs on biological fibers was realized through electrostatic and hydrogen bonding interactions between biological macromolecules and HBPAA molecules that were capped on the surface of AgNPs. Scanning electron microscopy (SEM) and X-ray photoelectron spectroscopy (XPS) were used to characterize AgNPs on the fiber surface. Antibacterial tests were carried out to evaluate their antibacterial activity.

In Chapter 3, different from HBPAA-guided self-assembly strategy, HBPAA was coated on the surface of silk fibers to evaluate its trapping effect of AgNPs. We further designed a complementary molecule namely hydroxyl-terminated hyperbranched poly(amine-ester)s (HBPAE) and related HBPAE-functionalised AgNPs. Because of the mutual recognition and combination between HBPAA and HBPAE, the self-assembly

of HBPAE-functionalised AgNPs on the HBPAA-modified fiber surface would be environmentally friendly and efficient.

In Chapter 3, we report an efficient and environmentally-friendly approach for the preparation of AgNP-coated silk fibers through self-assembly of HBPAE-functionalised AgNPs on HBPAA-modified silk fibers driven by intermolecular interactions between hydroxyl-terminated HBPAE and amino-terminated HBPAA. As-prepared HBPAE-functionalised AgNPs were characterized by dynamic light scattering (DLS), Ultraviolet–visible (UV–Vis) spectroscopy, Fourier-transform infrared (FTIR) spectroscopy, and transmission electron microscopy (TEM). The self-assembly process was conducted by successively impregnating silk fibers with HBPAA and AgNPs solutions. Their self-assembly behavior was detailedly studied to find out the optimal conditions for complete adsorption of AgNPs by silk fibers. Finally, the antibacterial activities of resulting silk fibers against *Staphylococcus aureus* and *Escherichia coli* were quantitatively evaluated.

In Chapter 4, we designed an environmentally-friendly and energy-efficient bottom-up nanocoating strategy for cotton fibers by the cooperative self-assembly of complementary AgNPs that are functionalised by HBPAA and HBPAE, respectively. Owing to intermolecular recognition and interactions between HBPAA and HBPAE, heterostructured AgNPs could be selectively assembled on the surface of cotton fibers. As-prepared heterostructured AgNP coatings were studied by SEM and XPS. The antibacterial activities of cotton fibers against *Staphylococcus aureus* and *Escherichia coli* were also evaluated.

In Chapter 5, special hierarchical structured Fe_3O_4 NPs/AgNPs dual-coated silk

fibers were prepared via a simple cooperative self-assembly technology. Specifically, silk fibers were sequentially immersed in solutions of positively charged HBPAA-functionalised AgNPs and negatively charged citric acid-capped Fe_3O_4 NPs. As-prepared hierarchical structured silk fibers were characterized by XRD, FESEM, and VSM. Besides, water-soluble hydroxyl-terminated hyperbranched poly(amino-ester) (HBPAE)-capped titanium dioxide nanocrystals (TiO_2 NCs) were also synthesized for coating a cotton fabric via an amino-terminated hyperbranched poly(amidoamine) (HBPAA)-mediated self-assembly strategy to produce a controllable and uniform TiO_2 coating on the cotton surface. It was demonstrated that hydroxyl-modified TiO_2 NCs were egg-shaped and had a narrow size distribution. A TiO_2 NC-coated cotton fabric was prepared by sequential impregnation with solutions of HBPAA and TiO_2 NCs. The attachment of HBPAA to TiO_2 NCs was evaluated by FTIR, FESEM, and XRD.

Finally, in Chapter 6, the conclusion of this study is described.

References:

[1] Balter M. Clothes Make the (Hu) Man. Science. 2009;325:1329.

[2] Kvavadze E, Bar-Yosef O, Belfer-Cohen A, Boaretto E, Jakeli N, Matskevich Z, et al. 30,000-Year-Old Wild Flax Fibers. Science. 2009;325:1359.

[3] Pillai CKS, Paul W, Sharma CP. Chitin and chitosan polymers: Chemistry, solubility and fiber formation. Progress in Polymer Science. 2009;34:641-78.

[4] Tang B, Sun L, Li J, Kaur J, Zhu H, Qin S, et al. Functionalization of bamboo pulp fabrics with noble metal nanoparticles. Dyes and Pigments. 2015;113:289-98.

[5] Reddy N, Yang Y. Introduction to Regenerated Protein Fibers. Innovative Biofibers from Renewable Resources. Berlin, Heidelberg: Springer Berlin Heidelberg; 2015. p. 213-.

[6] Qin Y. Alginate fibres: an overview of the production processes and applications in wound management. Polymer International. 2008;57:171-80.

[7] Jayakumar R, Prabaharan M, Sudheesh Kumar PT, Nair SV, Tamura H. Biomaterials based on chitin and chitosan in wound dressing applications. Biotechnology Advances. 2011;29:322-37.

[8] Bi H, Yin Z, Cao X, Xie X, Tan C, Huang X, et al. Carbon Fiber Aerogel Made from Raw Cotton: A Novel, Efficient and Recyclable Sorbent for Oils and Organic Solvents. Advanced materials. 2013;25:5916-21.

[9] Hopkins AM, De Laporte L, Tortelli F, Spedden E, Staii C, Atherton TJ, et al. Silk Hydrogels as Soft Substrates for Neural Tissue Engineering. Advanced Functional

Materials. 2013;23:5140-9.

[10] Mahltig B, Haufe H, Bottcher H. Functionalisation of textiles by inorganic sol-gel coatings. Journal of Materials Chemistry. 2005;15:4385-98.

[11] Simoncic B, Tomsic B. Structures of Novel Antimicrobial Agents for Textiles - A Review. Textile Research Journal. 2010;80:1721-37.

[12] Dastjerdi R, Montazer M. A review on the application of inorganic nano-structured materials in the modification of textiles: Focus on anti-microbial properties. Colloids and Surfaces B: Biointerfaces. 2010;79:5-18.

[13] Sapsford KE, Algar WR, Berti L, Gemmill KB, Casey BJ, Oh E, et al. Functionalizing Nanoparticles with Biological Molecules: Developing Chemistries that Facilitate Nanotechnology. Chemical reviews. 2013;113:1904-2074.

[14] Reiss P, Protière M, Li L. Core/Shell Semiconductor Nanocrystals. Small. 2009;5:154-68.

[15] Chen C, He H, Lu Y, Wu K, Ye Z. Surface Passivation Effect on the Photoluminescence of ZnO Nanorods. ACS applied materials & interfaces. 2013;5:6354-9.

[16] Protesescu L, Yakunin S, Bodnarchuk MI, Krieg F, Caputo R, Hendon CH, et al. Nanocrystals of Cesium Lead Halide Perovskites (CsPbX3, X = Cl, Br, and I): Novel Optoelectronic Materials Showing Bright Emission with Wide Color Gamut. Nano Letters. 2015;15:3692-6.

[17] Stewart ME, Anderton CR, Thompson LB, Maria J, Gray SK, Rogers JA, et al.

Nanostructured Plasmonic Sensors. Chemical reviews. 2008;108:494-521.

[18] Rycenga M, Cobley CM, Zeng J, Li W, Moran CH, Zhang Q, et al. Controlling the Synthesis and Assembly of Silver Nanostructures for Plasmonic Applications. Chemical reviews. 2011;111:3669-712.

[19] Georgakilas V, Tiwari JN, Kemp KC, Perman JA, Bourlinos AB, Kim KS, et al. Noncovalent Functionalization of Graphene and Graphene Oxide for Energy Materials, Biosensing, Catalytic, and Biomedical Applications. Chemical reviews. 2016.

[20] Lee N, Yoo D, Ling D, Cho MH, Hyeon T, Cheon J. Iron Oxide Based Nanoparticles for Multimodal Imaging and Magnetoresponsive Therapy. Chemical reviews. 2015;115:10637-89.

[21] Chng LL, Erathodiyil N, Ying JY. Nanostructured Catalysts for Organic Transformations. Accounts of chemical research. 2013;46:1825-37.

[22] Liu XY, Wang A, Zhang T, Mou C-Y. Catalysis by gold: New insights into the support effect. Nano Today. 2013;8:403-16.

[23] Mout R, Moyano DF, Rana S, Rotello VM. Surface functionalization of nanoparticles for nanomedicine. Chemical Society reviews. 2012;41:2539-44.

[24] Fresnais J, Yan M, Courtois J, Bostelmann T, Bée A, Berret JF. Poly(acrylic acid)-coated iron oxide nanoparticles: Quantitative evaluation of the coating properties and applications for the removal of a pollutant dye. Journal of Colloid and Interface Science. 2013;395:24-30.

[25] Qi H, Ghodousi M, Du Y, Grun C, Bae H, Yin P, et al. DNA-directed self-assembly

of shape-controlled hydrogels. Nature communications. 2013;4.

[26] Lan X, Wang Q. DNA-programmed self-assembly of photonic nanoarchitectures. NPG Asia Mater. 2014;6:e97.

[27] Zhang Y, Lu F, Yager KG, van der Lelie D, Gang O. A general strategy for the DNA-mediated self-assembly of functional nanoparticles into heterogeneous systems. Nat Nano. 2013;8:865-72.

[28] Reddy LH, Arias JL, Nicolas J, Couvreur P. Magnetic Nanoparticles: Design and Characterization, Toxicity and Biocompatibility, Pharmaceutical and Biomedical Applications. Chemical reviews. 2012;112:5818-78.

[29] Eckhardt S, Brunetto PS, Gagnon J, Priebe M, Giese B, Fromm KM. Nanobio silver: its interactions with peptides and bacteria, and its uses in medicine. Chemical reviews. 2013;113:4708-54.

[30] Levard C, Hotze EM, Lowry GV, Brown GE. Environmental Transformations of Silver Nanoparticles: Impact on Stability and Toxicity. Environmental science & technology. 2012;46:6900-14.

[31] Simoncic B, Tomsic B. Structures of Novel Antimicrobial Agents for Textiles - A Review. Textile Research Journal. 2010.

[32] Sun X, Li D, Guo S, Zhu W, Sun S. Controlling core/shell Au/FePt nanoparticle electrocatalysis via changing the core size and shell thickness. Nanoscale. 2016;8:2626-31.

[33] Prokopovich P, Köbrick M, Brousseau E, Perni S. Potent antimicrobial activity of

bone cement encapsulating silver nanoparticles capped with oleic acid. Journal of Biomedical Materials Research Part B: Applied Biomaterials. 2015;103:273-81.

[34] McLaren A, Valdes-Solis T, Li G, Tsang SC. Shape and Size Effects of ZnO Nanocrystals on Photocatalytic Activity. Journal of the American Chemical Society. 2009;131:12540-1.

[35] Pan D, Zhao N, Wang Q, Jiang S, Ji X, An L. Facile Synthesis and Characterization of Luminescent TiO2 Nanocrystals. Advanced materials. 2005;17:1991-5.

[36] Si S, Li C, Wang X, Yu D, Peng Q, Li Y. Magnetic Monodisperse Fe3O4 Nanoparticles. Crystal Growth & Design. 2005;5:391-3.

[37] Chen S, Liu W. Oleic acid capped PbS nanoparticles: Synthesis, characterization and tribological properties. Materials Chemistry and Physics. 2006;98:183-9.

[38] Zhou L, Gao C, Hu X, Xu W. General Avenue to Multifunctional Aqueous Nanocrystals Stabilized by Hyperbranched Polyglycerol. Chem Mater. 2011;23:1461-70.

[39] Fei X, Jia M, Du X, Yang Y, Zhang R, Shao Z, et al. Green Synthesis of Silk Fibroin-Silver Nanoparticle Composites with Effective Antibacterial and Biofilm-Disrupting Properties. Biomacromolecules. 2013;14:4483-8.

[40] Boca SC, Potara M, Gabudean A-M, Juhem A, Baldeck PL, Astilean S. Chitosan-coated triangular silver nanoparticles as a novel class of biocompatible, highly effective photothermal transducers for in vitro cancer cell therapy. Cancer Letters. 2011;311:131-40.

[41] Sun Y, Yin Y, Mayers BT, Herricks T, Xia Y. Uniform Silver Nanowires Synthesis by Reducing AgNO3 with Ethylene Glycol in the Presence of Seeds and Poly(Vinyl Pyrrolidone). Chemistry of Materials. 2002;14:4736-45.

[42] Sun Y, Xia Y. Shape-Controlled Synthesis of Gold and Silver Nanoparticles. Science. 2002;298:2176-9.

[43] Zeng F, Zimmerman SC. Dendrimers in Supramolecular Chemistry: From Molecular Recognition to Self-Assembly. Chemical reviews. 1997;97:1681-712.

[44] Chen S, Zhang X-Z, Cheng S-X, Zhuo R-X, Gu Z-W. Functionalized Amphiphilic Hyperbranched Polymers for Targeted Drug Delivery. Biomacromolecules. 2008;9:2578-85.

[45] Jin H, Huang W, Zhu X, Zhou Y, Yan D. Biocompatible or biodegradable hyperbranched polymers: from self-assembly to cytomimetic applications. Chemical Society reviews. 2012;41:5986-97.

[46] Skaria S, Thomann R, Gómez-Garcia CJ, Vanmaele L, Loccufier J, Frey H, et al. A convenient approach to amphiphilic hyperbranched polymers with thioether shell for the preparation and stabilization of coinage metal (Cu, Ag, Au) nanoparticles. Journal of Polymer Science Part A: Polymer Chemistry. 2014;52:1369-75.

[47] Kurniasih IN, Keilitz J, Haag R. Dendritic nanocarriers based on hyperbranched polymers. Chemical Society reviews. 2015;44:4145-64.

[48] Yu S-j, Yin Y-g, Liu J-f. Silver nanoparticles in the environment. Environmental Science: Processes & Impacts. 2013;15:78-92.

[49] Navarro E, Piccapietra F, Wagner B, Marconi F, Kaegi R, Odzak N, et al. Toxicity of Silver Nanoparticles to Chlamydomonas reinhardtii. Environmental science & technology. 2008;42:8959-64.

[50] Perelshtein I, Applerot G, Perkas N, Wehrschetz-Sigl E, Hasmann A, Guebitz GM, et al. Antibacterial Properties of an In Situ Generated and Simultaneously Deposited Nanocrystalline ZnO on Fabrics. ACS applied materials & interfaces. 2009;1:361-6.

[51] El-Shishtawy RM, Asiri AM, Abdelwahed NAM, Al-Otaibi MM. In situ production of silver nanoparticle on cotton fabric and its antimicrobial evaluation. Cellulose. 2011;18:75-82.

[52] Grzelczak M, Vermant J, Furst EM, Liz-Marzán LM. Directed Self-Assembly of Nanoparticles. ACS nano. 2010;4:3591-605.

[53] Jeffrey GA, Saenger W. Hydrogen bonding in biological structures: Springer Science & Business Media; 2012.

[54] Pal S, Deng Z, Ding B, Yan H, Liu Y. DNA-Origami-Directed Self-Assembly of Discrete Silver-Nanoparticle Architectures. Angewandte Chemie. 2010;122:2760-4.

[55] Nykypanchuk D, Maye MM, van der Lelie D, Gang O. DNA-guided crystallization of colloidal nanoparticles. Nature. 2008;451:549-52.

[56] Yap FL, Thoniyot P, Krishnan S, Krishnamoorthy S. Nanoparticle Cluster Arrays for High-Performance SERS through Directed Self-Assembly on Flat Substrates and on Optical Fibers. ACS nano. 2012;6:2056-70.

Chapter 2

Preparation and controlled coating of HBPAA-functionalized silver nanoparticles on cotton and silk fibers through self-assembly

Chapter 2 Preparation and controlled coating of HBPAA-functionalized silver nanoparticles on cotton and silk fibers through self-assembly

2.1 Introduction

Cotton fibers (CFs) are amongst the most popular and best-selling raw materials all over the world for their wide applications in clothes, home furnishings, and various textile-based industrial products such as toys, home accessories, and medical gauzes and bandages, due to the excellent mechanical and thermal properties including excellent hygroscopicity and breathability, satisfied strength and flexibility, and good thermal insulation. As a natural and abundant biomaterial, cotton is mainly composed of cellulose with polymerization degree ranged in 1×10^4-1×10^5. The supramolecular structure of cotton cellulose can be divided into three levels. Initially, dozens of cellulose macromolecules are combined to form a crystallized microfibril with a diameter of 6 nm through intermolecular interactions mainly dominated by hydrogen bonding. Several elementary fibrils are further assembled into fibrils with a diameter ranging in 10-25 nm. The fibrils further form macrofibrils that range from 0.1 to 1.5 μm in diameter and finally the cotton fiber.

The *Bombyx mori* silk fiber (SF) is a naturally created protein fiber, mainly consisting of a gummy outer layer (sericin) and two core filaments (fibroin) [1]. Sericin is an amorphous protein that can be removed by the degumming process. Silk fibroin is composed of numerous minute fibrils, which could be separated into β-sheet crystals with strong hydrogen bonding and a non-crystalline (amorphous) region with varying

degrees of hydrogen bonding. The amino acid sequence in the crystalline region of the silk fibroin is mainly composed of glycine residues alternating with alanine and serine and the sequence in the amorphous region contains a tyrosine-rich domain [2]. SFs are known to be one of the strongest natural fibers with excellent mechanical properties and have been used for textiles in the last several millennia.

Currently, CFs and SFs have also attracted considerable interest from researchers in the preparation of functional biomaterials in the fields such as biomedicine, tissue engineering, and biosensing because of their good mechanical properties, excellent biocompatibility, and controllable biodegradability [3-6]. Recently, functionalization of biological fibers by coating various nanomaterials has become an interesting subject in the field of materials science and nanotechnology because of their ability to combine the desirable properties of both nanoscale materials and biological fibers to improve mechanical, optical, electronic, or magnetic properties for potential applications in biomedicine [7]. Among the various nanomaterials, silver nanoparticles (AgNPs) are one of the most attractive nanomaterials because of their outstanding biomedical and optical performances [8-10]. Specifically, AgNPs exhibit excellent broad spectrum antimicrobial activity and relatively low bacterial resistance, which have made them extremely popular in antibacterial textiles. Because of these novel properties, surface coating of biological fibers with AgNPs has been intensively investigated to extend their utility in biomedical applications.

Most traditional assembly approaches of nanomaterials on biological substrates depend on a chemical or physical coating. Because of their poor compatibility with organic materials, it is hard to achieve complete attachment of inorganic nanoparticles

on biological fibers using chemical coating methods such as in situ deposition and sol–gel coating, causing inevitable environmental problems and waste of nanomaterials [11]. Physical coating methods that are able to make full use of nanomaterials such as sputtering and evaporation are only suitable for flat surfaces and the nanoparticles are exposed to the external environment, which is prone to oxidation. Thus, the assembly of nanomaterials, especially for nanometallic materials, on biological substrates in a facile, fast, and green manner remains challenging.

Supramolecular self-assembly is the spontaneous association of different materials under equilibrium conditions into a stable and structurally well-defined assembly mediated by intermolecular interactions such as non-covalent bonds or hydrogen bonds [12]. The advantage of this self-assembly technology is that inorganic nanomaterials can be spontaneously transferred and concentrated onto organic materials from their colloidal solution, making the fast, efficient, and environmentally friendly self-assembly of nanomaterials on fiber substrate possible [13, 14]. Notably, because the strengths of individual van der Waals interactions and hydrogen bonds are very weak compared with thermal energies, to gain sufficient driving force, molecules that are capped on the surface of nanoparticles should interact with substrates by a sufficient number of weak non-covalent interactions or multiple hydrogen bonds. Furthermore, these interactions between the capping molecules and the bio-substrates should overwhelm the entropic advantages of the disintegration of the ordered assembly into a dissociated state. In consideration of the low compatibility of AgNPs to biological fibers, the surface modification of AgNPs with dense functional groups is essential. Molecules capped on the surface of AgNPs should be water soluble, biodegradable, and biocompatible, able to protect AgNPs from oxidation and agglomeration, and possess a huge number of free

functional groups capable of forming strong chemical interactions with biomacromolecules. Currently, a variety of functional polymers can be used as capping agents to prepare water-soluble AgNPs, including linear polymers, hyperbranched polymers, and dendrimers. Polymeric modifiers can not only serve as multiple binding sites or nanoreactors to control the size and size distribution of nanoparticles but also provide sufficient steric hindrance and functional groups to prevent nanoparticle aggregation and improve their surface chemical activity [15]. Among them, linear polymers are cheap and effective modifiers; however, owing to linear chain entanglement, the synthetic nanoparticles usually show broad size distribution, lower stability, and less surface functional groups compared with hyperbranched polymers and dendrimers. Li Zhang et al. have compared the conventional capping agents including PEG, PVA, and PAA with hyperbranched polymers in the synthesis of various nanocrystals. It was shown that PEG-, PVA-, and PAA-modified nanocrystals showed bigger size, wider polydispersity, or poor stability in water compared with hyperbrached polyglycerol [15]. Although dendrimers can be used to prepare uniform and stable AgNPs, their synthesis is time consuming and complicated. By contrast, hyperbranched polymers have comparable properties to their dendrimer analogs including a three-dimensional structure, low viscosity, and abundant functional end groups, but they can be synthesized in a ‘‘one-step’’ reaction that is much easier than that of dendrimers [16]. To this end, amino-terminated hyperbranched poly(amine-amine) (HBPAA) is chosen as the capping agent for surface modification of AgNPs because of its biocompatibility, amphipathicity, abundant amino end groups, and torispherical nature, which not only controls the growth and stabilization of nanoparticles but also endows the NP surface with dense amino-functional groups [17]. Above positively-charged

HBPAA molecules on surfaces of AgNPs is able to recognize negatively-charged biological fibers and bind with receptor biomacromolecules on the fiber surface through electrostatic and hydrogen bonding interactions.

In this study, we present an efficient and environment-friendly assembly approach to prepare homogenously distributed AgNP-coated biological fibers through intermolecular self-assembly technology. AgNPs were capped by amino-terminated HBPAA to endow NPs with high binding ability towards polyanionic biomolecules. The use of HBPAA as the capping agent is because HBPAA possessing a three-dimensional spherical structure with a hydrophobic core and hydrophilic amino end groups not only stabilizes and protects AgNPs in aqueous phase but also have an ability of specific recognition for anionic biomolecules through multi-intermolecular interactions. In the experiment, we selected cotton fibers (CFs) silk fibers (SFs), and calcium alginate fibers (CAFs) as demonstrations to evaluate the self-assembly ability. Our studies showed that HBPAA-capped AgNPs (HBPAE/AgNPs) can completely assemble onto biological fibers at room temperature. Notably, the self-assembly ability of HBPAA/AgNPs on CFs, SFs, and CAFs is different. CAFs showed much stronger capture ability of AgNPs than SFs and CFs. Nevertheless, the self-assembly ability on CFs and SFs could be improved by increasing the incubation temperature. Antibacterial tests showed that all biological fibers had excellent antibacterial activities. In summary, the developed self-assembly technology may provide simple, efficient, and environment-friendly coating strategy for precise control of Ag content of antibacterial biological fibers, which is significant for quality control of antibacterial textiles.

2.2 Experimental

2.2.1 Materials

SFs were obtained from the Ueda Fujimoto Co., Ltd (Japan). CFs were obtained from Zhangjiagang Nellnano Nanotechnology Co., Ltd (China). CAFs were obtained from the Qingdao Bright Moon Group Co. (China). HBPAA was synthesized as described in our previous paper [18, 19]. Silver nitrate and nitric acid were purchased from Wako Pure Chemical Industries, Ltd. (Japan). *Staphylococcus aureus* (ATCC 6538) and *Escherichia coli* (ATCC 8099) were obtained from College of Life Science, Soochow University (China). Nutrient broth and nutrient agar were purchased from Scas Ecoscience Technology Inc. (China).

2.2.2 Preparation of HBPAA/AgNPs

HBPAA/AgNPs were synthesized by dissolving 18.75 μmol HBPAA in 45 mL deionized water and adding the HBPAA solution to 5 mL of 46.3 mM silver nitrate at 35 ^{o}C using a well-described procedure. The reaction mixture was slowly heated to 90 ^{o}C and kept stirring at 90 ^{o}C for 3 h. This resultant solution was dialyzed against distilled water for 72 h.

2.2.3 Characterization of HBPAA/AgNPs

The morphology and size of HBPAA/AgNPs were characterized using a JEM-2100F transmission electron microscope (TEM) (JEOL, Japan). The hydrodynamic size and surface charge of AgNPs in the aqueous solution were evaluated using a Nano ZS90 Zetasizer (Malvern, UK). The ultraviolet-visible (UV-vis) spectra from 250 to 700 nm were recorded on a Shimadzu UV-2700 spectrophotometer (Shimadzu, Japan). The Fourier transform infrared spectroscopy (FT-IR) images were

collected on a Perkin Elmer Spectrum 100 FT-IR spectrometer (Perkin Elmer, USA). The silver content was measured by the inductively coupled plasma atomic emission spectroscopy (ICP-AES) method.

2.2.4 Self-assembly between HBPAA/AgNPs and biological fibers

2.2.4.1 Self-assembly of HBPAA/AgNPs on CFs

The influence of Ag concentration on the self-assembly of HBPAA/AgNPs on CFs was evaluated by incubating one gram of CFs in 100 mL of AgNP solutions with Ag concentrations ranging in 5−100 mg/L at 35 ^{o}C for 180 min. To study the effect of temperature on the self-assembly, 1 g of CFs were incubated in 100 mL of AgNP solution (100 mg/L) for 180 min under different temperature conditions (35, 45, 55, 65, 75, 85, and 95 ^{o}C). The resulting CFs were rinsed by deionized water and cured at 120 ^{o}C for 20 min. As a control, CFs were treated with 0.3 mM HBPAA solution at 95 ^{o}C for 180 min.

2.2.4.2 Self-assembly of HBPAA/AgNPs on SFs

Similar to CFs, the influence of Ag concentration on the self-assembly of HBPAA/AgNPs on SFs was evaluated by incubating 1 g of SFs in 100 mL of AgNP solutions with Ag concentrations in the range of 5−100 mg/L at 35 ^{o}C for 180 min. To study the effect of temperature on the self-assembly, 1 g of SFs were incubated in 100 mL of AgNP solution (400 mg/L) under different temperature conditions (35, 45, 55, 65, 75, 85, and 95 ^{o}C) for 180 min. The resulting CFs were rinsed by deionized water and cured at 120 ^{o}C for 20 min. As a control, SFs were treated with 0.3 mM HBPAA solution at 95 ^{o}C for 180 min.

2.2.4.3 Self-assembly of HBPAA/AgNPs on CAFs

The influence of Ag concentration on the self-assembly of HBPAA/AgNPs on CAFs was evaluated by incubating 1 g of CAFs in 100 mL of AgNP solutions with Ag concentrations in the range of 100−400 mg/L at 35 ºC for 180 min. The resulting CAFs were rinsed by deionized water and cured at 120 ºC for 10 min. As a control, CAFs were treated with 0.3 mM HBPAA solution at 35 ºC for 180 min.

2.2.5 Characterization of HBPAA/AgNP-coated biological fibers

The morphology of HBPAA/AgNP-coated biological fibers were observed using a Hitachi S-5000 field emission scanning electron microscope (FESEM) (Hitachi, Japan). Surface analysis by X-ray photoelectron spectroscopy (XPS) was performed using a Kratos Axis Ultra DLD spectrometer (Kratos Analytical, Japan). The collected spectra were analyzed using a curvefitting program, XPSPEAK 4.1.

The Ag content in the biological fibers was measured via a Vista MPX inductively coupled plasma atomic emission spectroscope (Varian, USA). A total of 10 mg of the sample was dissolved in 10 mL HNO_3 solution (65%) and diluted to 100 mL with deionized water. A total of 1 mL of the diluted solution was then drawn to measure the concentration of silver ion (C*ion*, mg/L). Silver content C*ag*, mg/g) in the fibers was calculated by Equation (1):

$$Cag = Cion \tag{1}$$

2.2.6 Antibacterial test

The antimicrobial activity of biological fibers was tested against *E. coli* and *S.*

aureus by a shake-flask method according to GB/T 20944.3-2008 (China). A sample of testing fibers (0.75 g) was immersed into a flask containing 70 mL 0.3 mM phosphate-buffered saline (PBS, monopotassium phosphate, pH ~7.2) culture solution with cell concentration of 1×10^5–4×10^5 colony forming units (cfus)/mL. The flask was then shaken at 150 rpm on a rotary shaker at 24 °C for 18 h. Samples of 1 mL were taken at a specified time, diluted 10-fold in saline, and then transferred onto nutrient agar plates (Difco). All plates were incubated at 37 °C for 24 h and the colonies formed were counted. The percentage reduction (cfu, %) was determined as in Equation (2):

$$cfu\ (\%) = \frac{c - a}{c} \times 100 \qquad (2)$$

Where c and a are the bacterial colonies of pristine fibers and the HBPAA/AgNP-coated fibers, respectively. All experiments were performed in triplicate with three substrates and the mean values were calculated.

2.3 Results and discussion

2.3.1 Characterization of HBPAA/AgNPs

Amino-functionalised HBPAA/AgNPs were prepared by hydrothermal reaction using HBPAA as the reducing and capping agent, which can prevent NPs from aggregation, oxidation, and degradation, as well as endow the particle surface with positive charges and abundant amino groups.

The synthesis of HBPAA/AgNPs can be directly observed during the experiment. Upon heating of a silver nitrate/HBPAA mixture at 90 °C, the solution slowly turned yellow and finally dark red after several hours. The formation of AgNPs can also be

verified using an UV-vis spectrophotometer [Figure 2.1(a))]. The UV-vis spectra of as-prepared AgNPs exhibited a strong absorption band at 404 nm corresponding to the characteristic surface plasmon resonance of metallic AgNPs [20]. The sharp band of AgNPs indicated the presence of well-separated AgNPs with narrow size distribution in water. This was further confirmed by the TEM image of AgNPs [Figure 2.1(c)], which revealed that the monodispersed AgNPs had an average diameter of about 8.9 nm and a narrow dispersion. The observed large-scale HBPAA/AgNPs with a regular spherical structure indicated HBPAA has a good control of particle shape. The hydrodynamic size of these AgNPs is around 10.1 nm (3–85 nm), which agreed very well with the anticipated size [Figure 2.1(b)].

The small size and narrow size distribution of as-prepared AgNPs were due to the unique structure of HBPAA. Because of its spherical three-dimensional structure with inner nano-cavities and numerous internal secondary amino groups, HBPAA can entrap the silver ions into the confined inner cavity, reduce them to form small-sized silver nanocrystals, and prevent them from further aggregation through electrostatic and steric hindrance effects.

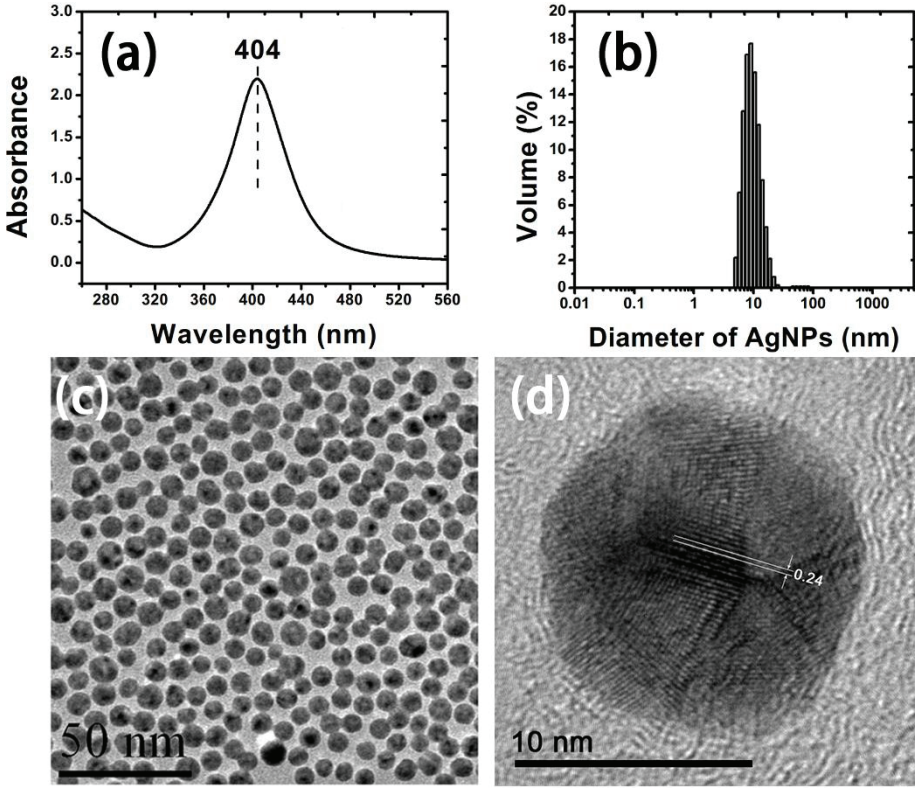

Figure 2.1 (a) UV-vis adsorption spectra of the solution of HBPAA/AgNPs. (b) In situ size distribution of HBPAA/AgNPs. (c) TEM and (d) high resolution TEM images of HBPAA/AgNPs.

To examine more closely the nature of the Ag/HBPAA interface, in particular the possible chemical interactions between the HBPAA and AgNPs, FTIR spectroscopy was employed to detect the chemical transformation. Figure 2.2 displays the FTIR spectra of HBPAA and HBPAA/AgNPs. The overall FT-IR spectra of HBPAA/AgNPs showed similar pattern to that of HBPAA, indicating HBPAA was successfully attached onto the surface of AgNPs and no major chemical structure transformations in HBPAA in the chemical reaction. However, some distinct features in amino/amide regions were observed. The adsorption peaks of amino A, amide B, amide I, and amide II at 3288, 3065, 1645, and 1549 cm^{-1} slightly shifted to 3285, 3067, 1643, and 1558 cm^{-1},

respectively. In addition, the adsorption peak of amide III at 1273 cm^{-1} greatly strengthened and shifted obviously to 1305 cm^{-1}. These changes indicated that some chemical interactions formed between HBPAA molecules and AgNPs, probably owing to the coordination between N and Ag. Finally, the zeta potential test found that the as-prepared AgNPs had positive surface charge (+38 mV), also suggesting capping by a surface layer of HBPAA.

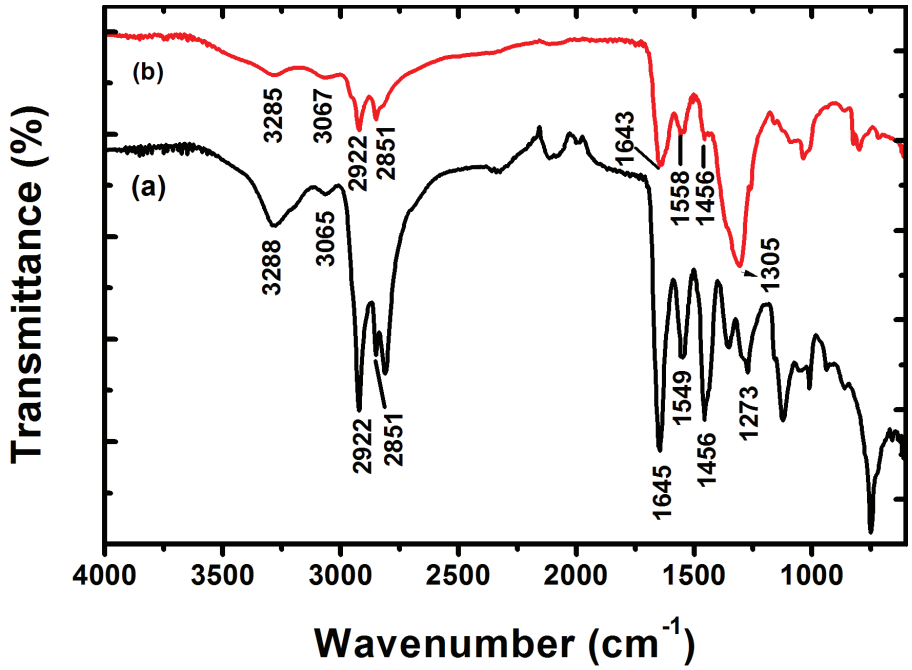

Figure 2.2 FTIR spectra of (a) HBPAA and (b) HBPAA/AgNPs.

2.3.2 Preparation of HBPAA/AgNP-coated CFs, SFs, and CAFs

The mechanism of self-assembly of HBPAA/AgNPs on the surface of biological fibers could be explained on the basis of electrostatic and hydrogen bonding interactions between the negatively charged carboxyl/hydroxyl groups in biological fibers and positively charged amino groups that are coated on the surface of AgNPs, as shown in Scheme 2.1. By virtue of the acidity of their hydroxyl and carboxyl constituent units,

CFs, SFs, and CAFs exhibit a net negative charge in weakly acidic aqueous medium. Conversely, HBPAA/AgNPs possessed a positive charge with the zeta potentials of +38 mV. Therefore, when biological fibers were incubated in AgNPs solution (pH=8.2), positively-charged AgNPs can adsorb onto the oppositely-charged biomacromolecules in biological fibers by electrostatic and hydrogen-bonding interactions. In addition, because of the abundant amino end groups, quasispherical branched architecture, good solubility, and polycationic nature, HBPAA/AgNPs can easily bind to biological fibers via intermolecular hydrogen bonding between amino end groups and pendent carboxylate and/or hydroxyl groups of biomacromolecules.

Theoretically, the self-assembly ability between HBPAA/AgNPs and biological fibers is highly dependent on the surface chemical activity of biological fibers. Therefore, SFs is expected to possess stronger adsorption ability for HBPAA/AgNPs because most hydroxyl pendent groups in cotton cellulose is passivated, thereby leading to relatively weak surface chemical activity. Similarly, HBPAA/AgNPs are expected to have strong binding affinity to carboxyl-containing biological fibers. Therefore, we chose CAFs as a control to explore the effect of surface functional groups on the self-assembly.

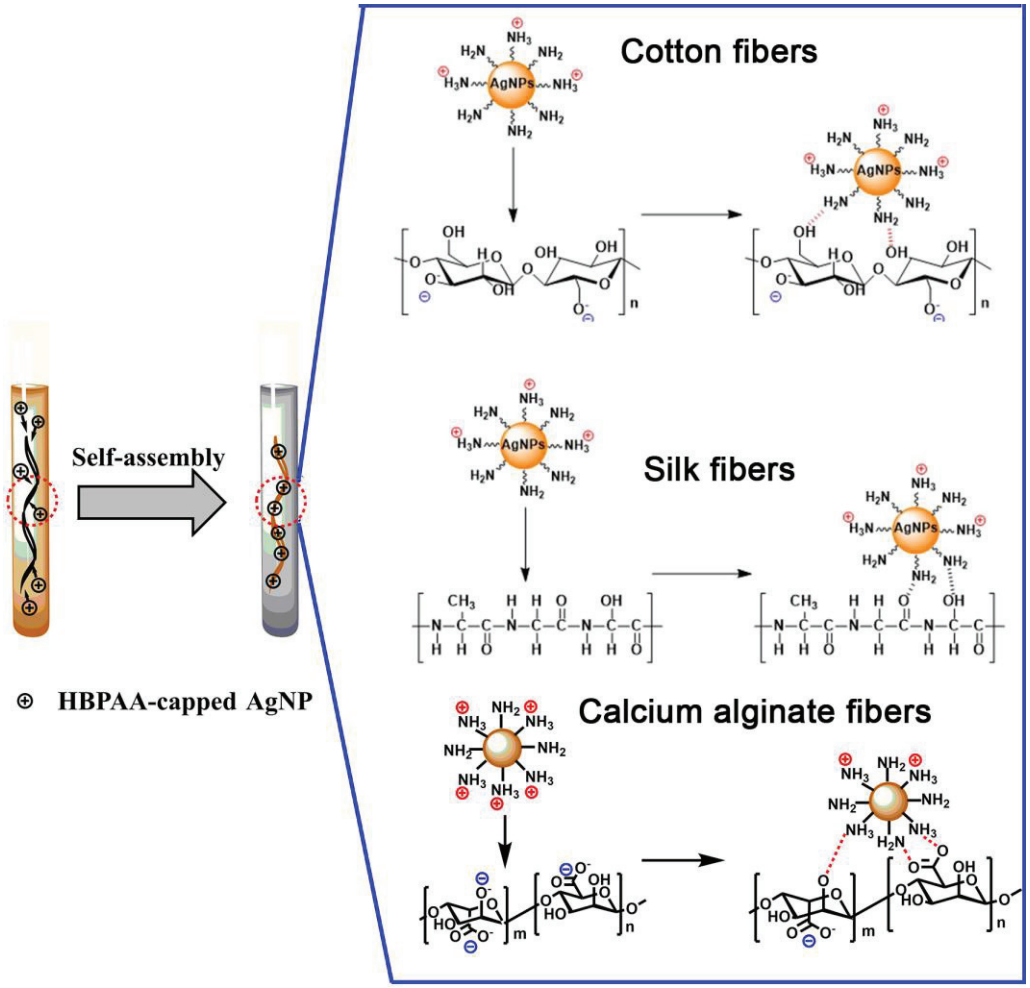

Scheme 2.1 Schematic illustration of HBPAA-mediated assembly of AgNPs on the surface of CFs, SFs, and CAFs.

To prove our speculation, the adsorption ability of AgNPs by CFs, SFs, and CAFs was explored. Figure 2.3-2.7 showed the AgNPs concentration-dependent Ag content in CFs, SFs, and CAFs at room temperature (35 ºC). In the case of CFs, by increasing the AgNP concentration from 5 to 100 mg/L, their adsorption by cotton showed an initial increase (5-15 mg/L) and then a decrease (15-100 mg/L). The maximum capacity for complete adsorption of HBPAA/AgNPs was only 1.5 mg/g. Conversely, SFs showed a much higher adsorption ability. Up to 35 mg/L of HBPAA/AgNPs were completely

adsorbed on SFs, indicative of their higher compatibility than CFs. This is because silk protein possesses more active functional groups on the silk surface than on the cotton surface.

In the case of CAFs, with increasing the concentration of AgNPs from 100 to 400 mg/L, the Ag content of CAFs increased proportionally from 10 to 30 mg/g, and then reached a plateau beyond 300 mg/L (Figure 2.7). The adsorption efficiency of AgNPs decreased from near 100 % to 75.2% (red line). The capacity for the complete adsorption of HBPAA/AgNPs by CAFs can reach up to 30 mg/g, which was 10 times higher than by silk and cotton.

Based on above analyses, two important conclusions were as follows.

Firstly, HBPAA/AgNPs are very sensitive to surface functional groups of biological fibers. In our experiment, HBPAA/AgNPs show much stronger binding ability to carboxyl-containing CAFs than to hydroxyl-containing CFs and SFs. Secondly, the adsorption ability was highly dependent on the Ag concentration. When the Ag concentration increased to a high value, the adsorption ability of HBPAA/AgNPs was inhibited because of the increased electrostatic repulsion among NPs.

Interestingly, although CFs and SFs showed weak adsorption for HBPAA/AgNPs at room temperature compared to CAFs, their adsorption ability can be improved by elevating the temperature. As shown in Figure 2.4 and 2.6, by rising the incubation temperature from 35 to 95 ^{o}C, the adsorption capacity of HBPAA/AgNPs by CFs and SFs increased up to 8.05 and 21 mg/g, respectively. This is probably contributed by the improvement of chemical activity of HBPAA and biomacromolecules in high temperature.

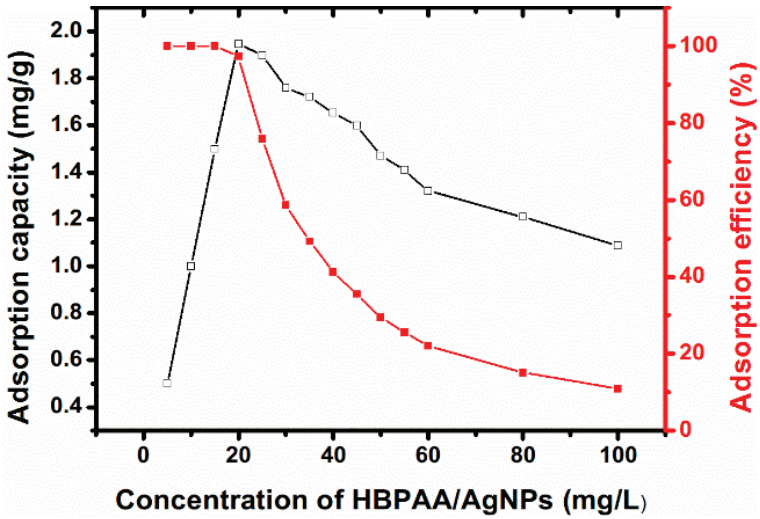

Figure 2.3 Ag concentration dependent-Ag content in CFs (black line) at room temperature and the corresponding adsorption efficiency of AgNPs by CFs (red line).

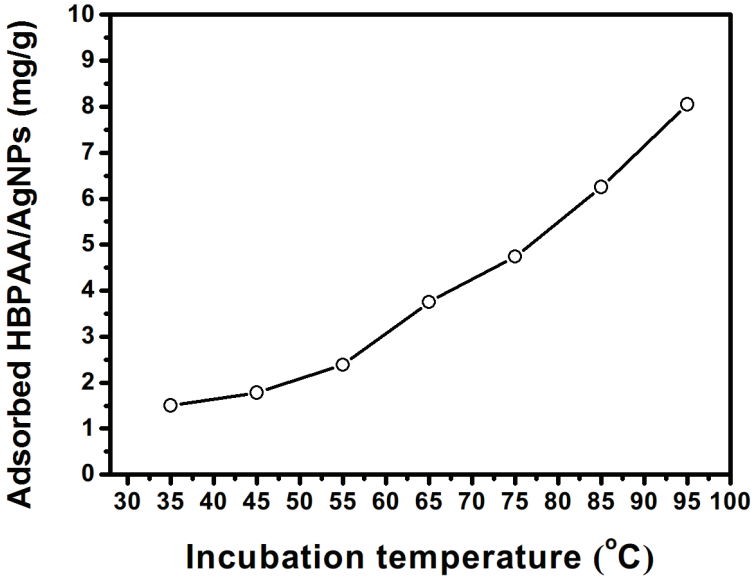

Figure 2.4 Temperature dependent-Ag content in CFs. The concentration of HBPAA/AgNPs was set as 100 mg/L.

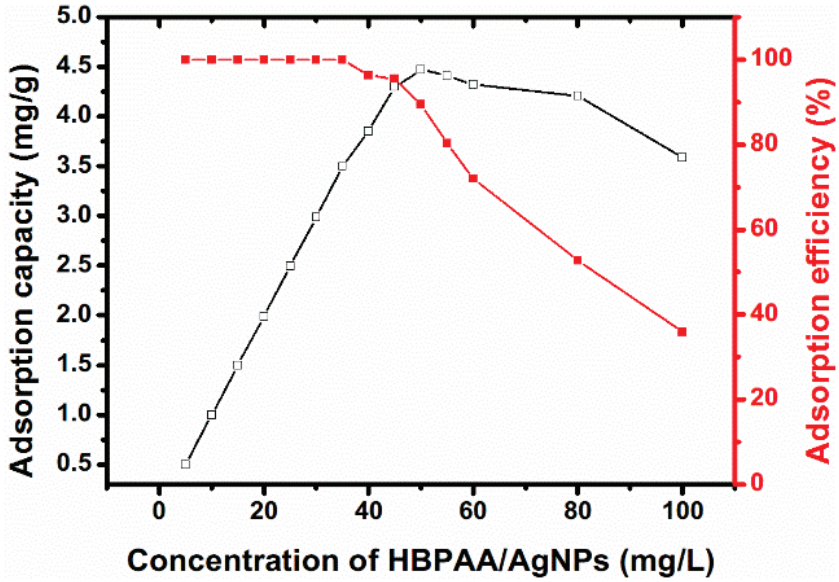

Figure 2.5 Ag concentration dependent-Ag content in SFs (black line) and the corresponding adsorption efficiency of AgNPs by CFs (red line).

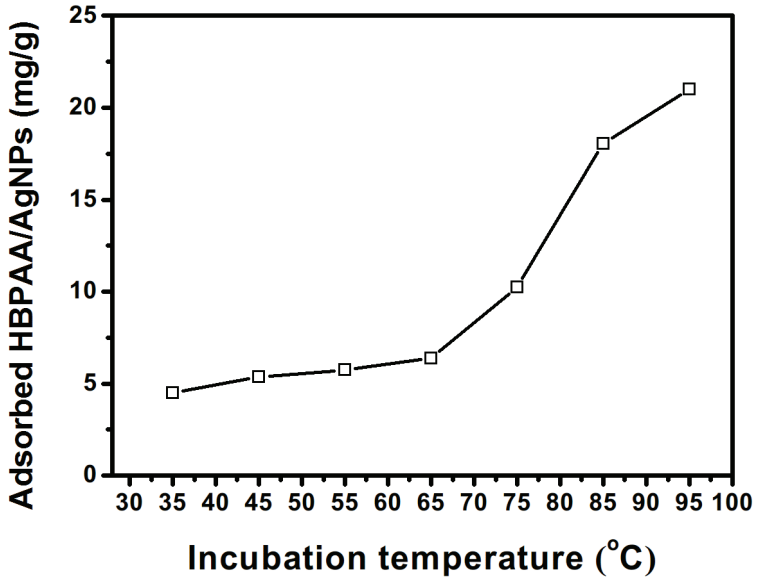

Figure 2.6 Temperature dependent-Ag content in SFs. The concentration of HBPAA/AgNPs was 400 mg/L.

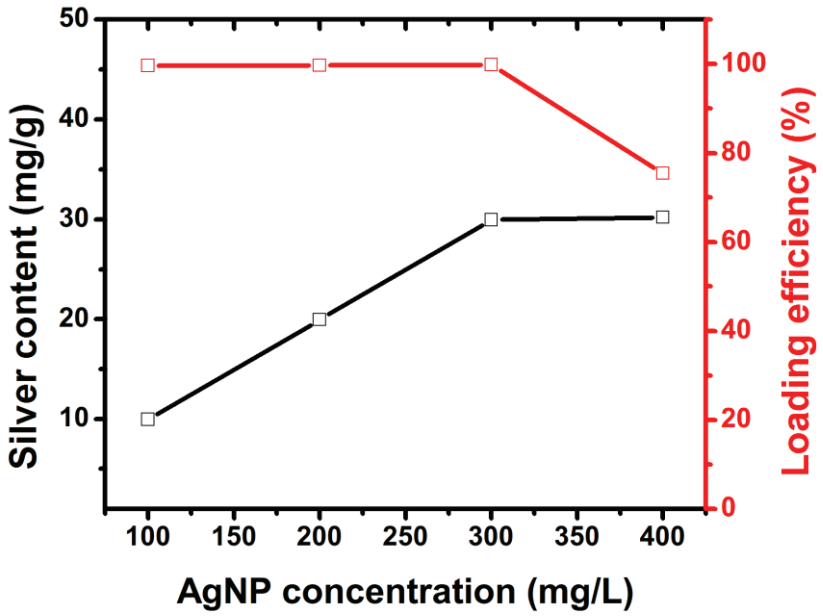

Figure 2.7 Ag concentration dependent-Ag content in CAFs (black line) and the corresponding adsorption efficiency of AgNPs by CAFs (red line).

2.3.3 SEM morphology of the HBPAA/AgNP-coated CFs, SFs, and CAFs

The characteristic microstructure of CFs can be observed by FESEM. As displayed in inset of Figure 2.8(a), the convolution of CFs was clearly observed at a low magnification (1,000 times). The CFs showed dense paralleled macrofibrils and a clean and smooth surface at a magnification of 20,000 × [Figure 2.8(b)], in good agreement with the morphology characteristics of CFs. The texture of CFs at nanoscale level was shown in Figure 2.8(b). Grooves with irregular shapes were found among fibrils although the whole surface appeared smooth. Conversely, HBPAA/AgNP-coated CFs exhibited a much rougher surface [Figure 2.8(c)]. After the assembly of HBPAA/AgNPs on a cotton surface, numerous well-dispersed NPs were found on the surface of CFs compared with pure CFs. The diameter of the spherical particles was found to vary from 10 to 100 nm [Figure 2.8(d)], which was in line with the morphological features of HBPAA/AgNPs that were determined by TEM. Interestingly,

although HBPAA/AgNPs densely bond to cotton cellulose, they followed the same distribution rules, i.e., monodispersion. This mainly contributed by electrostatic repulsion among HBPAA/AgNPs. It also indicates that HBPAA was responsible for the attachment and distribution of HBPAA/AgNPs on the surface of CFs.

Figure 2.9 shows the FESEM images of pure SFs and HBPAA/AgNPs-coated SFs (20 mg/g). Unlike CFs, pure SFs exhibited a much smoother surface as shown in Figure 2.9(a) and 2.9(b). Nevertheless, we found several polymeric attachments on the SF surface, mainly belonging to unremoved sericin during the degumming process. By treatment SFs with HBPAA/AgNPs at high temperature, high density of NPs, actually HBPAA/AgNPs, appeared on the SF surface [Figure 2.9(c)], indicative of their high self-assembly efficiency. Notably, these HBPAA/AgNPs were monodispersed on the surface of SFs, compliant with distribution rules on the surface of CFs. An advantage of such interesting characteristic is that we can control the coating thickness and coating layer number of NPs on biological substrates or even design a heterostructured NP coating by Layer-by-Layer (LbL) self-assembly technology (see our studies in chapter 3 and 4).

SEM images of the surface of blank CAFs and the AgNP-coated CAFs are shown in Figure 2.10. Pure CAFs displayed a flat, dense, and smooth surface [Figures 2.10(a) and 2.10(b)]. Unlike pure CAFs, high-density of white spots uniformly spread around on a surface of coated CAF [Figure 2.10(c)], which indicated a high level of adhesion of HBPAA/AgNPs on the fiber surface. As can be seen in Figure 2.10(d), these particles were fairly monodisperse and exhibited nearly circular cross-sections. The diameter of particles was in range of 1–100 nm, also suggesting that the AgNPs were fairly

monodisperse. These results suggest that the functionalized HBPAA/AgNPs have been successfully attached to the fiber surface and no further aggregation of the AgNPs occurred on the surface of CAFs.

In summary, the HBPAA-guided self-assembly of HBPAA/AgNPs on CFs, SFs, and CAFs are simply, effective, and exhibited good monodispersity, mainly owing to supramolecular interactions between HBPAA and cotton cellulose.

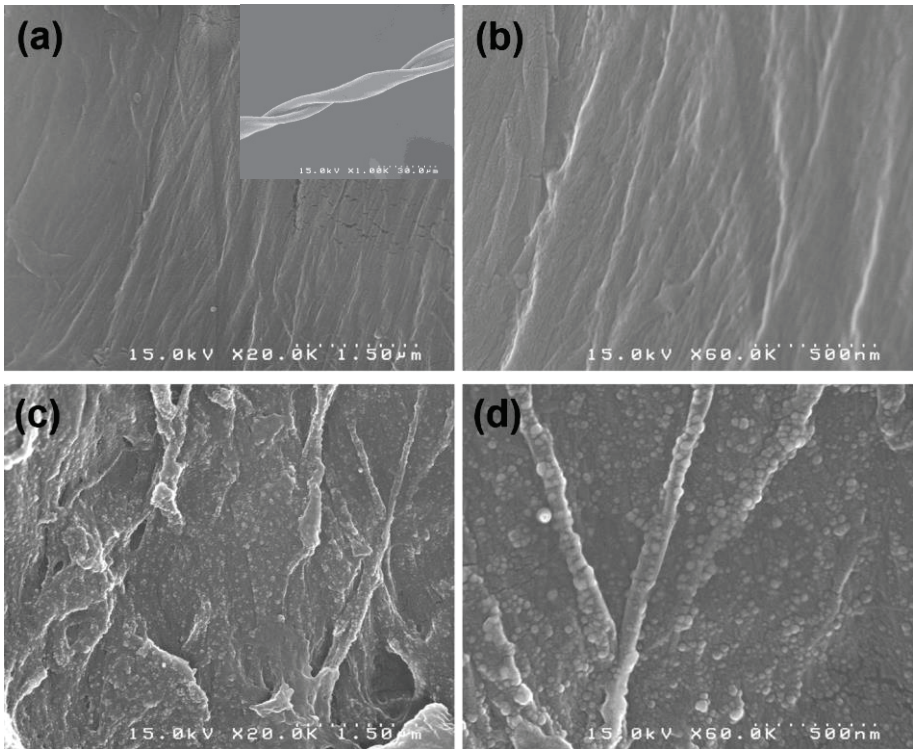

Figure 2.8 SEM images of the ((a) × 20,000; (b) × 60,000) blank CFs and ((c) × 20,000; (d) × 60,000) HBPAA/AgNP-coated CFs (8 mg/g).

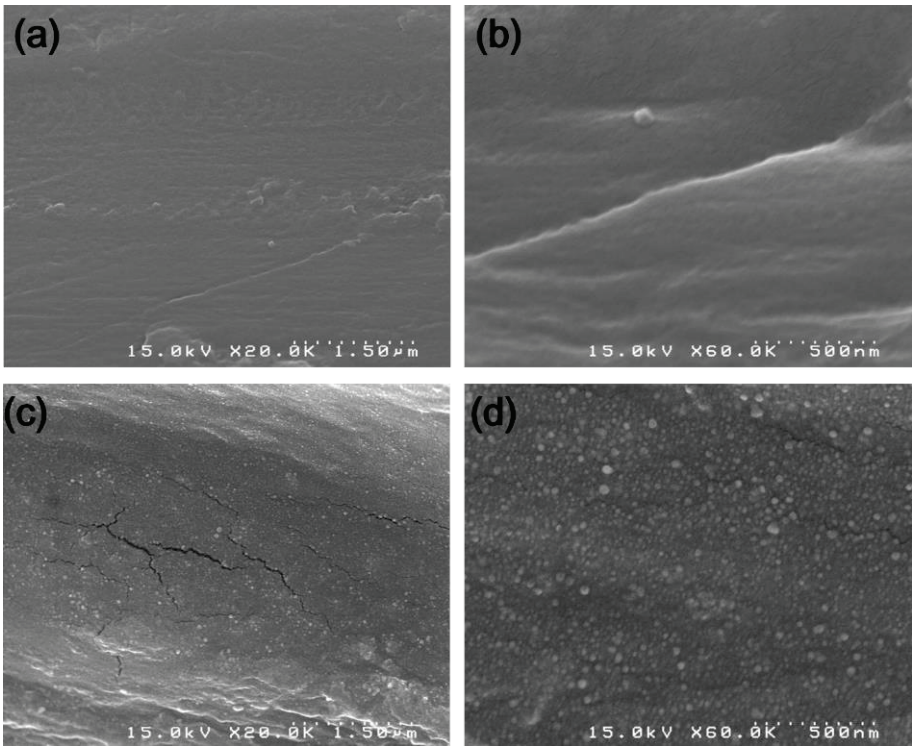

Figure 2.9 SEM images of the ((a) × 20,000; (b) × 60,000) blank SFs and the ((c) × 20,000; (d) × 60,000) HBPAA/AgNP-coated SFs (20 mg/g).

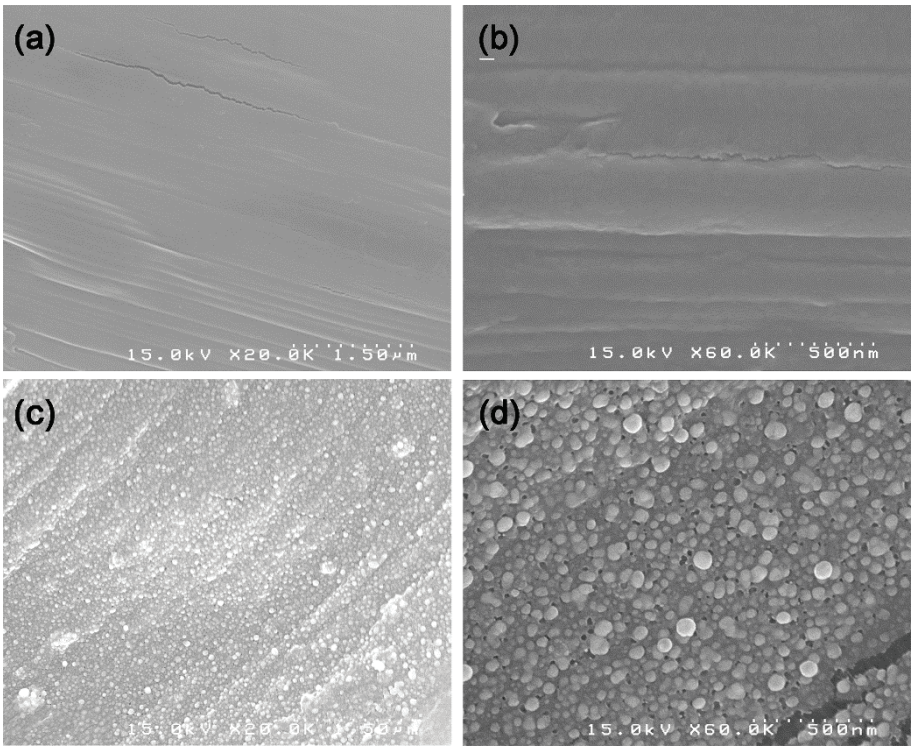

Figure 2.10 SEM images of the ((a) × 20,000; (b) × 60,000) blank CAFs and the ((c) × 20,000; (d) × 60,000) HBPAA/AgNP-coated CAFs (30 mg/g).

2.3.4 XPS analysis of the HBPAA/AgNP-coated CFs, SFs, and CAFs

XPS analysis was performed to identify the presence of AgNPs on the surface of CFs, SFs, and CAFs. As shown in Figure 2.11(a), 2.12(a), and 2.13(a), all recorded XPS survey spectra showed signals for C, O, and Ag species. The presence of C and O signals are expected because they are the main constituent elements of CFs, SFs, and CAFs. Besides of above elements, for CAFs, a signal of Ca2s was also detected, which was in line with the chemical structure of CAFs. Two peaks at around 368 and 374 eV observed in all spectra were responsible for Ag3d, indicating AgNPs were successfully bound to the fiber surface.

To identify the valence state of HBPAA/AgNPs on the fiber surface, high-resolution scans were also conducted on the Ag3d XPS for HBPAA/AgNP-coated CFs, SFs, and CAFs. As shown in Figure 2.11(b), 2.12(b), and 2.13(b), all HBPAA/AgNPs coated on CFs, SFs, and CAFs have a single predominant valence state. The binding energy corresponding to the $Ag3d_{5/2}$ peaks for CFs, SFs, and CAFs were around 368.2 eV, indicative of metallic Ag [21]. Similarly, their binding energy of the $Ag3d_{3/2}$ peaks were around 374.2 eV. As a result, the difference between the binding energy of $Ag3d_{5/2}$ and $3d_{3/2}$ peaks for all biological fibers were approximately 6.0 eV, also suggesting the characteristic of metallic Ag3d states [21]. Our studies indicated that HBPAA/AgNPs were able to maintain their metallic state, indicating HBPAA have a good protection effect.

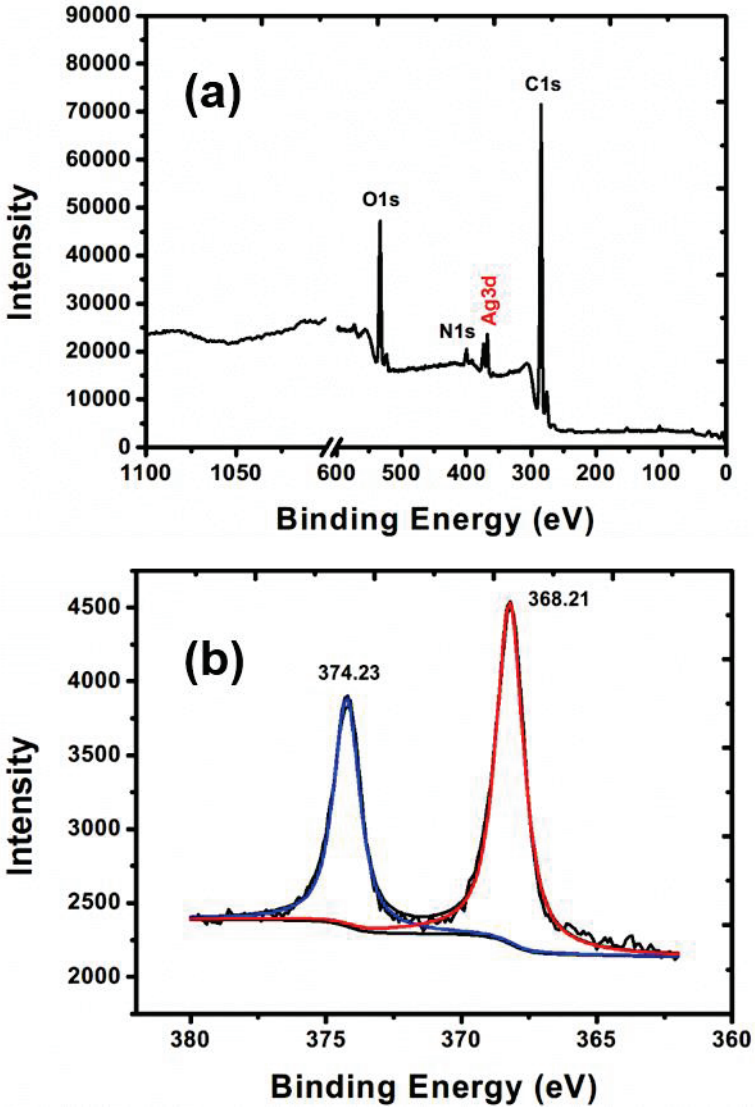

Figure 2.11 (a) Broad scan XPS spectrum of HBPAA/AgNP-coated CFs and (b) the high-resolution Ag3d XPS spectrum of HBPAA/AgNP-coated CFs (8 mg/g).

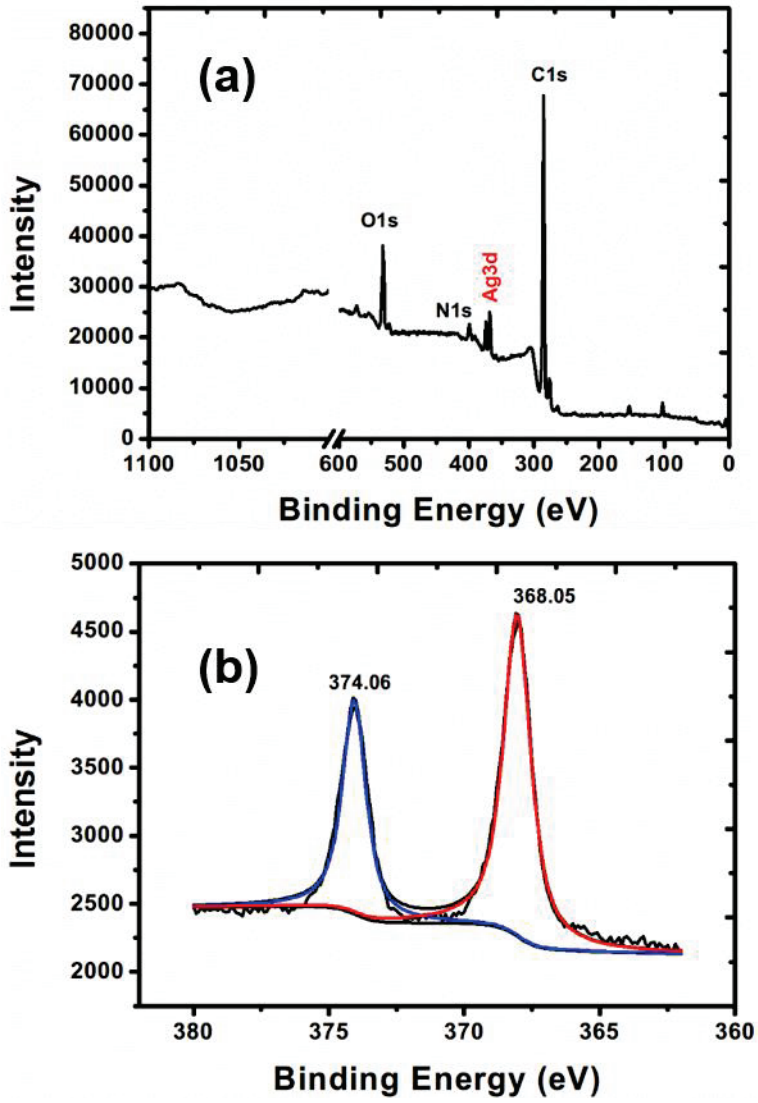

Figure 2.12 (a) Broad scan XPS spectrum of HBPAA/AgNP-coated SFs and (b) the high-resolution Ag3d XPS spectrum of HBPAA/AgNP-coated SFs (20 mg/g).

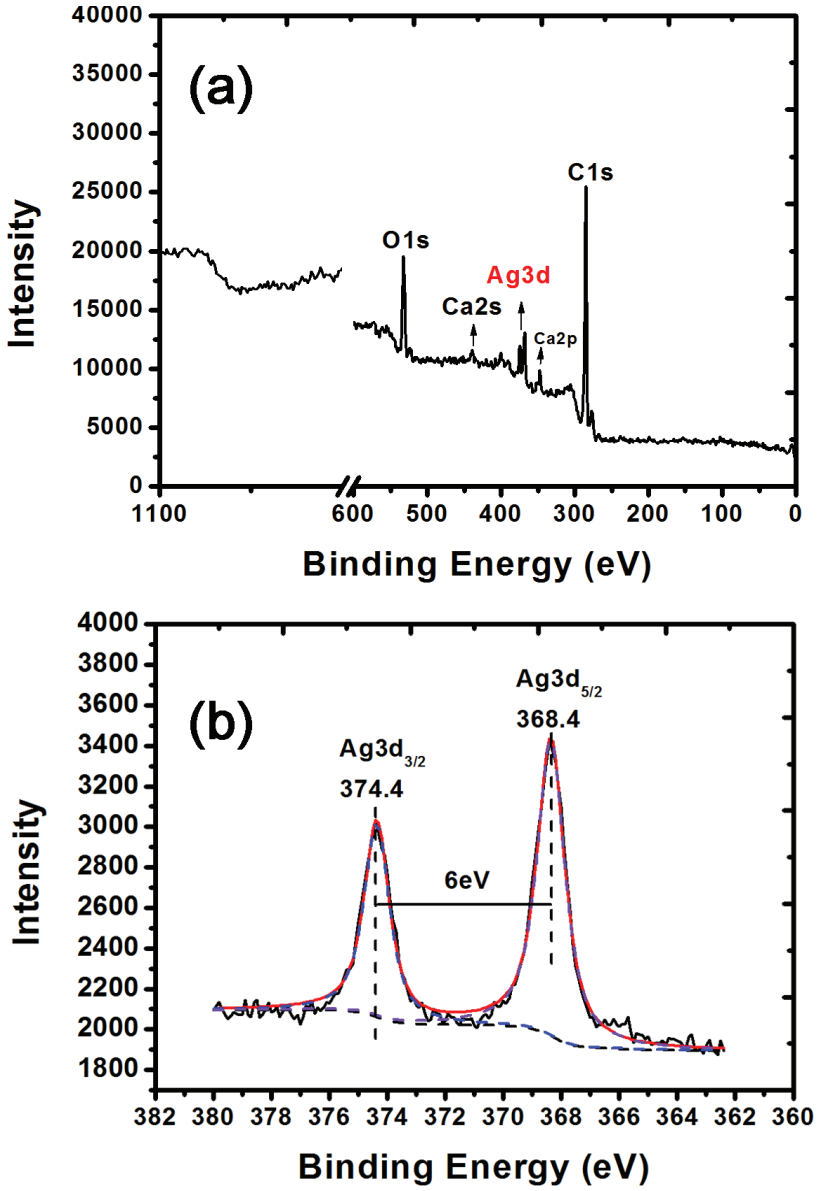

Figure 2.13 (a) Broad scan XPS spectrum of HBPAA/AgNP-coated CAFs and (b) the high-resolution Ag3d XPS spectrum of HBPAA/AgNP-coated CAFs (30 mg/g).

2.3.5 Antibacterial activity of HBPAA/AgNP-coated CFs, SFs, and CAFs

The antibacterial activity of CFs, SFs, and CAFs was qualitatively evaluated using gram-negative *E. coli* and gram-positive *S. aureus* bacteria cells with blank CFs, SFs, and CAFs as the controls, respectively, the results of which are presented in Table 2.1.

In the cases of CFs and SFs, because of their excellent biocompatibility, the increase of surviving cells indicates they were no antibacterial activities against *S. aureus* or *E. coli*. After coated with HBPAA/AgNPs, the antibacterial activities of HBPAA/AgNP-coated CFs and SFs showed good inhibition effects. CFs and SFs showed high antibacterial effects with antibacterial rates over 98 % against *S. aureus* or *E. coli* when Ag content was as low as 0.5 mg/g, indicative of high antibacterial activities of HBPAA/AgNPs. Similarly, CAFs did not show antibacterial activities against *S. aureus* or *E. coli*, indicating they was insufficient to inhibit the bacterial growth. By contrast, HBPAA/AgNP-coated CAFs exhibited excellent antibacterial activities. The bacterial reduction rates of both *S. aureus* and *E. coli* can reach above 99% when the Ag content was over 1 mg/g.

The antimicrobial activities of AgNP-coated CFs, SFs, and CAFs are Ag content-dependent. In the case of CFs, with the increase of HBPAA/AgNPs from 1 to 5 mg/g, the bacterial reduction rates of *S. aureus* increased from 98.3% to 99.99% and *E. coli* from 98.92% to 99.99%. In the case of SFs, HBPAA/AgNPs showed similar antibacterial efficiencies against *S. aureus* and *E. coli*. However, HBPAA/AgNP-coated CAFs exhibited weaker antibacterial activities. When the Ag content of coated CAFs increased from 0.5 mg/g to 5 mg/g, their antibacterial rates increased from 97.31% for *S. aureus* and 98.38% for *E. coli* to 99.92% and 99.63%, respectively, which were much lower than that of CFs and SFs. Nevertheless, the growth of *S. aureus* and *E. coli* could be completely inhibited when Ag content was up to 10 mg/g. The related weak antibacterial activities of HBPAA/AgNP-coated CAFs are because CAFs showed much stronger binding ability for both HBPAA/AgNPs and Ag cation, finally preventing their release from the solid organic surface to aqueous phase.

Based on this experiment, it is concluded that the HBPAA/AgNP-coated CFs, SFs, and CAFs produced using our practical procedure demonstrated dose-dependent antibacterial activities.

The high antibacterial activity of HBPAA/AgNP-coated fibers is attributed to the excellent antibacterial properties of AgNPs. Generally, the antibacterial activity of AgNPs to bacteria can be explained by two mechanisms. One is the oxidative stress generated by reactive oxygen species (ROS), including oxygen superoxide ($\cdot O_2^-$), hydrogen peroxides (H_2O_2), and the hydrogen radical ($\cdot OH$) formed at the surface of the AgNPs. The other is the interaction of silver cations with sulfhydryl groups of vital enzymes and proteins, causing their denaturation [22, 23]. Therefore, assembling AgNPs on biological fibers can provide them with excellent antibacterial properties.

Table 2.1 Antibacterial activity of CAFs

Antibacterial activity					
Sample		*S. aureus*		*E. coli*	
	silver content (mg/g)	Surviving cells (CFU/mL)	Reduction (%)	Surviving cells (CFU/mL)	Reduction (%)
CFs	0	8.46×10^6	-	2.85×10^6	-
SFs	0	1.2×10^7	-	2.17×10^6	-
CAFs	0	2.37×10^6	-	8.70×10^6	-
HBPAA/AgNP-coated CFs	0.5	3.41×10^3	98.3	3.24×10^3	98.92
	1	1.66×10^3	99.17	1.17×10^3	99.61
	1.5	1.24×10^3	99.4	6.65×10^3	99.78

	2	1.82×10^{2}	99.91	1.84×10^{2}	99.94
	5	17	99.99	13	99.99
HBPAA/AgNP-coated SFs	0.5	2.5×10^{3}	98.75	4.71×10^{3}	98.43
	1	8.07×10^{2}	99.6	6.9×10^{3}	99.77
	1.5	1.67×10^{2}	99.92	62	99.98
	2	64	99.97	35	99.99
	5	11	99.99	21	99.99
HBPAA/AgNP-coated CAFs	0.5	2.14×10^{4}	97.31	4.86×10^{3}	98.38
	1	1.44×10^{3}	99.28	2.70×10^{3}	99.1
	1.5	1.28×10^{3}	99.4	1.83×10^{3}	99.39
	2	5.8×10^{3}	99.71	1.29×10^{3}	99.57
	5	1.64×10^{2}	99.92	1.11×10^{3}	99.63
	10	0	100	0	100

2.4 Conclusions

A supramolecular self-assembly strategy for preparation of HBPAA/AgNP-coated CFs, SFs, and CAFs in the AgNP solution was presented in this work. The self-assembly of HBPAA/AgNPs on biological fibers was guided by HBPAA molecules that are capped on the surface of AgNPs. HBPAA/AgNPs were synthesized by reduction of Ag nitrate in aqueous solution using HBPAA as the reducing and capping agent. The as-prepared HBPAA/AgNPs exhibited small size and narrow size distribution. The average size of AgNPs measured by dynamic light scattering (DLS) was around 10.1 nm. Due to its unique quasi-spherical structure and large numbers of amino end groups, HBPAA/AgNPs were endowed with positive charges and high binding affinity towards biological fibers such as CFs, SFs, and CAFs. Our test showed that the assembly ability of AgNPs on CFs, SFs, and CAFs was Ag concentration and temperature-dependent. The maximum Ag content of coated CFs, SFs, and CAFs can reach up to 8.05, 21, and 30 mg/g. Both SEM and XPS analysis showed that the high density of metallic AgNPs uniformly distributed on surfaces of CFs, SFs, and CAFs, indicating the supramolecular self-assembly technology was efficient. Finally, the antibacterial property of coated fibers was measured by the shake-flask method. The HBPAA/AgNP-coated CFs and SFs showed excellent antibacterial activities with antibacterial rates over 99% at Ag content of 1.5 mg/g although HBPAA/AgNP-coated CAFs showed weaker antibacterial activities.

References

[1] Tansil NC, Koh LD, Han M-Y. Functional Silk: Colored and Luminescent. Adv Mater. 2012;24:1388-97.

[2] Lin N, Meng Z, Toh GW, Zhen Y, Diao Y, Xu H, et al. Engineering of Fluorescent Emission of Silk Fibroin Composite Materials by Material Assembly. Small. 2015;11:1205-14.

[3] Drummy LF, Phillips DM, Stone MO, Farmer BL, Naik RR. Thermally Induced α-Helix to β-Sheet Transition in Regenerated Silk Fibers and Films. Biomacromolecules. 2005;6:3328-33.

[4] Correia C, Bhumiratana S, Yan L-P, Oliveira AL, Gimble JM, Rockwood D, et al. Development of silk-based scaffolds for tissue engineering of bone from human adipose-derived stem cells. Acta Biomaterialia. 2012;8:2483-92.

[5] Kim D-H, Viventi J, Amsden JJ, Xiao J, Vigeland L, Kim Y-S, et al. Dissolvable films of silk fibroin for ultrathin conformal bio-integrated electronics. Nat Mater. 2010;9:511-7.

[6] Mou Z-L, Duan L-M, Qi X-N, Zhang Z-Q. Preparation of silk fibroin/collagen/hydroxyapatite composite scaffold by particulate leaching method. Mater Lett. 2013;105:189-91.

[7] Yu D, Kang G, Tian W, Lin L, Wang W. Preparation of conductive silk fabric with antibacterial properties by electroless silver plating. Appl Surf Sci. 2015;357, Part A:1157-62.

[8] Rycenga M, Cobley CM, Zeng J, Li W, Moran CH, Zhang Q, et al. Controlling the synthesis and assembly of silver nanostructures for plasmonic applications. Chemical reviews. 2011;111:3669-712.

[9] Yuan G, Cranston R. Recent Advances in Antimicrobial Treatments of Textiles. Text Res J. 2008;78:60-72.

[10] Dallas P, Sharma VK, Zboril R. Silver polymeric nanocomposites as advanced antimicrobial agents: classification, synthetic paths, applications, and perspectives. Adv Colloid Interface Sci. 2011;166:119-35.

[11] Petkova P, Francesko A, Fernandes MM, Mendoza E, Perelshtein I, Gedanken A, et al. Sonochemical Coating of Textiles with Hybrid ZnO/Chitosan Antimicrobial Nanoparticles. Acs Appl Mater Interfaces. 2014;6:1164-72.

[12] Grzelczak M, Vermant J, Furst EM, Liz-Marzán LM. Directed Self-Assembly of Nanoparticles. ACS nano. 2010;4:3591-605.

[13] Kuzyk A, Schreiber R, Fan Z, Pardatscher G, Roller E-M, Hogele A, et al. DNA-based self-assembly of chiral plasmonic nanostructures with tailored optical response. Nature. 2012;483:311-4.

[14] Shenhar R, Norsten TB, Rotello VM. Polymer-Mediated Nanoparticle Assembly: Structural Control and Applications. Adv Mater. 2005;17:657-69.

[15] Zhou L, Gao C, Hu X, Xu W. General Avenue to Multifunctional Aqueous Nanocrystals Stabilized by Hyperbranched Polyglycerol. Chem Mater. 2011;23:1461-70.

[16] Caminade A-M, Yan D, Smith DK. Dendrimers and hyperbranched polymers. Chem Soc Rev. 2015;44:3870-3.

[17] Wang D, Zhao T, Zhu X, Yan D, Wang W. Bioapplications of hyperbranched polymers. Chem Soc Rev. 2015;44:4023-71.

[18] Zhang F, Chen Y, Lin H, Lu Y. Synthesis of an amino-terminated hyperbranched polymer and its application in reactive dyeing on cotton as a salt-free dyeing auxiliary. Color Technol. 2007;123:351-7.

[19] Zhang D, Zhang G, Liao Y, Wang C, Chen Y, Lin H, et al. Synthesis of ZnO nanoparticles in aqueous solution by hyperbranched polymer. Mater Lett. 2013;102–103:98-101.

[20] Rycenga M, Cobley CM, Zeng J, Li W, Moran CH, Zhang Q, et al. Controlling the Synthesis and Assembly of Silver Nanostructures for Plasmonic Applications. Chemical reviews. 2011;111:3669-712.

[21] Zanna S, Saulou C, Mercier-Bonin M, Despax B, Raynaud P, Seyeux A, et al. Ageing of plasma-mediated coatings with embedded silver nanoparticles on stainless steel: An XPS and ToF-SIMS investigation. Applied Surface Science. 2010;256:6499-505.

[22] Levard C, Hotze EM, Lowry GV, Brown GE, Jr. Environmental transformations of silver nanoparticles: impact on stability and toxicity. Environmental science & technology. 2012;46:6900-14.

[23] Kim JS, Kuk E, Yu KN, Kim J-H, Park SJ, Lee HJ, et al. Antimicrobial effects of silver nanoparticles. Nanomedicine: Nanotechnology, Biology and Medicine.

2007;3:95-101.

Chapter 3

Preparation and controlled coating of HBPAE-functionalised silver nanoparticles on silk fibers through HBPAA-guided self-assembly

Chapter 3 Preparation and controlled coating of HBPAE-functionalised silver nanoparticles on silk fibers through HBPAA-guided self-assembly

3.1 Introduction

In Chapter 2, we demonstrated the excellent binding ability of HBPAA-functionalised silver nanoparticles (HBPAA/AgNPs) towards silk fibers (SFs) and cotton fibers (CFs), suggesting the strong combining capacity between HBPAA and hydroxyl- and/or carboxyl-dominated biomolecules. We believe that its remarkable physicochemical properties including three-dimensional (3D) cavity structure, amphiphilic nature, high density of amino end groups, and positive surface charges should be responsible for the good compatibility between HBPAA/AgNPs and cotton cellulose and silk fibroin. Inspired by this, HBPAA possesses a possibility of serving as trapping molecules for various molecule-capped AgNPs, independently. Theoretically, with coating HBPAA on the surface of biological fibers, HBPAA-modified bio-substrates are capable of trapping hydrogen acceptor and/or anionic molecule-functionalised inorganic NPs. To verify our concept, we further designed and synthesized hydroxyl-terminated hyperbranched poly(amine-ester)s-functionalised silver nanoparticles (HBPAE/AgNPs) as a special model to verify the strong supramolecular interactions between the hydrogen-donor and hydrogen-acceptor polymers. HBPAE is designed to possess the same physicochemical structure as HBPAA except its functional end groups. Particularly, HBPAA owns high density of amino end groups whereas HBPAE has rich hydroxyl end groups. This interesting

differences impart them with diverse chemical properties, i.e., one is a hydrogen donor and the other is hydrogen acceptor, this endowing them with an ability of mutual recognition and combination. Together with their opposite surface charges, their supramolecular interactions may overwhelm electrostatic repulsion among NPs and their kinetic energy, probably achieving high adsorption capacity for HBPAE/AgNPs at room temperature. In the experiment, we chose SFs as the bio-substrate because of their clean, smooth, and compact surface, which can reduce the interference from impurities on fiber surface.

In summary, we aim to develop an efficient and environment-friendly assembly approach to fabricate homogenously distributed AgNPs coated SFs through suparmolecular self-assembly technology. To gain a powerful driving force, SFs and AgNPs were modified by HBPAA and HBPAE, respectively. HBPAA is a three-dimensional spherical polymer with a unique structure consisting of a hydrophobic core and a hydrophilic shell possessing dense amino end groups, capable of self-assembly onto the surface of SFs by supramolecular interactions between HBPAA and silk macromolecules. Similarly, HBPAE is a 3D spherical polymer with numerous hydroxyl end groups. This interesting structural characteristic provides application possibilities not only as a capping agents for NPs, but also as a guiding molecule to HBPAA due to molecular recognition between HBPAA and HBPAE. Duo to the strong electrostatic and hydrogen bonding interactions, high concentration of HBPAE/AgNPs can assembled completely onto HBPAA-modified SFs (HBPAA/SFs) in a very short time at room temperature. Thus, the developed self-assembly technology may provide simple, efficient, and environment-friendly coating strategy for precise control of Ag content of coated fibers, which is significant for quality control of

antibacterial textiles.

3.2 Experimental

3.2.1 Materials

SFs were obtained from the Ueda Fujimoto Co., Ltd. (Japan). HBPAA was synthesized as described in chapter 2. 1,1,1-Tris(hydroxymethyl) propane (TMP), 2,2′-iminodiethanol, p-toluenesulfonic acid (p-TSA), methyl acrylate, acetic anhydride,methanol, silver nitrate ($AgNO_3$), sodium borohydride ($NaBH_4$), potassium hydroxide, and nitric acid were purchased from Wako Pure Chemical Industries, Ltd. (Japan). *Staphylococcus aureus* (ATCC 6538) and *Escherichia coli* (ATCC 25922) were obtained from College of Life Science, Soochow University (China). Nutrient broth and nutrient agar were purchased from Scas Ecoscience Technology Inc. (China).

3.2.2 Synthesis of HBPAE

HBPAE was synthesized as follows [1]: methyl acrylate (0.24 mol, 18.66 g), 2,2'-iminodiethanol (0.24 mol, 25.23 g), and methanol (24 mL) were mixed in a three necked glass reactor equipped with a gas inlet pipe for N_2 addition. The mixture was allowed to react at 35 °C for 4 h under a N_2 atmosphere. The oily AB_2 type monomer was synthesized and then the mixture was transferred to an eggplant-shaped flask for an automatic rotary vacuum evaporator. After removing the methanol under low pressure, TMP (10 mmol, 0.134 g) and *p*-TSA (0.9 g) were added into the flask. The flask was then placed in an oil bath previously heated to 110 °C. After 10 h of reaction under a N_2 atmosphere, a vacuum was applied for 2 h before the reaction mixture was removed from the flask. This solution was dialyzed against distilled water using Slide-a-Lyzer dialysis cassettes (Pierce, molecular weight cut-off 3,500) for 1 day to remove

impurities. The dry polymer was obtained by freeze drying.

3.2.3 Synthesis of HBPAE/AgNPs

HBPAE/AgNPs were synthesized by adding 10 mL of 7.8 g/L $AgNO_3$ solution into 40 mL of 20 g/L HBPAE aqueous solution using a well-described procedure. This was followed by adding 1 mL of 1 g/L $NaBH_4$ to the above mixture. The colloidal solution was stored in a brown colored bottle at 5 °C. The concentrations for the experiments were prepared by dilution of the solution using deionized water.

3.2.4 Sequential assembly of HBPAA and HBPAE/AgNPs on SFs

The process assembly for SFs were similar. Specifically, two grams of fiber samples was first immersed into a beaker containing 100 mL of 10 g/L HBPAA solution at 98 °C. After 1 h of contact time, samples were removed from the solution and rinsed thoroughly with water to remove unattached HBPAA. The as-prepared HBPAA-coated SFs were then dipped in 100 mL of colloidal solution of HBPAE/AgNPs (10–100 mg/L, pH~7.8) for 10 min. The resultant samples were subsequently dried at 90 °C for 30 min. As a control, HBPAE/HBPAA dual-coated SFs (HBPAE/HBPAA/SFs) were prepared by impregnating HBPAA/SFs in 100 mL of HBPAE solution following the same procedure as above.

3.2.5 Characterization of HBPAE/AgNPs

The morphology and crystal structure of HBPAE/AgNPs were investigated using a JEOL-2100F transmission electron microscope (TEM) (JEOL, Japan) operating at an accelerating voltage of 120 kV. The Zeta potential of AgNPs as a function of pH in the aqueous solution was evaluated by dynamic light scattering using the Zetasizer Nano

ZS system (Malvern, UK). Ultraviolet–visible (UV–Vis) spectra were obtained using UV–Vis adsorption spectrophotometry (Shimadzu, Japan). For Fourier-transform infrared (FTIR) measurement, the AgNPs solution was poured into acetone and the resulting precipitates were dried for characterization. The FTIR spectra were performed on a Shimadzu FTIR, IR Prestige-21 infrared spectrometer (Shimadzu).

3.2.6 Antibacterial activity evaluation of HBPAE/AgNPs

HBPAE/AgNPs in a colloidal solution was first tested for antimicrobial activity by the agar well-diffusion method. The agar plate was prepared by pouring the solid culture onto sterile circular plates and allowing it to solidify. One milliliter of microbial culture (1×10^6–5×10^6 cfu/mL) was uniformly distributed on each plate. Three millimeter oxford cups were placed on the plates and filled with water, HBPAE solution, and HBPAE/AgNPs colloidal solution (10 mg/L). The plates were placed in an incubator for 24 h at 37 °C. The diameter of the zone of inhibition was then measured and recorded. The antimicrobial activity of colloidal solutions of AgNPs was further tested by studying the growth kinetics of *E. coli* and *S. aureus* by measuring the optical density of the microbial culture at 546 nm after 0–24 h of incubation using a UV–Vis spectrophotometer. In addition, the effect of the concentration of AgNPs on antimicrobial activity was tested by measuring the optical density of the microbial culture at 546 nm after 4 h of incubation [2].

3.2.7 Characterization of HBPAE/AgNP-coated HBPAA/SFs

The morphology and size of SFs were observed using a field-emission scanning electron microscope (FESEM) (S4800; Hitachi, Japan). The surface chemical structure of the fiber was characterized using an X-ray diffractometer (AXIS Ultra DLD; Krotos,

Japan). The crystal structures were examined by an X-ray diffractometer (XRD) (D8 ADVANCE, Bruker, Germany). The Ag content was measured in acidified solutions by a Vista MPX inductively coupled plasma atomic emission spectrometer (Varian, USA).

3.2.8 Antibacterial activity evaluation of HBPAE/AgNP-coated HBPAA/SFs

The antimicrobial activity of composite fibers was assessed according to the standard shake-flask method according to GB/T 20944.3-2008 (China) [3]. The antimicrobial activity was investigated against two types of bacteria (*E. coli* and *S. aureus*). A sample of treated fibers (0.75 g) was dipped into a flask containing 0.3 mM phosphate-buffered saline (70 mL, PBS, monopotassium phosphate, pH~7.2) culture solution with cell concentration of 1×10^5–4×10^5 colony-forming units (cfu)/mL. The flask was then shaken at 150 rpm on a rotary shaker at 24 °C for 18 h. Samples of 1 mL were taken at a specified time, diluted tenfold in saline, and then transferred onto nutrient agar plates (Difco). All plates were incubated at 37 °C for 24 h, and the colonies formed were counted. The percentage reduction (*cfu*, %) was determined as follows:

$$cfu(\%) = \frac{\mathrm{C-A}}{\mathrm{C}} \times 100, \quad (1)$$

where C and A are the bacterial colonies of blank fibers and treated fibers, respectively. All experiments were performed in triplicate with three substrates and the mean values were calculated.

3.3 Results and discussion

3.3.1 Synthesis of HBPAE/AgNPs

HBPAE was synthesized by a one-step procedure by alcoholysis at 110 °C using TMP and N,N-diethylol-3-amine methylpropionate (AB_2 monomer) with *p*-TSA as the esterification catalyst [4], as shown in Scheme 3.1. A major requirement for the synthesis of polymer-functionalised AgNPs is that the capping polymer should be chemically compatible to metallic Ag. HBPAE consists of ester backbone linkages, interior tertiary amino groups, and numerous hydroxyl end groups on the outer shell, possessing high binding affinity to metallic AgNPs. Furthermore, owing to their amphiphilic feature, HBPAE are capable of forming micelles in aqueous solution, where three-dimensional template HBPAE served as a spatially restricted reaction vessel.

UV–vis spectroscopy is an effective structural characterization technique for AgNPs. The position, magnitude, and shape of the absorption peak are strongly dependent on particle shape and size. As shown in Figure 3.1(a), compared with $AgNO_3$/HBPAE mixture solution, the absorption spectrum of HBPAE/AgNPs solution showed a strong absorption band with a maximum of 416.5 nm, which could not only verify the formation of metallic AgNPs in the solution but also their spherical features. The sharp band of AgNPs indicates the presence of well-separated AgNPs with a narrow size distribution. The inset of Figure 3.1(a) is a typical photograph of a colloidal solution of HBPAE/AgNPs that formed in the reaction. The wine-red color of the solution derived from localized surface plasmon resonance (LSPR) effect of AgNPs was clearly observed, also suggesting the formation of AgNPs. Figure 3.1(c) is a typical low-magnification TEM of HBPAE/AgNPs. It shows that the monodispersed AgNPs

with nearly spherical shapes possessed an average diameter of 11.8 nm. The corresponding high-resolution TEM image in Figure 3.1(d) shows the lattice spacing with a d spacing of 0.24 nm, in good agreement with the lattice spacing of (111) planes of face-centered-cubic Ag (JCPDS No. 04-0783). The obvious (111) crystal plane and regular shape indicate high crystalline quality. The high crystallinity is also supported by the SAED pattern as shown in the inset of Figure 3.1(c), which showed a strong diffraction ring composed of several individual spots indexed as (111), (220), and (311). The advantage of HBPAE/AgNPs is their abundant free hydroxyl groups, imparting the NPs with ultra-high binding affinity towards cationic hydrogen-bond donor molecules, making HBPAA-templated self-assembly possible.

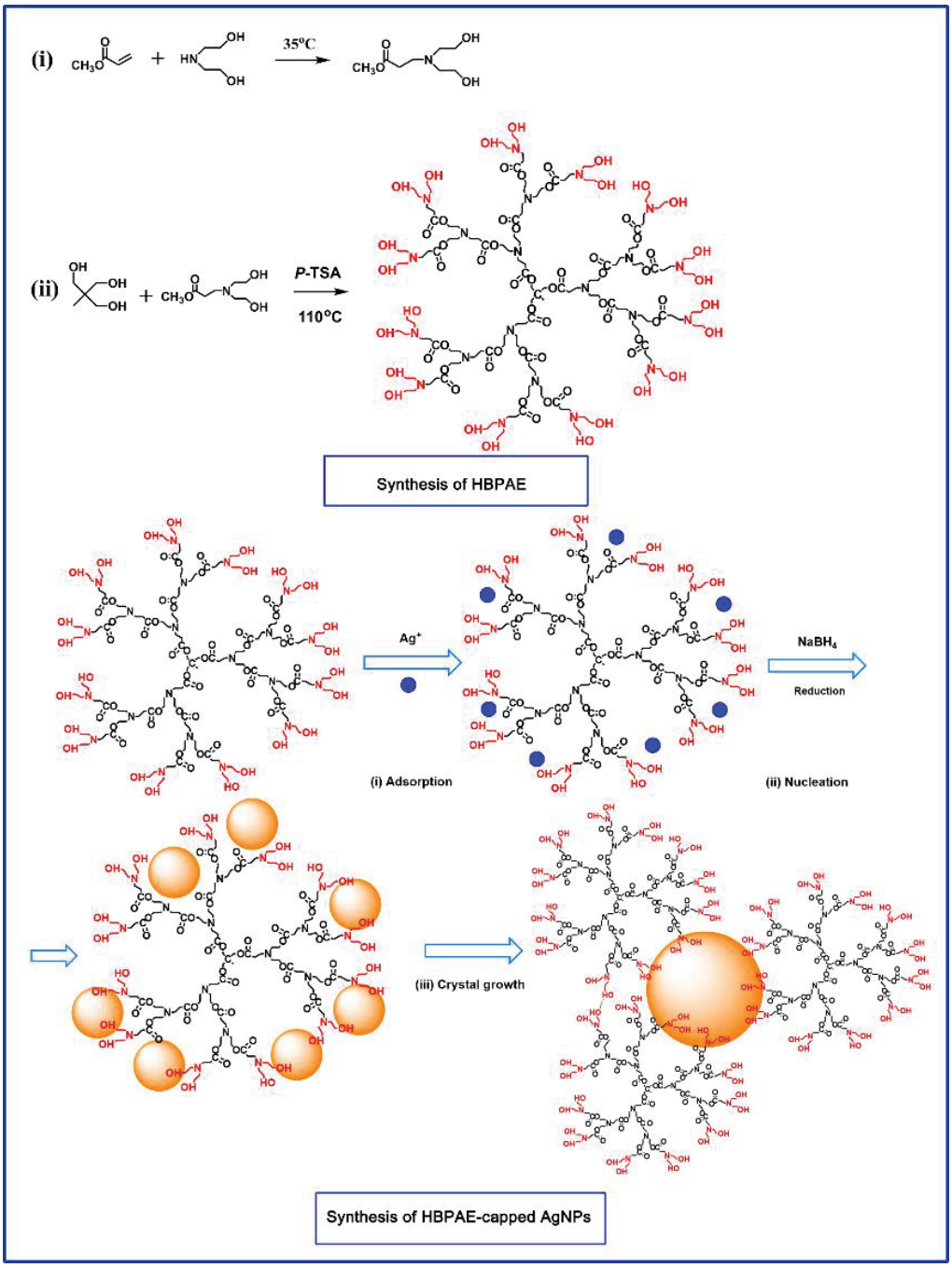

Scheme 3.1 Synthesis of HBPAE and HBPAE/AgNPs

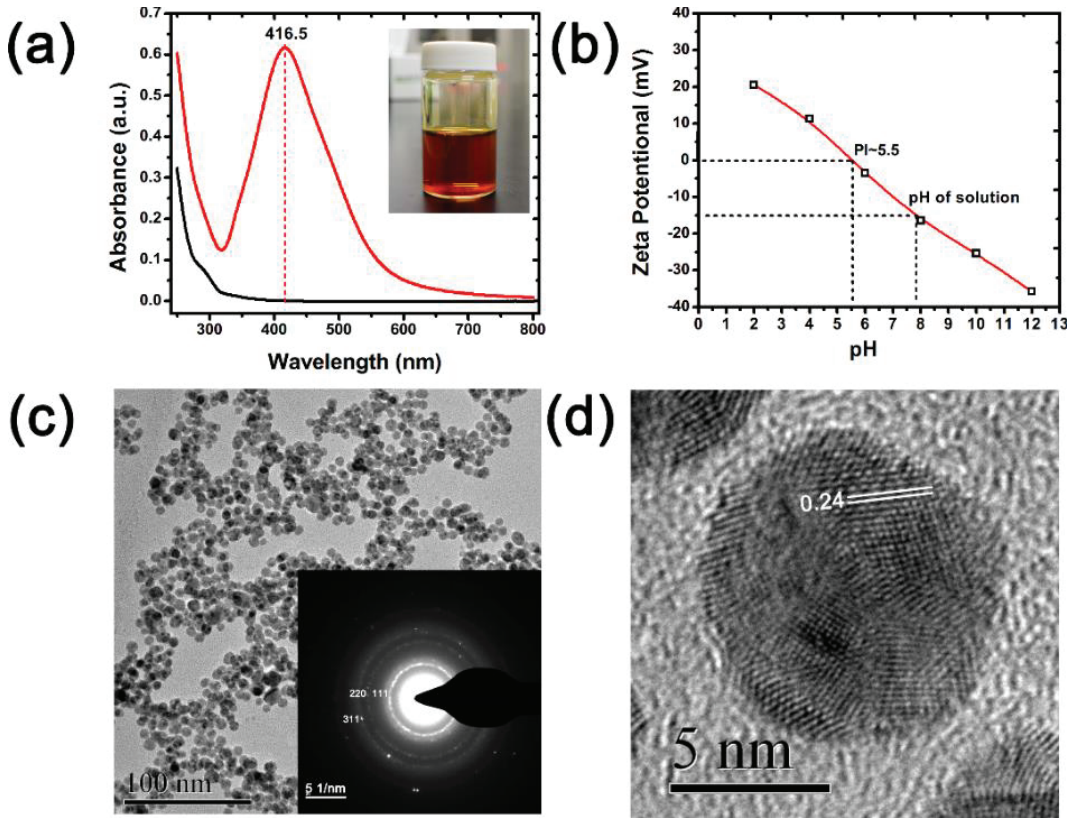

Figure 3.1 (a) UV-vis adsorption spectra of the (black) mixture solution of $AgNO_3$/HBPAE and (red) colloidal solution of HBPAE/AgNPs, (b) Zeta potential of HBPAE/AgNPs as a function of pH, and (c) TEM and (d) high resolution TEM images of HBPAE/AgNPs. The inset of figure 1a displays the typical photograph of as-prepared HBPAE/AgNPs solution. The inset of figure 1c shows the SAED pattern of HBPAE/AgNPs.

As shown in Figure 3.1(b), the zeta potential of hydroxyl-functionalised AgNPs was measured as approximately −15 mV. It is believed that the chemical interactions between the hydroxyl groups and Ag was responsible for the attachment of HBPAE on the surface of AgNPs, which was confirmed by the FTIR spectra. As shown in Figure 3.2, the characteristic absorption peaks of the C=O stretch (around 1729 cm^{-1}), C–N stretch (around 1608 cm^{-1}), and C–O–C antisymmetric stretch (around 1184 and 1028

cm^{-1}) were present both in the HBPAE and HBPAE/AgNPs, indicating the presence of HBPAE on the surface of hybrid NPs. Conversely, HBPAE also showed characteristic O–H stretching vibration and in-plane bending bands centered at 3331 and 1361 cm^{-1}. However, there are several differences for HBPAE capped on the Ag surface. The absorption peak of the O–H stretching vibration was obviously broadened and greatly shifted towards a lower frequency for HBPAE/AgNPs, which can be attributed to the interactions between the OH groups of the HBPAE and Ag. Furthermore, the O–H in-plane bending band greatly strengthened, probably associating with the enhanced polarization of O–H via OH–Ag interactions. The weakened C=O stretching vibration adsorption and blue shifted C–N stretch vibration band suggest the interior amide groups of HBPAE may also be responsible for the combination.

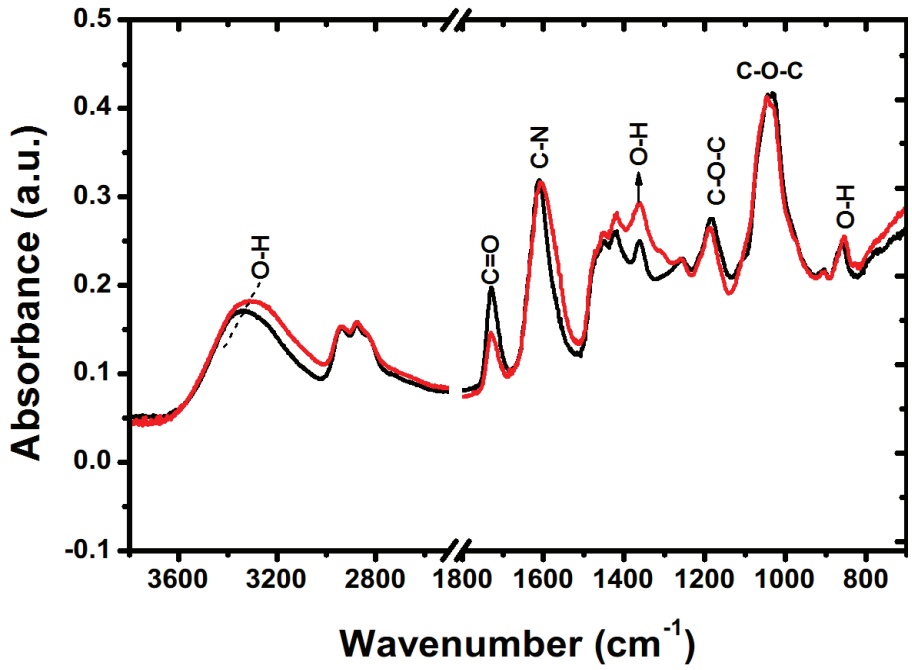

Figure 3.2 FTIR spectra of (black) pure HBPAE and (red) HBPAE/AgNPs.

3.3.2 Antibacterial activity of HBPAE/AgNPs

To evaluate the antibacterial activity of HBPAE/AgNPs, the inhibition zone method was first carried out by using deionized water and HBPAE as the control. *E. coli* and *S. aureus* were selected as a demonstrate strain here. Figure 3.3(a) reveals the images of the inhibition zone of deionized water, HBPAE, and HBPAE/AgNPs. No inhibition zone around the oxford cups of the deionized water and HBPAE were found, indicating that HBPAE has no antibacterial effects. On the contrary, HBPAE/AgNPs on the bacteria inoculated surfaces killed all the bacteria around them, and a distinct inhibition zone was clearly visible surrounding the samples [Figure 3.3(a)]. The observed zone of inhibition is a result of the release of active biocidal species Ag ions from the HBPAE/AgNPs into the surrounding aqueous medium. This also demonstrates that their good antibacterial activities against *E. coli* and *S. aureus* derives from AgNPs. Notably, the antimicrobial activity of HBPAE/AgNPs was highly dependent on the concentration of the AgNPs. As shown in Figure 3.3(b), by increasing the concentration of HBPAE/AgNPs from 0.5 to 3 mg/L, the antimicrobial activity was significantly improved. No significant increase in antimicrobial activity was observed beyond 4 mg/L, which seems to be the minimum concentration that should be used. Figure 3.3(c) shows the growth kinetics of *E. coli* and *S. aureus* in the presence of HBPAE/AgNPs. Compared with the pristine sample, the growth of both *E. coli* and *S. aureus* was greatly inhibited indicating the strong antibacterial activity of HBPAE/AgNPs. In addition, the absorption of two types of bacteria tended to be gradually decreased with the increase of contact time between HBPAE/AgNPs and bacteria. This implies that HBPAE/AgNPs have antibacterial effects resulting not only in the inhibition of bacterial growth but also in killing bacteria. AgNPs exhibit good antimicrobial activity owing to their strong binding to the electron-donating groups in the bacterial cells. Once Ag ions are released

into the pathogenic environment, they could attach to the surface of the bacterial cells and even penetrate into them, resulting in the antimicrobial activity [5].

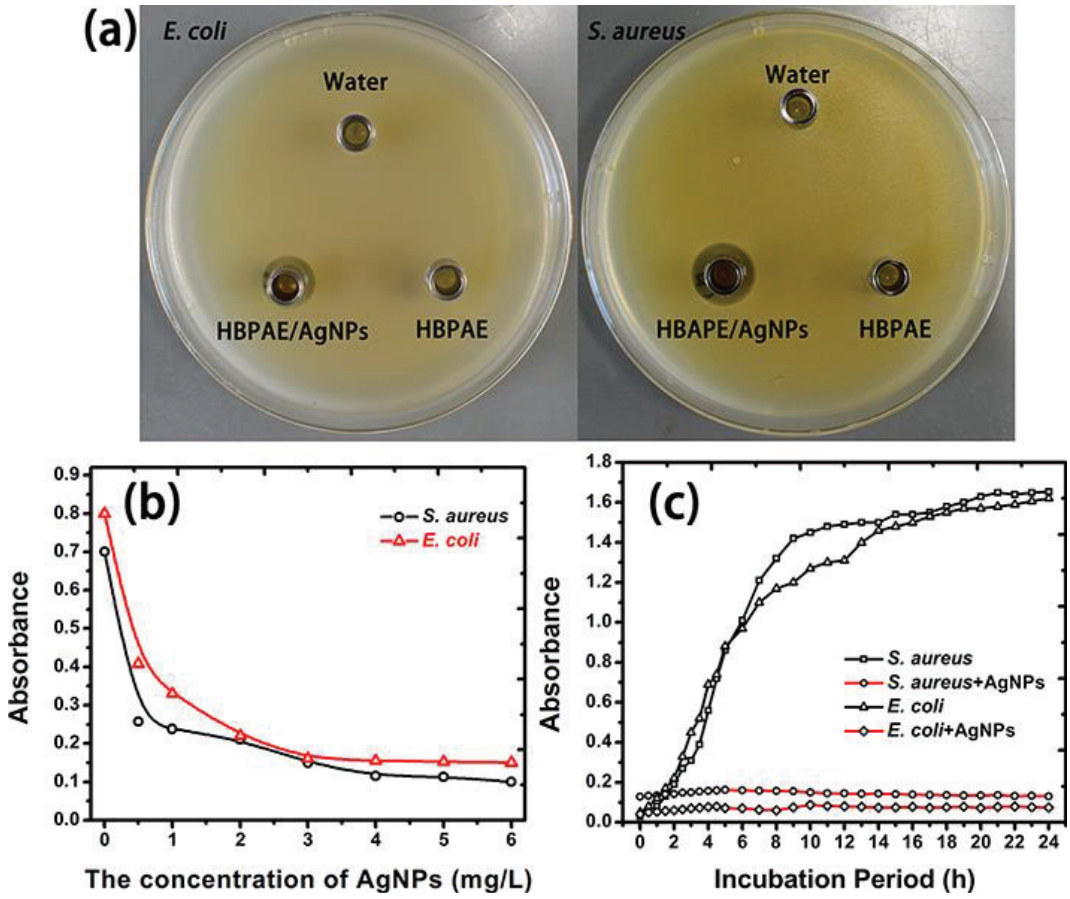

Figure 3.3 (a) The inhibition zones of deionized water, HBPAE, and HBPAE/AgNPs against *E. coli* and *S. aureus* (the concentration of AgNPs: 10 mg/L), (b) the effect of concentration on antimicrobial activity of HBPAE/AgNPs against *E. coli* and *S. aureus*, and (c) the growth kinetics of *E. coli* and *S. aureus* in the presence and absence of HBPAE/AgNPs (4 mg/L).

3.3.3 Assembly of HBPAE/AgNPs onto HBPAA/SFs

The HBPAE/AgNP-coated HBPAA/SFs were prepared by sequential impregnation of SFs in a colloidal solution of HBPAA and HBPAE/AgNPs (pH=7.8). As shown in

Scheme 3.2, prior to AgNP coating, to improve the binding ability towards HBAPE/AgNPs, SFs were first modified with HBPAA by impregnation in HBPAA solution at 98 °C for 1 h. The surface modification of HBPAA introduced positive charges and abundant amino groups onto the SF surface.

The attachment of HBPAA was confirmed by FTIR. As shown in Figure 3.4, the FTIR spectra of the SFs and HBPAA/SFs provided the same pattern. For pure silk, the characteristic IR bands of amide I and amide II were observed in the ranges of 1700–1550 cm^{-1} and 1550–1450 cm^{-1}, respectively. The bands of HBPAA/SFs showed almost the same features. Because amino I and amino II are sensitive to secondary structures such as α-helices and *β*-sheets, this indicates that there were no significant conformational transformations during the self-assembly process. However, some slight differences in the bands of the CH_2 stretching vibration and amino III were observed. The weak absorption peaks of the CH_2 asymmetric and symmetric stretching vibration at 2924 and 2850 cm^{-1} were enhanced greatly, obviously owing to the enhancement effect of the strong adsorption of the CH_2 asymmetric and symmetric stretching vibration in HBPAA. Furthermore, the amino III region at approximately 1260 cm^{-1} was also strengthened, which could be attributed to the superposition of amino III from HBPAA. Furthermore, it is noticed that no new absorption peaks appeared in HBPAA/SFs, suggesting no chemical reaction occurred during HBPAA/SFs formation. In summary, it is concluded that HBPAA has been anchored onto the silk and does not change the chemical structure of the silk fibroin molecule.

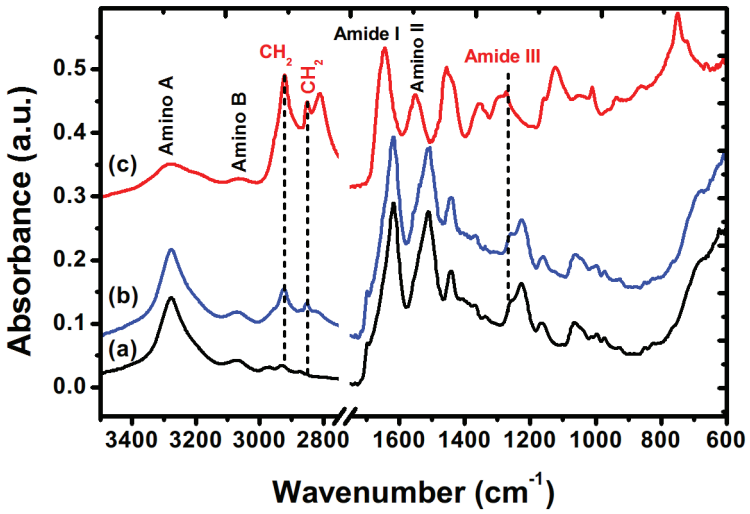

Figure 3.4 FTIR spectra of (a) pure SFs, (b) HBPAA/SFs, and (c) HBPAA.

To introduce the AgNP coating, HBPAA-coated SFs were immersed in the colloidal solution of HBPAE/AgNPs (pH=7.8) at room temperature for 10 min as shown in Scheme 3.2. They were subsequently rinsed for 1 min in deionized water and dried in an oven. Owing to strong electrostatic and hydrogen-bonding interactions, HBPAE/AgNPs could self-assemble onto HBPAA-coated SFs from their colloidal solution in a very short time.

The assembly process of AgNPs on the SF surface can be followed by UV–Vis. As shown in Figure 3.5(a), the UV–Vis absorption spectrum of HBPAE/AgNPs had a broad UV absorption band in the UV–Vis region, and had a characteristic peak of AgNPs at 416.5 nm. After impregnation for 10 min, this characteristic peak almost disappeared, indicative of complete adsorption of AgNPs on the surface of HBPAA/SFs [6]. Furthermore, the phenomenon of the transfer of HBPAE/AgNPs from the liquid phase to the organic surface of HBPAA/SFs can be observed directly. Figures 3.5(b) shows the typical photographs of color transformation from the AgNPs solution to HBPAA/SFs during the assembly procedure. Specifically, the characteristic yellow color of the

AgNPs faded gradually in the solution during the self-assembly process and finally the solution was colorless and transparent. In contrast, the color of HBPAA/SFs changed from white to bright yellow, further verifying that AgNPs in the colloidal solution were successfully assembled onto the surfaces of HBPAA/SFs.

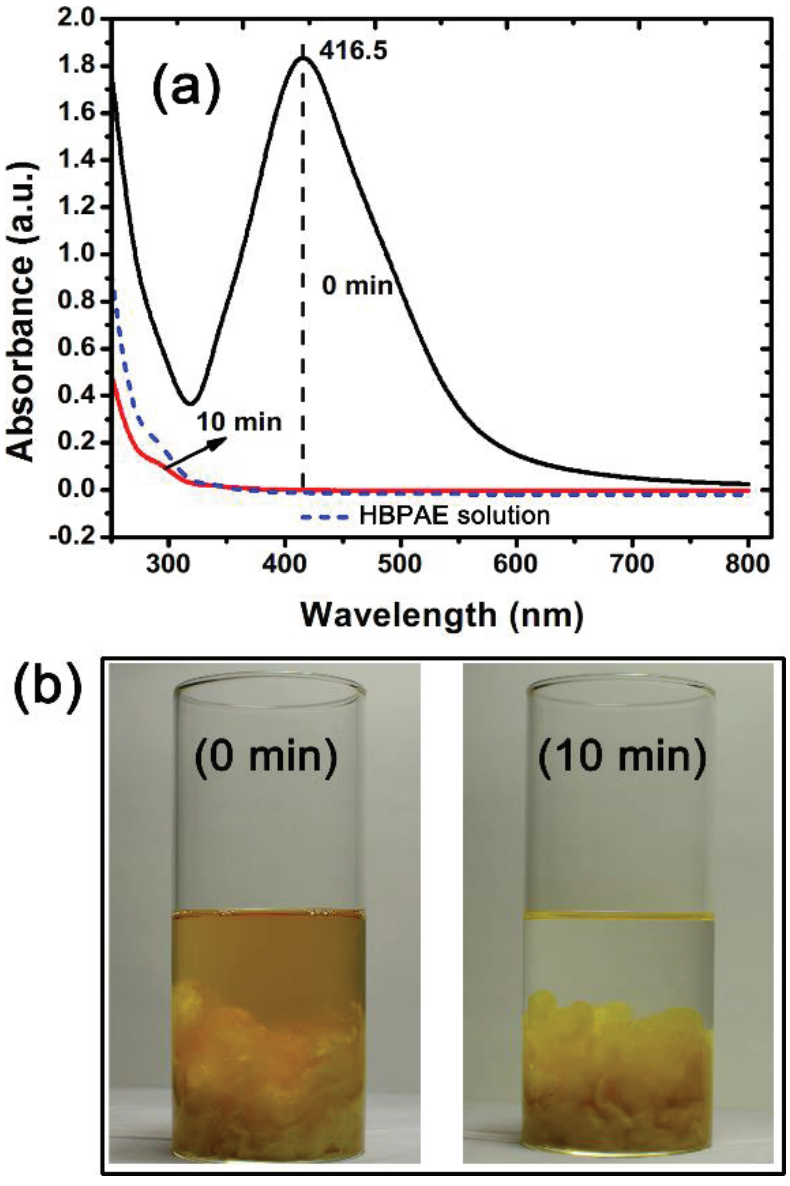

Figure 3.5 (a) UV–Vis adsorption spectra of a solution of HBPAE/AgNPs (black) before and (red) after the assembly process; the blue line represents the HBPAE solution without AgNPs. (b) Photographs of HBAPE/AgNPs solution and HBPAA/SFs

before and after the assembly process. The concentration of AgNPs used in the above experiments was 30 mg/L.

Scheme 3.2 presents a schematic of the self-assembly of HBPAE/AgNP-coated HBPAA/SFs through intermolecular-induced self-assembly between HBPAA, silk macromolecules, and HBPAE. Silk fibroin fiber is composed of β-sheet crystals with strong hydrogen bonding and an amorphous non-crystalline region with varying degrees of hydrogen bonding. The crystalline region of silk fibroin is mainly composed of glycine residues alternating with alanine and serine, whereas the sequence in the amorphous region contains a tyrosine-rich domain. The unconjugated tyrosine residues and amide residues along the protein backbone in the amorphous region are capable of forming intermolecular hydrogen-bonding interactions with hydrogen-donor or acceptor molecules, endowing the silk surface with certain intermolecular assembly ability. Nevertheless, this binding ability is greatly weakened owing to the high crystallinity of silk fibroin and the lack of unconjugated functional groups in the amorphous region. To modify the chemical activity of the silk surface, HBPAA was employed to modulate the surface chemistry of silk fibroin through intermolecular self-assembly technology. Because HBPAA possesses a huge number of active amino end groups on the outer surface, it can readily assemble onto the SF surface through electrostatic and multi-hydrogen bonding interactions. Moreover, because of its three-dimensional quasi-spherical structure, the high density of amino active groups of the unbound HBPAA hemisphere maintains its ultrahigh affinity towards hydrogen bond acceptor molecules. Conversely, naked AgNPs cannot assemble onto the surface of the silk fibroins directly because of the lack of functional groups. The modification of the capping ligands to make the nanoparticles compatible with HBPAA is also required. To

accomplish this, the AgNPs were functionalized by modification of the nanoparticle surface with HBPAE. Because of the huge number of hydroxyl end groups, HBPAE/AgNPs could be anchored to HBPAA in a facile manner through molecule recognition and self-assembly.

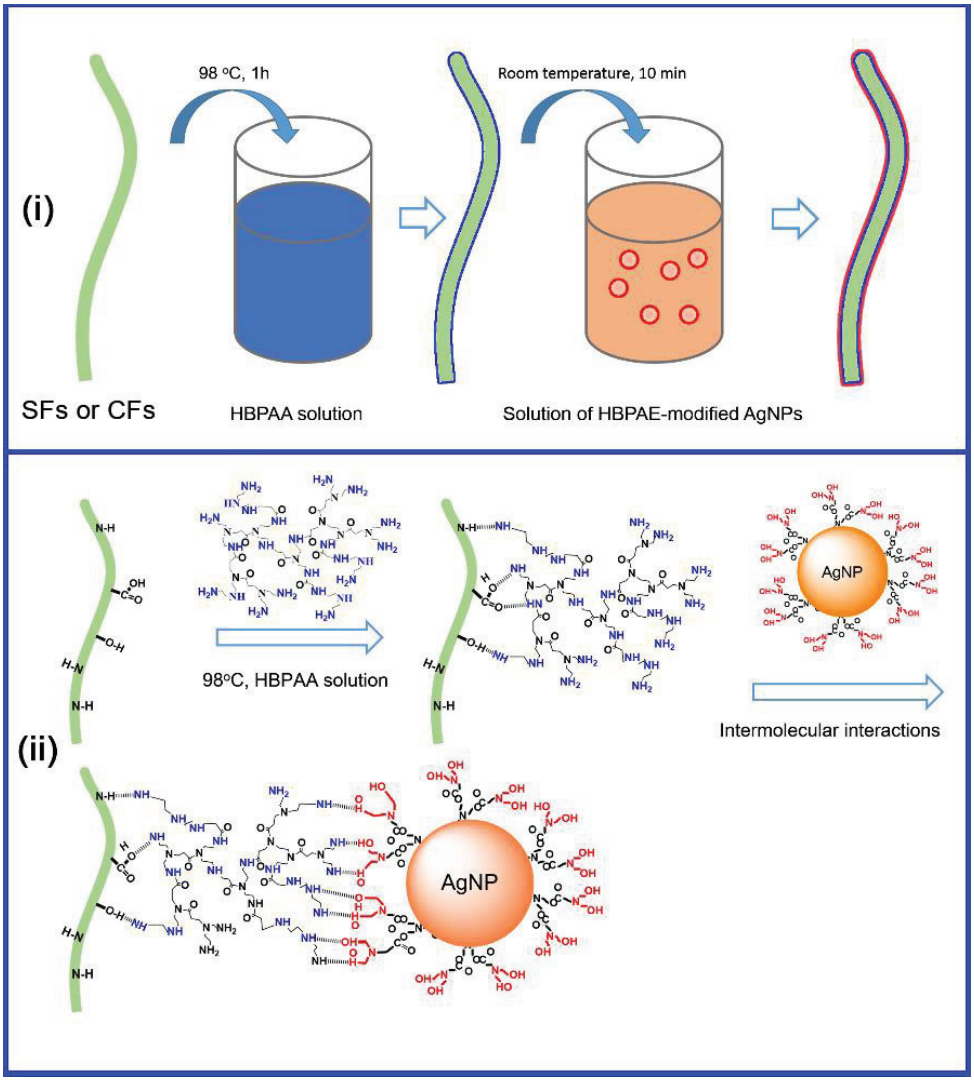

Scheme 3.2 (i) Steps involved in the fabrication of HBPAE/AgNP-coated HBPAA/SFs by intermolecular self-assembly. (ii) The corresponding mechanism of self-assembly of HBPAE/AgNPs on the surface of HBPAA/SFs.

3.3.4 Self-assembly ability of AgNPs on surface of SFs

The self-assembly ability was further quantitatively analyzed by measuring the Ag content of the SFs as a function of concentration of the HBPAE/AgNPs. Figure 3.6 depicts the concentration-dependent Ag content of HBPAA/SFs. It is demonstrated that the amount of attached AgNPs on the HBPAA/SF surface increased with increasing Ag concentration. Up to 160 mg/L of HBPAE/AgNPs can completely self-assemble onto HBPAA/SFs within 10 min at room temperature. This implies that up to 8 mg/g of AgNP-coated SFs can be obtained with complete adsorption. Most importantly, because the Ag content can be controlled by simply adjusting the concentration of HBPAE/AgNPs, the assembly process would be fast, controllable, and quantifiable. Although some recently developed, solution-based coating methods such as in-situ deposition, sol–gel coating, and layer-by-layer assembly can introduce even higher density AgNP coatings, the precise control of Ag content and complete loading of AgNPs on fibers remain as insurmountable obstacles. Our developed intermolecular self-assembly may provide an efficient and environmentally-friendly solution.

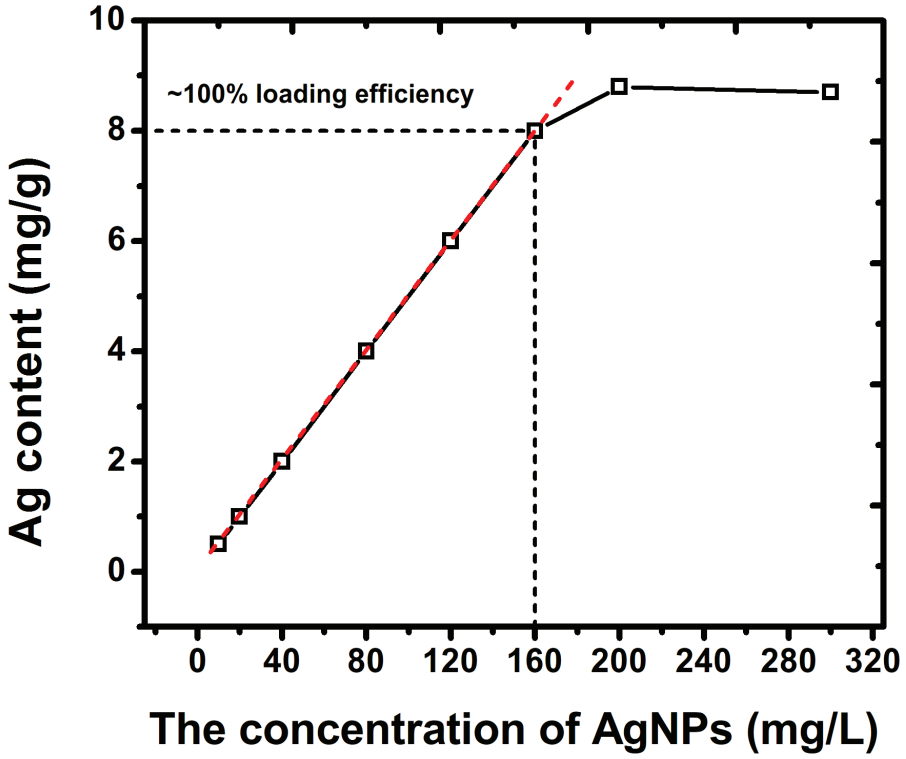

Figure 3.6 The concentration-dependent Ag content of HBPAA/SFs at room temperature with an impregnation time of 10 min.

3.3.5 Antimicrobial tests

After developing a robust and practical procedure for producing AgNP-coated SFs, their antimicrobial activity was further evaluated, which is very important for biomedical applications. In the case of SFs, to test the antimicrobial effects, *E. coli* and *S. aureus* were selected as test organisms, and SFs, HBPAA/SFs, HBPAA/HBPAE/SFs, and HBPAE/AgNP-coated HBPAA/SFs were evaluated qualitatively according to the standard shake-flask method (China) (GB/T 20944.3-2008). As shown in Table 3.1, SFs showed no inhibition effects on *E. coli* and *S. aureus*, confirming pristine silk had no influence on the antibacterial activity. Because silk fibroin consists of (Gly-Ala-Gly-Ala-Gly-Ser) repeating amino acid sequences, SFs are believed to be in

favor of bacteria growth. A slight decrease in colony formation was detected for HBPAA/SFs, verifying the weak antibacterial activity of HBPAA against *E. coli* and *S. aureus*, which was attributed to the abundant amino end groups and the cationic features of HBPAA. It is known that the outer membrane of Gram-positive bacteria such as *E. coli* consists of lipopolysaccharides containing phosphate and pyrophosphate groups, while Gram-negative bacteria such as *S. aureus* contains peptidoglycan, both of which render the cell surface negatively charged [7]. Thus, cationic HBPAA can entrap negatively charged bacteria, interact with the cell membranes, and influence the bio-function of the cell membrane, thereby leading to cell death. With further binding of HBPAE to the surface of HBPAA, the antibacterial activity of SFs showed a slight decrease, suggesting HBPAE did not promote the antibacterial activity of HBPAA. The weakened antibacterial activity could result from the inactivation of HBPAA as it forms strong electrostatic and hydrogen-bonding interactions with HBPAE. In contrast, by binding HBPAE/AgNPs to HBPAA/SFs, HBPAE/AgNP-coated HBPAA/SFs showed very high antibacterial activity. The minimum antibacterial rates of HBPAE/AgNP-coated HBPAA/SFs against *E. coli* and *S. aureus* were both over 98 %, compared with 23.04 % and 11.05 % for HBPAE/HBPAA/SFs. This proves that the strong antibacterial ability of HBPAE/AgNP-coated HBPAA/SFs is mainly related to the antibacterial effect of AgNPs. Moreover, the antimicrobial ability of HBPAE/AgNP-coated HBPAA/SFs was concentration dependent [8]. When the Ag content increased from 0.5 to 1.5, and 8 mg/g, the bacterial reduction rates against *E. coli* and *S. aureus* increased from 98.46 % and 98.14 %, to 99.91 % and 99.69 %, and then over 99.9%, indicative of a positive correlation between inhibition ability and Ag content. To achieve a stable antibacterial effect, the minimum inhibitory content of

AgNPs on SFs was determined as 1.5 mg/g.

Notably, the aforementioned self-assembly ability experiments clearly revealed that the capacity for complete loading of HBPAE/AgNPs on HBPAE/SFs was up to 8 mg/g, which is about 5 times higher than the minimum inhibitory value. Therefore, two advantages are expected: (i) Stable antibacterial activity can be obtained by precisely controlling the Ag content of the SFs and (ii) the Ag content can be controlled to a very low value, avoiding excessive loading of AgNPs and saving costs.

Table 3.1 Antibacterial activities of the SFs.

Silk samples	Ag content (mg/g)	Antibacterial activities			
		E. coli		*S. aureus*	
		Surviving cells (cfu/mL)	% Reduction	Surviving cells (cfu/mL)	% Reduction
SFs	-	2.11×10^{6}	-	6.48×10^{6}	-
HBPAA/SFs	-	1.23×10^{5}	46.52	2.53×10^{5}	33.42
HBPAA/HBPAE /SFs	-	1.77×10^{5}	23.04	3.38×10^{5}	11.05
HBPAE/AgNP-coated HBPAA/SFs	0.5	3.54×10^{3}	98.46	7.07×10^{3}	98.14
	1	1.08×10^{3}	99.53	3.12×10^{3}	99.18
	1.5	2.07×10^{2}	99.91	1.18×10^{3}	99.69
	2	1.61×10^{2}	99.93	1.03×10^{3}	99.73
	5	13	99.99	1.14×10^{2}	99.97
	8	11	99.99	27	99.99

3.3.6 SEM analysis

The surface morphology of the SFs was investigated by FESEM. Figure 3.7 displays FESEM photographs of the SF, HBPAA/SF, and HBPAE/AgNP-coated HBPAA/SF. Pure SF exhibited a clean and smooth surface with dense paralleled microfibrils [Figures 3.7(a) and 3.7(b)], verifying successful removal of sericin from the silk surface after degumming. By contrast, HBPAA/SF exhibited a rough surface morphology in the nanoscale [Figure 2.7(d)], which was probably because of the random assembly of HBPAA nano-quasispheres along the microfibrils of SF. As expected, HBPAE/AgNP-coated HBPAA/SF showed a similar surface pattern to HBPAA/SF. Nevertheless, except for the rugged microfibrils, numerous raised nanoparticles were observed and were well distributed on the HBPAA/SF surface [Figures 2.7(e) and 2.7(f)], which is attributed to the attachment of AgNPs on the surface of HBPAA/SF through intermolecular interactions. Conversely, the diameter of these monodispersed spherical nanoparticles shown in Figure 2.7(f) ranged from 10 to 100 nm, which was in line with the morphological characteristics of AgNPs determined by TEM. In general, the aggregation state of AgNPs on the fiber surface strongly affects the antibacterial activity of AgNPs and the stability of the products because AgNP aggregation will lead to loss of an inhibitory effect on bacterial growth. The good distribution of HBPAE/AgNPs on HBPAA/SF may contribute to obtaining stable antibacterial effects.

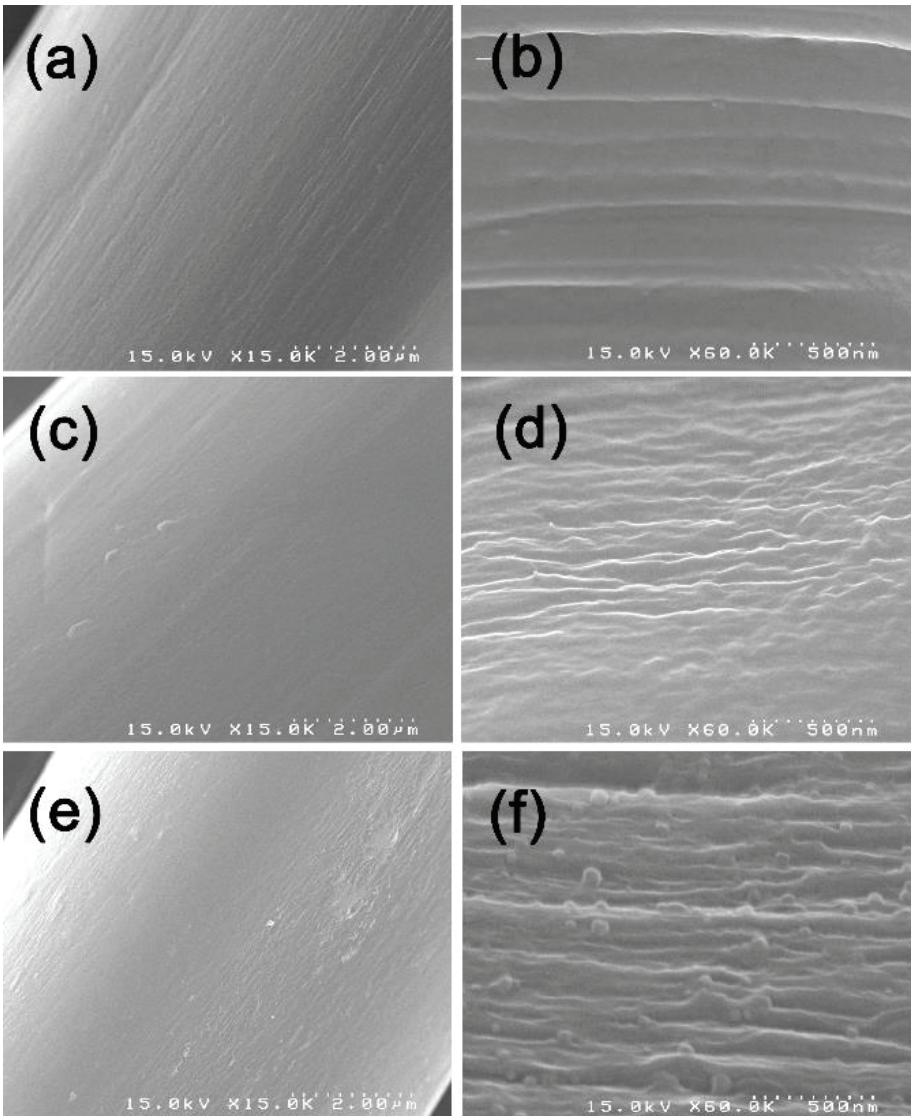

Figure 3.7 FESEM photographs of (a×15,000, b×60,000) pristine SF, (c×15,000, d×60,000) HBPAA/SF, and (e×15,000, f×60,000) HBPAE/AgNP-coated HBPAA/SF (2 mg/g).

3.3.7 XPS and XRD analysis

To gain a better understanding of the surface chemical state of the SFs, XPS analysis was performed. The survey spectrum of SFs [Figure 3.8(a))] showed that pure SFs mainly contain carbon (C), oxygen (O), and nitrogen (N). After assembly of

HBPAA on SFs, the relative intensity of the N in HBPAA/SFs increased significantly, confirming that HBPAA had been successfully anchored to the surface of the SFs because HBPAA has a much higher content of N than SFs. This was further supported by comparing the high-resolution N1s spectra of SFs and HBPAA/SFs. Figures 3.8(b)–8(d) show the fitting curves of the N1s XPS spectra of SFs, HBPAA/SFs, and HBPAE/AgNP-coated HBPAA/SFs. The N1s peak could actually be deconvoluted into two major peaks at 398.9 and 399.7 eV, attributed to amino and acylamide groups [9]. For HBPAA/SFs, the proportion of functional amino groups greatly increased after the HBPAA coating. As amino-dominated HBPAA possesses much more amino end groups than SFs, it is confirmed that the increased proportion of amino groups was mainly attributed to the HBPAA coating. Notably, after further assembly of HBPAE/AgNPs onto the surface of HBPAA/SFs, the relative intensity of N decreased and that of O increased, suggesting that the hydroxyl-dominated HBPAEs were anchored to the surface of the HBPAA/SFs, as analyzed from wide-scan XPS in Figure 3.8(a). Moreover, the concentration of amino groups on HBPAA/SF surface decreased, as observed from the deconvoluted N1s spectra of HBPAE/AgNP-coated HBPAA/SF in Figure 3.8(d). Considering XPS is a highly surface-sensitive probing technique, the weakened N intensity may be because of the combined shielding effects of hydroxyl-dominant HBPAE and AgNPs. Therefore, it is demonstrated that HBPAA and HBPAE/AgNPs successively assembled onto the SF surface, further verifying our presumption about the self-assembly mechanism.

Furthermore, the presence of AgNPs on the HBPAE/AgNP-coated HBPAA/SF can be evidenced by the photoelectron lines of the wide-scan XPS. As shown in Figure 3.8(a), besides C, O, and N, two new doublet peaks at round 370 eV were observed

when compared with SFs and HBPAA/SFs, which can be attributed to $Ag3d_{3/2}$ and $Ag3d_{5/2}$, indicative of successful attachment of AgNPs on the surface of the SFs. In the high-resolution Ag3d XPS spectra in Figure 3.8(e), the peaks of $Ag3d_{5/2}$ and $Ag3d_{3/2}$ at 368.16 and 374.17 eV were at the characteristic positions of metallic AgNPs, indicating no change to the chemical valence state of the AgNPs after their transfer from water to the air/SF interface [10]. The good chemical stability may be attributed to their high crystallinity and good protection from HBPAE.

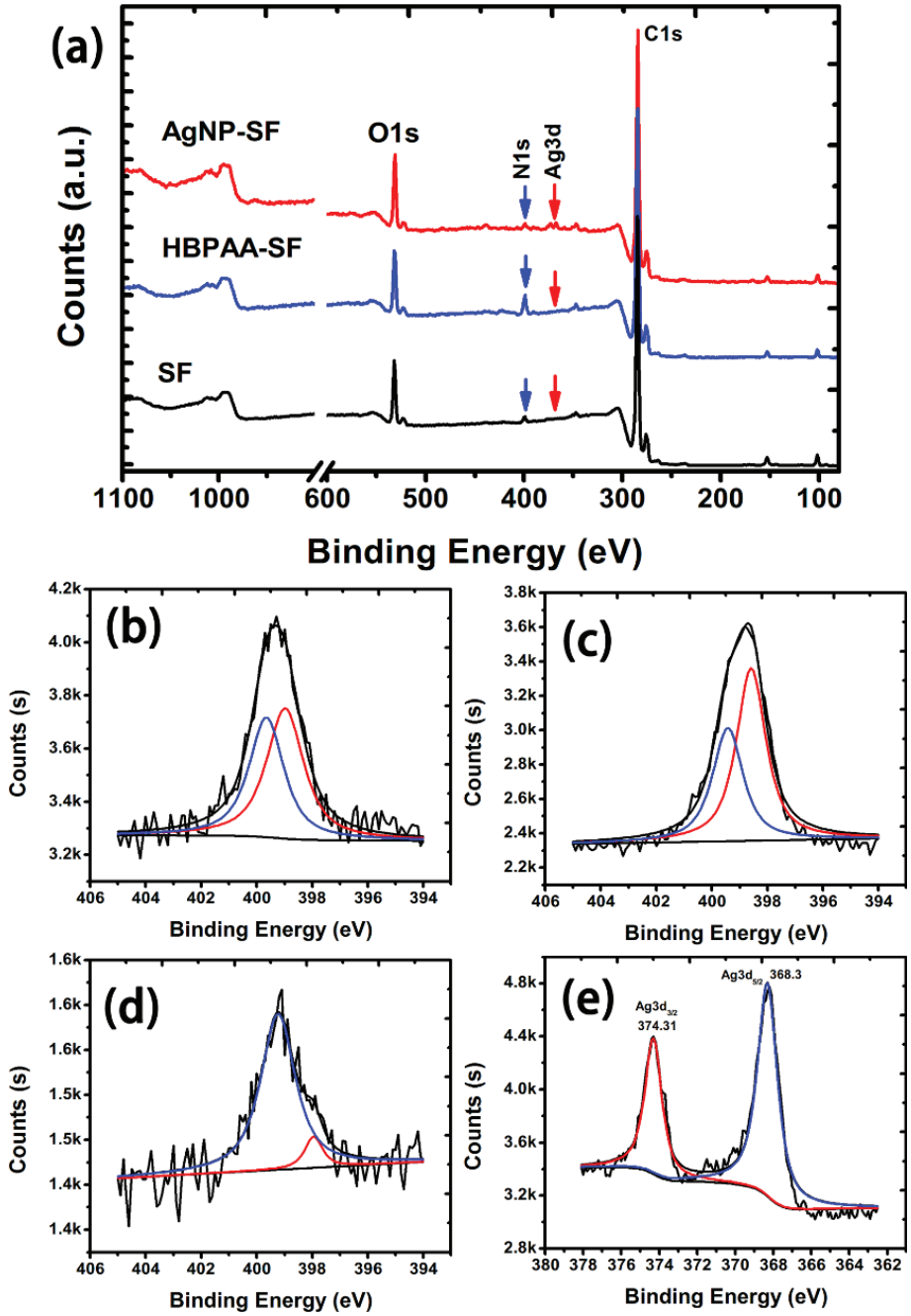

Figure 3.8 XPS spectra: (a) wide scan, N1s spectra of (b) SFs, (c) HBPAA/SFs, and (d) HBPAE/AgNP-coated HBPAA/SFs, and (e) Ag3d spectra of HBPAE/AgNP-coated HBPAA/SFs (1.5 mg/g).

The crystal structure of the SF was further evaluated by XRD. Figure 3.9 displays XRD patterns of SFs, HBPAA/SFs, and HBPAE/AgNP-coated HBPAA/SF. The

pristine silk generated the diffraction peaks at around 9.2°, 20.6°, and 24.3°, which can be indexed to the (100), (210), and (211) diffractions of the β-sheet crystalline structure of the silk fibroin, respectively [11]. After sequentially coating HBPAA and HBPAE/AgNPs on SFs, the characteristic peaks of the silk fibroin exhibited little change, indicating the assembly process did not influence the microcrystalline structure of the silk fibroin. Furthermore, the XRD pattern of HBPAE/AgNP-coated HBPAA/SF showed four additional diffraction peaks at around 38.3°, 44.3°, 64.4°, and 74.5°, which can be indexed to the (111), (200), (220), and (311) diffractions of the face-centered-cubic phase metallic Ag (JCPDS No. 04-0783), respectively, suggesting good chemical stability of AgNPs [12]. This also verifies that AgNPs with an excellent crystalline structure were successfully assembled onto the HBPAA/SFs. The good crystallinity, excellent chemical stability, and monodispersity of AgNPs on the silk surface are important for the physical and chemical properties of the functional SFs. These advantages guaranteed the quality of the final product.

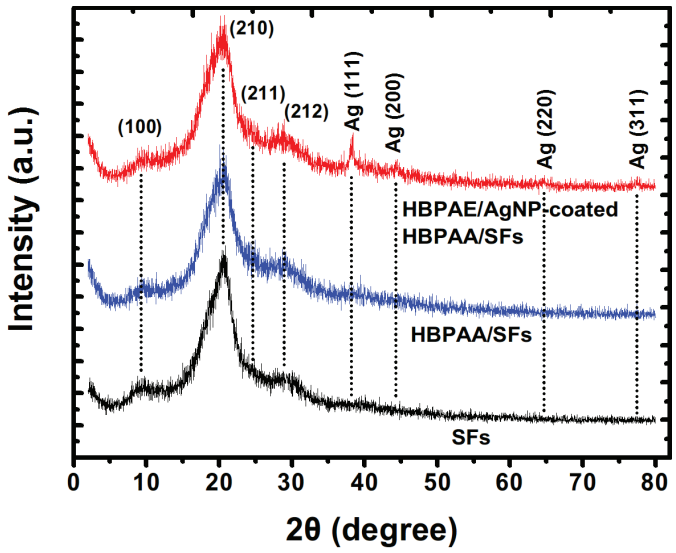

Figure 3.9 XRD of (back) SFs, (blue) HBPAA/SFs, and (red) HBPAE/AgNP-coated

HBPAA/SFs (8 mg/g).

3.4 Conclusions

The assembly of AgNPs on the surface of natural SFs was demonstrated. It was achieved through the intermolecular self-assembly of HBPAE/AgNPs on HBPAA/SFs. HBPAE/AgNPs were synthesized through a simple reduction of $AgNO_3$ in the liquid phase, employing three-dimensional structured HBPAE as the template and capping agent. Because of the space limitation of HBPAE micelles, the as-prepared AgNPs exhibited uniform morphology with an average particle diameter of 11.8 nm. Further research confirmed that HBPAE were successfully bonded to the surface of AgNPs through chemical interactions between the hydroxyl/amide groups and the Ag atom.

The binding of HBPAA onto the molecules in the silk endowed the SF surface with cationic charges and a huge number of amino end groups, allowing further assembly of hydroxyl-dominated HBPAE/AgNPs. Because up to 160 mg/L of AgNPs can be rapidly and completely adsorbed from a colloidal solution to the surface of HBPAA/SFs (2 g) at room temperature, the Ag content of SFs up to 8 mg/g can be accurately controlled by simply adjusting the concentration of the HBPAE/AgNPs. The antibacterial tests showed that HBPAE/AgNP-coated HBPAA/SFs exhibited excellent inhibition activities against both *E. coli* and *S. aureus*. The antibacterial activity was concentration dependent and the minimum content of AgNPs for antibacterial activity was determined as 1.5 mg/g. Furthermore, FESEM, XPS, and XRD analyses confirmed that the assembly of AgNPs on the surface of the SFs exhibited high monodispersity, good crystallinity, and excellent chemical stability, owing to the trapping effect of HBPAA and protective effect of HBPAE. In summary, our developed intermolecular-induced assembly procedure is efficient, controllable, and environmentally friendly. The precise control of the Ag content of coated fibers can

ensure the stability of the product quality and reduce unnecessary waste of resources, which may offer a new approach for controlled preparation of antibacterial textiles.

In summary, our study well verified our previous speculation. This technology can be used for environmental-friendly preparation of various inorganic NPs, without limited by the surface chemistry of fibers.

References:

[1] Qiu T, Song C, Yu J, Li X. The Photoluminescence Properties of Hyperbranched Poly(ester-amine)/ZnS Particle Self-Assembled Multilayer Films. Polym J. 2009;41:358-62.

[2] Zhang F, Chen Y, Ling H, Zhang D. Synthesis of HBP-HTC and its application to cotton fabric as an antimicrobial auxiliary. Fibers Polym. 2009;10:141-7.

[3] Fu X, Shen Y, Jiang X, Huang D, Yan Y. Chitosan derivatives with dual-antibacterial functional groups for antimicrobial finishing of cotton fabrics. Carbohydr Polym. 2011;85:221-7.

[4] Zhu B-K, Wei X-Z, Xiao L, Xu Y-Y, Geckeler KE. Preparation and properties of hyperbranched poly(amine-ester) films using acetal cross-linking units. Polym Int. 2006;55:63-70.

[5] Dallas P, Sharma VK, Zboril R. Silver polymeric nanocomposites as advanced antimicrobial agents: classification, synthetic paths, applications, and perspectives. Adv Colloid Interface Sci. 2011;166:119-35.

[6] Tang B, Zhang M, Hou X, Li J, Sun L, Wang X. Coloration of Cotton Fibers with Anisotropic Silver Nanoparticles. Ind Eng Chem Res. 2012;51:12807-13.

[7] Bhawana, Basniwal RK, Buttar HS, Jain VK, Jain N. Curcumin Nanoparticles: Preparation, Characterization, and Antimicrobial Study. J Agr Food Chem. 2011;59:2056-61.

[8] Xiu Z-m, Zhang Q-b, Puppala HL, Colvin VL, Alvarez PJJ. Negligible

Particle-Specific Antibacterial Activity of Silver Nanoparticles. Nano Lett. 2012;12:4271-5.

[9] Gu J, Yang X, Zhu H. Surface sulfonation of silk fibroin film by plasma treatment and in vitro antithrombogenicity study. Materials Science and Engineering: C. 2002;20:199-202.

[10] Zanna S, Saulou C, Mercier-Bonin M, Despax B, Raynaud P, Seyeux A, et al. Ageing of plasma-mediated coatings with embedded silver nanoparticles on stainless steel: An XPS and ToF-SIMS investigation. Applied Surface Science. 2010;256:6499-505.

[11] Drummy LF, Phillips DM, Stone MO, Farmer BL, Naik RR. Thermally Induced α-Helix to β-Sheet Transition in Regenerated Silk Fibers and Films. Biomacromolecules. 2005;6:3328-33.

[12] Lu Z, Xiao J, Wang Y, Meng M. In situ synthesis of silver nanoparticles uniformly distributed on polydopamine-coated silk fibers for antibacterial application. J Colloid Interface Sci. 2015;452:8-14.

Chapter 4

Eco-friendly preparation of antibacterial cotton fibers by the cooperative self-assembly of HBPAA- and HBPAE-functionalized silver nanoparticles

Chapter 4 Eco-friendly preparation of antibacterial cotton fibers by the cooperative self-assembly of HBPAA- and HBPAE-functionalized silver nanoparticles

4.1 Introduction

Recently, scientists focused extensive research on the surface modification of biological fibers to improve their physical and chemical properties or impart new properties. One of interesting strategies is to coat nanomaterials on the natural fiber, with the purpose of turning the natural fiber into a multifunctional material that not only integrate the advantages of both the macroscopic natural fiber and the nanomaterial but also overcome their instinct drawbacks or even create new performances from their intrinsic properties [1, 2]. Such functional biological fibers will be helpful to transform natural fibers into high-tech and high-added-value products with advanced functionalities. Thereinto, one of hotspots for research is design and engineering of antimicrobial textiles by integration of antimicrobial nanomaterials into textile fibers [3-7].

Since ancient times, metallic silver has been very known by mankind for its antimicrobial properties [6]. With the booming development of nanoscience and nanotechnology and an increased risk of bacterial resistance compared to existing organic antimicrobial agents, a new form of silver namely silver nanoparticles (AgNPs) have become a popular subject due to their superiority compared to bulk silver and organic antibiotics including robust and broad-spectrum antimicrobial activity, low

bacterial resistance, and good biosafety. Although exact antimicrobial mechanism is still subject to debate, researchers are inclined to believe that the antimicrobial ability of AgNPs mainly derives from the interaction of Ag ions that are released from NP surfaces with important proteins and enzymes and the oxygen stress caused by peroxides such as O_2^- and OH^- that are formed on surfaces of AgNPs [8]. Owing to the excellent antimicrobial activity and unique antimicrobial mechanism, AgNPs have been widely used in food preservation, water disinfection, and medical devices. Nevertheless, recently studies indicate that AgNPs may pose a potential threat to eco-environment. Toxicity of AgNPs has been found for unicellular aquatic flora and fauna, which are the basis of the biological chain. Therefore, reduce of waste AgNPs is of great concern for their further development. In general, AgNPs can be discharged to the environment in every phase of manufacture and use of antibacterial products. To eliminate potential environment risks, researches recently have been devoted to design a green synthesis approach for AgNPs and biocompatible AgNPs by carefully engineering their core-shell structure. Surprisingly, few researches dedicate in the elimination of discharged AgNPs during the production process of antibacterial fibers/textiles. We point out that the waste AgNPs produced during the manufacture process may pose an even greater threaten because the continuous emission of AgNP-containing wastewater in certain area may not only quickly change the ecological structure due to their strong antimicrobial effects and but also has an adverse effect on humanity by bioaccumulation and concentration of Ag element through water food chain.

Molecular-induced NP self-assembly on the biomolecule surface is described as spontaneous spatial arrangement of NPs functionalized by functional polymers that can recognize biomolecular targets. This spatial arrangement is driven by electrostatic

attraction, hydrogen bonding, host-guest interactions. As such, the self-assembly may may provide an alternatively eco-friendly method for generating NP coatings that can overcome the above-mentioned shortcomings. The advantages of such bottom-up strategies lie in the simplicity and high-efficiency of the preparation process. In previous chapters, AgNPs functionalized by amino-terminated hyperbranched poly(amidoamine) (HBPAA) were successfully designed and found capable of being completely adsorbed by carboxyl-rich calcium alginate fibers (CAFs) and hydroxyl-containing silk fibers (SFs) depending on strong molecular interactions between the capping molecule and the biomolecule on the fiber surfaces. However, this strategy achieves lower efficiency for cotton compared with CAFs and SFs because of the relatively inert hydroxyl groups on cotton surface. Consequently, weaker intermolecular driving forces were compared with electrostatic repulsion forces among HBPAA-functionalized AgNPs (HBPAA/AgNPs). In fact, the surface AgNP charges adversely influence AgNP properties in the following manners: (i) the charges improve AgNP water stability and provide electrostatic attractions towards the oppositely charged organic surface or (ii) inhibit their attachment on the oppositely charged organic surface because of the charge repulsion among NPs. To overcome this barrier, we developed an NP cooperative self-assembly technology by designing two distinct AgNPs with the NP surface functionalized with amino-terminated HBPAA and hyperbranched poly(amine-ester)s (HBPAE) capable of mutual recognition and combination to overcome the charge steric hindrance. Such charge steric hindrance was surmounted by converting the electrostatic repulsion among NPs to electrostatic attractions. Particularly, the AgNP coating was constructed by the alternate self-assembly of positively charged HBPAA/AgNPs and negatively charged

hydroxyl-terminated HBPAE-functionalised AgNPs (HBPAE/AgNPs) on the cotton surfaces. HBPAA and HBPAE were selected as capping agents because of their similarly unique advantages of 3D spatial structure, amphipathicity, and dense functional end groups. As such, the agents afforded the AgNPs with good protection from agglomeration and corrosion. Meanwhile, the agents also enabled mutual recognition and combination because of their opposite charges and ability to form hydrogen bonding through amino-hydroxyl interactions.

In this study, we designed a highly efficient and eco-friendly self-assembly approach to fabricate heterostructured AgNP-coated cotton fibers by NP cooperative self-assembly technology. In such system, cotton fibers served as the substrate, whereas the positively charged amino-dominated HBPAA/AgNPs and negatively charged hydroxyl-dominated HBPAE/AgNPs served as the cooperative building blocks. The surface modification of HBPAA and HBPAE aimed to enhance the agents' binding capacity to hydroxyl-dominated cotton cellulose, impart high water and chemical stability to the AgNPs, and generate heterogeneous NPs that can mutually recognize and combine depending on the collective supramolecular interactions of long-range electrostatic attractions and short-range hydrogen-bonding interactions. AgNP coating was formed by the circular introduction of HBPAA/AgNPs and HBPAE/AgNPs to the cotton surface through a simple cyclic impregnation method. To realize the concept of environmental protection, HBPAA/AgNPs and HBPAE/AgNPs were completely adsorbed on the cotton surface by appropriately adjusting experimental conditions. The physical–chemical properties of the coated cotton were evaluated by Fourier transform infrared spectroscopy (FTIR), scanning electron microscopy (SEM), X-ray photoelectron spectroscopy (XPS), and X-ray diffraction (XRD).

4.2 Experimental

4.2.1 Materials

Cotton fibers were purchased from Zhangjiagang Nellnano Nanotechnology Co., Ltd (China). HBPAE and HBPAA were synthesized by previously reported methods. Silver nitrate ($AgNO_3$), ethanol (99.5%), sodium borohydride ($NaBH_4$), and nitric acid (HNO_3, ~70%) were purchased from Wako Pure Chemical Industries, Ltd. (Japan). *Escherichia coli* (ATCC8099) and *Staphylococcus aureus* (ATCC 6538) were obtained from the College of Life Science, Soochow University (China). Nutrient broth and nutrient agar were purchased from Wako Pure Chemical Industries, Ltd (Japan).

4.2.2 Synthesis of HBPAA/AgNPs and HBAPE/AgNPs

Different from Chapter 2 and 3, prior to synthesis of functional AgNPs, HBPAE and HBPAA were dialyzed against deionized water using SnakeSkin® dialysis tubings (Thermo scientific, molecular weight cut-off 3500 Da) for 24 h to remove oligomers. Therefore, the as-prepared NPs were a little different from that synthesized in Chapter 2 and 3.

HBPAA/AgNPs were synthesized as described by our as our previously reported method. Specifically, HBPAA/AgNPs were fabricated by dissolving 2 g of HBPAA in 45 mL of deionized water and adding HBPAA solution to 5 mL of 7.8 g/L $AgNO_3$ aqueous solution at 35^{o}C using a well-described procedure. The reaction mixture was slowly heated to 90 ^{o}C and kept stirring at 90 ^{o}C for 3 h. The resulting product was maintained in the refrigerator.

HBPAE/AgNPs: Briefly, 5 mL of 7.8 g/L $AgNO_3$ aqueous solution was mixed with 45 mL of 12 g/L HAPAE solution under magnetic stirring at 30 °C. This was followed by the addition of 5 mL of 1 g/L of $NaBH_4$ to the $AgNO_3$/HBPAE mixture. The HBPAE-capped AgNPs sample thus was stored in refrigerator.

4.2.3 Cooperative self-assembly of HBPAA/AgNPs and HBPAA/AgNPs on CFs

The heterostructured AgNP coating was constructed by alternately coating HBPAA/AgNPs and HBAPE/AgNPs on CFs with final high-temperature curing. Primarily, their concentration ratio was set as 1:1 to ensure that HBPAA/AgNPs and HBPAE/AgNPs could be completely adsorbed by CFs through their cooperative adsorption. The bottleneck of the self-assembly was the initial adsorption of HBPAA/AgNPs by cotton fibers because their binding ability was much weaker than between HBPAA/AgNPs and HBPAE/AgNPs. Therefore, to guarantee the complete uptake of HBPAA/AgNPs, the optimal conditions should be first determined.

The effect of Ag concentration and incubation temperature on the adsorption of single HBPAA/AgNPs by cotton fibers was investigated to find their optimal conditions for the complete uptake of HBPAA/AgNPs by cotton fibers. Specifically, 1 g of fiber samples was completely infiltrated by pre-impregnation in deionized water for 10 min. The wet cotton fibers were then transformed onto 100 mL of solution of HBPAA/AgNPs with concentrations ranging from 10–100 mg/L. The mixture was then stirred for 120 min at 35–95 °C. The HBPAA/AgNP-coated cotton fibers were removed and washed with deionized water three times. The remaining concentration of HBPAA/AgNPs in the solution was measured by inductively coupled plasma atomic emission spectrometry (ICP–AES). The Ag content of the treated cotton fibers was then calculated by the following formula:

$$C_{ag} = \frac{C_o - C_t}{10} \quad (1)$$

where Cag, Co, and Ct are the Ag content of coated cotton fibers, initial concentration of HBPAA/AgNPs, and the concentration of HBPAA/AgNPs in the residual solution, respectively.

The as-prepared HBPAA/AgNP-coated cotton fibers prepared under optimal conditions were circularly incubated with 100 mL of solutions of HBPAE/AgNPs and HBPAA/AgNPs with the above-determined concentration and temperature and incubation time of 0.5 h under stirring. After several times of treatment (including initial treatment by single HBPAA/AgNPs), a dense and controllable nanocoating was formed on the cotton surface. Finally, the as-prepared fiber samples were cleaned by tap water several times, cured in an oven at 120 °C for 20 min, and stored in a seal sample bag.

4.2.4 Sample characterization

AgNP morphology was studied by transmission electron microscopy (TEM; JEM-2100F, JEOL, Japan). The hydrodynamic size and surface AgNP charge in the aqueous solution were evaluated using the Nano ZS90 Zetasizer (Malvern, UK). The UV–vis spectra at 300–700 nm were obtained using a UV-2700 spectrophotometer (Shimadzu, Japan). The Ag content was measured in acidified solutions by ICP–AES (Vista MPX; Varian, USA).

The morphology and size of AgNPs on the fiber were characterized and analyzed by scanning electron microscopy SEM (Hitachi S-3000N, Hitachi, Japan) and field emission SEM (FESEM; Hitachi S-5000, Hitachi, Japan). The FTIR was collected on a Perkin Elmer Spectrum 100 FTIR spectrometer (Perkin Elmer, USA), which converted

fiber samples into powder using the KBr pellet infrared spectrometer test under a scan number of 32 and resolution of 4 cm−1. The chemical states and crystal structures of samples were analysed by XPS (AXIS Ultra DLD; Krotos, Japan) and XRD (D8 ADVANCE, Bruker, Germany).

4.2.5 Evaluation of the antibacterial activity of CFs

The antimicrobial activity of CFs was measured against *E. coli* and *S. aureus* using a shake-flask method [GB/T 20944.3-2008 (China)]. Briefly, test and control CFs (0.75 g) were immersed into a flask containing 70 mL 0.3 mM PBS (monopotassium phosphate, pH~7.2) culture solution with cell concentration of 1×10^5~4×10^5 colonyforming units (cfu)/mL in triplicates. Subsequently, the flasks were subjected to incubation on a rotary shaker at 24 ºC for 18 h. The colonies formed after incubation were counted by spread-plating serial dilutions on an agar plate at 24 h. The percentage reduction (C, %) was determined using the following formula:

$$C = \frac{B - A}{B} \quad (1)$$

where C and A are the bacterial colonies of the control CFs and treated CFs, respectively.

4.3 Results and Discussion

4.3.1 Characterization of HBAPA/AgNPs and HBPAE/AgNPs

Given the weak interactions between cotton and metallic AgNPs which is mainly

dominated by van der Waals forces, the poor compatibility of metallic AgNPs with biological fibers usually leads to low assembly efficiency, weak adhesive strength, and high environmental risks. Therefore, recent research focus has shifted to promoting their binding affinity by various strategies, such as modifying or grafting the fiber surface with cationic polyelectrolytes or cationic groups. Collectively, these strategies aim to convert weak van der Waals forces to robust long/short-range intermolecular forces, such as electrostatic, hydrophobic, and hydrogen-bonding forces, with final improvement of their combination. However, this approach suffers from certain deterioration of mechanics and gloss of fibers. Recently, we adopted the opposite supramolecular self-assembly strategy: capping the AgNP surface with amino-terminated HBPAA to guide and immobilize NPs to the fiber surface by intermolecular electrostatic and hydrogen-bonding interactions while avoiding potential fiber damages. However, such approach remains sensitive to the surface chemical properties of biological fibers.

To remedy this limitation, we further developed a supramolecular cooperative self-assembly by alternate self-assembly of mutual recognized donator/acceptor molecule-capped AgNPs on the fiber surface mediated by supramolecular interactions among HBPAA, HBPAE, and cotton cellulose. The detailed self-assembly mechanism and procedure were illustrated in Figure 4.1. We first synthesized two heterostructured AgNPs separately functionalized with amino-terminated HBPAA and hydroxyl-terminated HBPAE. HBPAA and HBPAE were used as capping agents because these substances possess similar molecular features, including amphiphilicity, 3D quasi-spherical structure, and abundant functional end groups suitable for protecting and stabilizing of AgNPs. Meanwhile, these agents endow two heterostructured AgNPs

with a special ability of mutual recognition and combination derived from the intermolecular electrostatic attraction and multiple hydrogen bonding interactions between HBPAA and HBAPE. The self-assembly is initially triggered by electrostatic and hydrogen bonding interactions between amino-functionalized HBPAA/AgNPs and hydroxyl-dominated cotton cellulose because HBPAA anchored to AgNPs surfaces possesses much higher binding ability to cotton cellulose than does hydroxyl-terminated HBPAE depending on their dense functional amino groups and polycationic features (Figure 4.1). Nevertheless, given the relatively chemical inertness of semicrystalline cotton cellulose, such intermolecular interactions are unsufficient to overcome combined obstacles of thermal energies and electrostatic repulsion among HBPAA/AgNPs, which is necessary to guide the massive HBPAA/AgNPs onto the cotton surface. Nonetheless, this disadvantage could be reversed by the alternate introduction of HBPAA/AgNPs and HBPAE/AgNPs onto the cotton surface for transforming electrostatic repulsion into electrostatic attraction. By circular incubation with oppositely charged HBPAE/AgNPs and HBPAA/AgNPs, the attached heterostructured AgNPs shift turns to serve as trapping agents for oppositely charged AgNPs and further form multi-hydrogen bonding interactions, resulting in co-attachment of heterostructured AgNPs on cotton surfaces. Theoretically, a dense AgNP coating with controllable Ag content and environmental-friendly assembly procedure can be achieved by multi-cycle incubation of two reversed AgNPs and by ensuring the complete adsorption of AgNPs in each step through the careful design of experimental conditions.

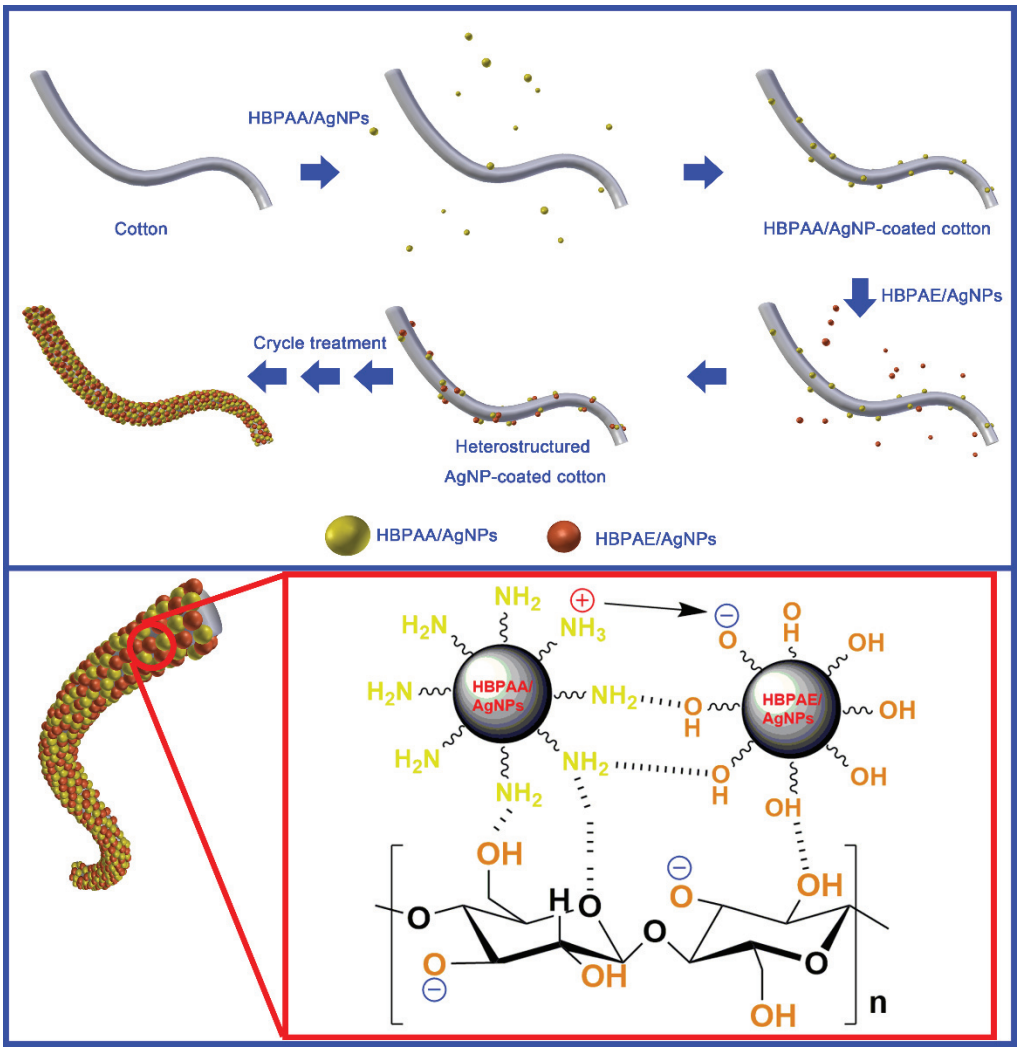

Figure 4.1 Schematic representation of cooperated self-assembly of HBPAA/AgNPs and HBPAE/AgNPs on a surface of the CF.

The synthetic methods of HBPAA/AgNPs and HBPAE/AgNPs were slightly dissimilar. HBPAA/AgNPs were synthesized by the hydrothermal reduction of $AgNO_3$, with HBPAA acting as the reducing and capping agent because of its reductive amino groups. By contrast, HBPAE/AgNPs were prepared by reducing an aqueous solution of $AgNO_3$ using $NaBH_4$ at ambient temperature with HBPAE only serving as the capping agent because of HBPAE' weak reducibility. Because of narrower molecular weight distribution of HBPAA and HBPAE after the dialysis, synthetic NPs should be

re-characterized. Figure 4.2(a) shows the TEM image of monodispersed HBPAA/AgNPs with about 14.9 nm average diameter, in line with the hydrodynamic size measured by DLS [inset of Figure 4.2(a)]. The observed large-scale HBPAA/AgNPs exhibited a uniform size and a regular spherical structure, which were probably contributed by the relatively low reaction rate and rigorous space restriction of HBPAA. In comparison, the average hydrodynamic size of HBPAE/AgNPs possesses a much smaller hydrodynamic size of around 4.4 nm [inset of Figure 4.2(b)] and a slight wide size-distribution was observed from their TEM images [Figure 4.2(b)]. The smaller size is because the narrower molecular weight distribution of HBPAE compared with that synthesized in Chapter 3. Moreover, HBPAA and HBPAE not only impart nano-size and good water stability to AgNPs but also opposite surface charges and complementary surface functional groups capable of mutual recognition and combination. As shown in Figure 4.2(e), The HBPAA/AgNPs possess a positive surface potential (+40.8 mV) derived from the numerous cationic amino groups in HBPAA. Conversely, HBPAE/AgNPs exhibited a slightly negative charge (-15.8 mV) attributed to weak acidic nature of HBPAE [Figure 4.2(f)]. The binding of HBPAA and HBPAE has been proved in our previous studies. The good capping effects of HBPAA and HBPAE on AgNPs are probably due to their three-dimensional (3D) cavity structure, abundant functional end groups, and their amphipathic characteristic.

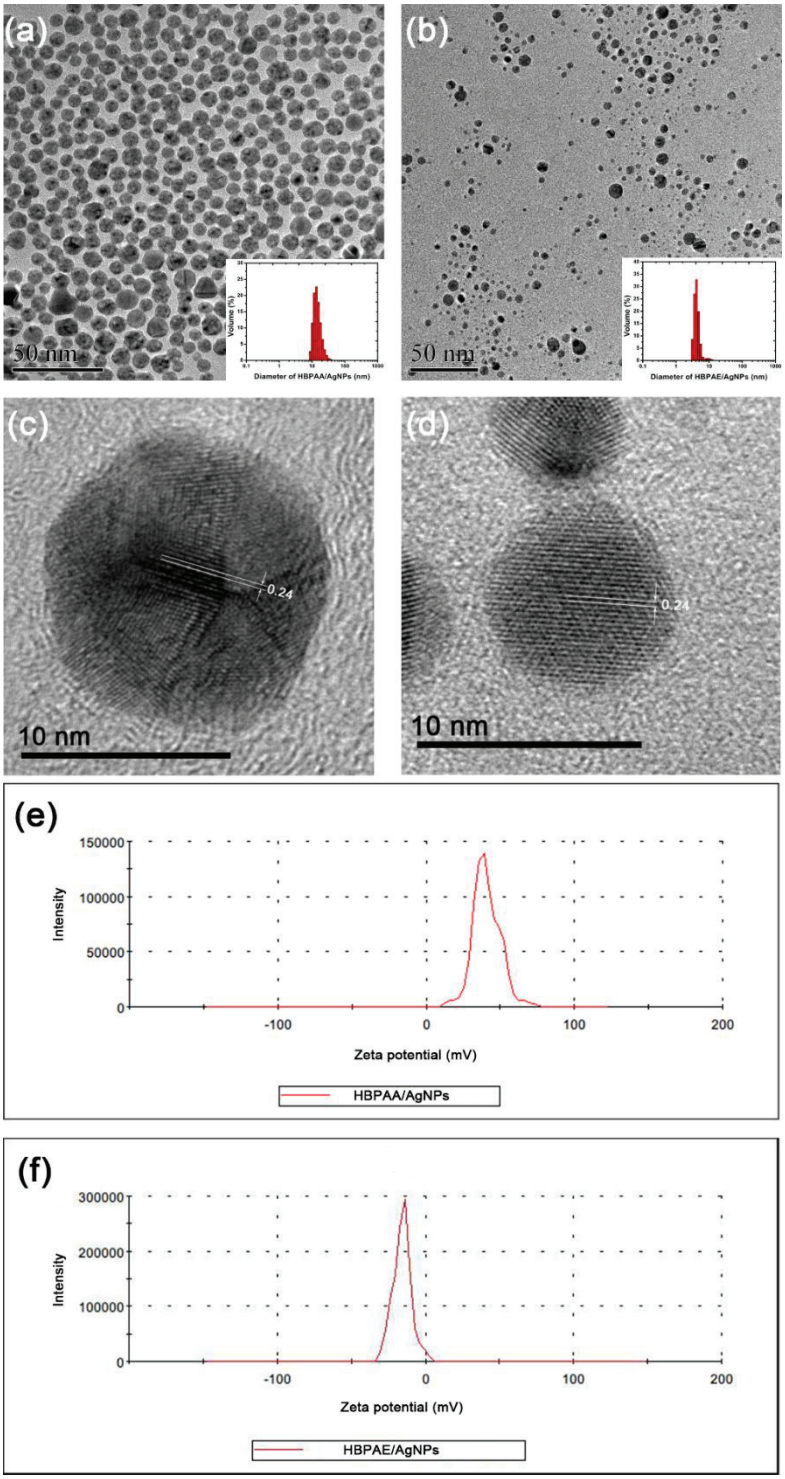

Figure 4.2 TEM and high-resolution TEM images of (a, c) HBPAA/AgNPs and (b, d) HBPAE/AgNPs. Zeta potential of (e) HBPAA/AgNPs and (f) HBPAE/AgNPs. In situ size distribution measured by DLS of HBPAA/AgNPs and HBPAE/AgNPs were shown

in the inset of Figures 4.2(a) and 4.2(b), respectively.

4.3.2 Cooperative self-assembly of HBPAA/AgNPs and HBPAE/AgNPs on CFs

To eliminate potential environmental risks during the treatment, a fundamental principle is that two hereostructured AgNPs should adsorb onto CFs completely in each step. Thus, the concentration ratio between HBPAA/AgNPs and HBPAE/AgNPs was set as 1:1 to ensure their synergistically complete adsorption by CFs. In our experiment, coating CFs with heterostructured AgNPs was performed by cycle incubation of CFs with colloidal solutions of HBPAA/AgNPs and HBPAE/AgNPs. Specifically, CFs are first incubated with a colloidal solution of HBPAA/AgNPs for 2 h. HBPAA/AgNPs were used as the starting coating solution because of their much stronger binding affinity to cotton cellulose than that of HBPAE/AgNPs attributed to the former' opposite positive charges and high number of amino surface groups.

As indicated in Chapter 2, only 15 mg/L HBPAA/AgNPs were completely adsorbed onto cotton fibers at room temperature. However, when the incubation temperature rises to 85 ^{o}C, 10-60 mg/L HBPAA/AgNPs can be completely adsorbed onto the cotton surface, i.e., 1-6 mg/g of HBPAA/AgNP-coated cotton can be obtained by the complete adsorption, as shown in Figure 4.3. Therefore, the concentration of HBAA/AgNPs was set as 10-60 mg/L. For fabrication of cotton fibers with low Ag content, the temperature can be set as a low value (i.e. room temperature). In contrast, for fabrication of cotton fibers with Ag content over 10 mg/g, rising the temperature can decrease the treatment times.

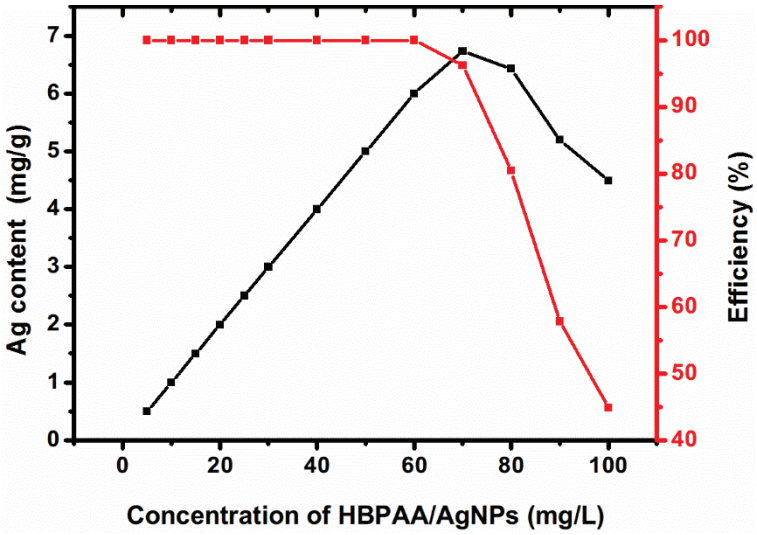

Figure 4.3 Adsorption of HBPAA/AgNP by the cotton as a function of HBPAA/AgNP concentration in the colloidal solution (incubation temperature: 85 ^{o}C; incubation time: 2 h). The red line represents the adsorption efficiency of HBPAA/AgNPs by cotton as a function of the HBPAA/AgNP concentration.

By coating the cotton surface with HBPAA/AgNPs, the subsequent cooperative self-assembly between HBPAA/AgNPs and HBPAE/AgNPs was much highly simplified because their ultra-strong intermolecular interactions. HBPAA/AgNP-coated CFs prepared by the aforementioned optimum experimental conditions were circularly transferred into colloidal solutions of HBPAE/AgNPs and HBPAA/AgNPs with the same concentration (as determined above) under continuous stirring. Our study showed that the complete adsorption between HBPAA/AgNPs and HBPAE/AgNPs could achieve at room temperature within 30 min. This occurrence can be attributed to the supramolecular recognition and combination between HBPAA and HBPAE.

Given that AgNPs were completely assembled onto cotton surface, the Ag content (Ccot,, mg/g) of coated cotton fibers can be calculated by the following formula:

$$C_{cotton} = \frac{C_{Ag} \times n}{10}$$

where C_{Ag} (mg/L) and n are the concentrations of AgNPs and treatment times, respectively. The concentrations of HBPAA/AgNPs and HBPAE/AgNPs were equal.

4.3.3 FTIR analysis

HBPAA and HBPAE capping of the AgNP surface play a vital role in self-assembly because the agents impart the surfaces of heterostructured AgNPs with functional 3D polymer shells that possess opposite surface charges and abundant electron-donating or electron-acceptor groups, respectively. These groups not only protect and stabilize the AgNPs in colloidal solution but also endow the AgNPs with certain molecular recognition and combination ability. Therefore, NP transfer onto the cotton surface would accompany the chemical combination of HBPAA HBPAE, and cotton cellulose. FTIR spectroscopy is a useful tool for representation of the chemical composition, spatial configuration, and functional groups of organic materials. As such, FTIR can be utilized to confirm the existence of HBPAA and HBPAE and analysis the potential physiochemical influence of HBPAE and HBPAA on cotton. As shown in Figure 4.4(b), the FTIR spectrum of the pristine CFs shows typical characteristic peaks of cotton cellulose [10]. The broad band ranged from 3200 to 3500 cm^{-1} could be assigned to O-H stretching (intermolecular hydrogen bonds). The vibrations located at around 2918 and 2850 cm^{-1} are attributed to CH_2 asymmetric stretching, which originates from the cellulose in the cell walls of cotton and wax substances attached on the cotton fiber surface. The band centered at around 1640 cm^{-1} corresponds to the deformation vibration of absorbed water molecules through hydrogen bonding in

amorphous regions of the cellulose macromolecules. The bands of 1250-800 cm^{-1} represent the fingerprint of cotton cellulose, which could be assigned to vibrations of COH in-plane bending, antisymmetric bridge $C_{(1)}$-O-$C_{(4)}$ stretching, and C-O stretching. Notably, the vibrations located at 1161 and 896 cm^{-1} were attributed to β-D-glucoside bond, and their position and intensity were associated with the molecular weight of cotton cellulose. After introducing various densities of heterostructured AgNP coatings to CFs, the main chemical bonds and related intensity of cotton cellulose, including O-H stretching, asymmetric C-H stretching, COH in-plane bending, C-O-C stretching, and C-O stretching, remained unchanged. This result implied the absence of major molecular structural change and secondary conformation during the cooperative self-assembly process.

The absorption bands and the intensity of combined water at 1650 cm^{-1} and CH_2 symmetric deformation at around 1429 cm^{-1} indirectly represent the proportion of amorphous and crystalline cellulose. In the case of 3 mg/g of heterostructured AgNP-coated cotton fibers, these absorption bands show almost the same intensity as that of the pristine cotton fibers, suggesting that the cooperative assembly process did not affect the crystal structure of cotton. Conversely, when Ag content increased to 15 mg/g, obvious changes in vibrations from 1750 cm^{-1} to 1350 cm^{-1} were observed. The characteristic adsorption band of combined water around 1650 cm^{-1} was covered completely by absorption bands of amide I, amide II, and C–H vibrations in HBPAA and C=O, C–N, and C–H vibrations in HBPAE. This result suggests that HBPAE and HBPAA were anchored to the cotton, and their content were positively correlated to Ag content. The finding also implies that the cooperative self-assembly of the AgNPs achieved an important association with their functional capping molecules.

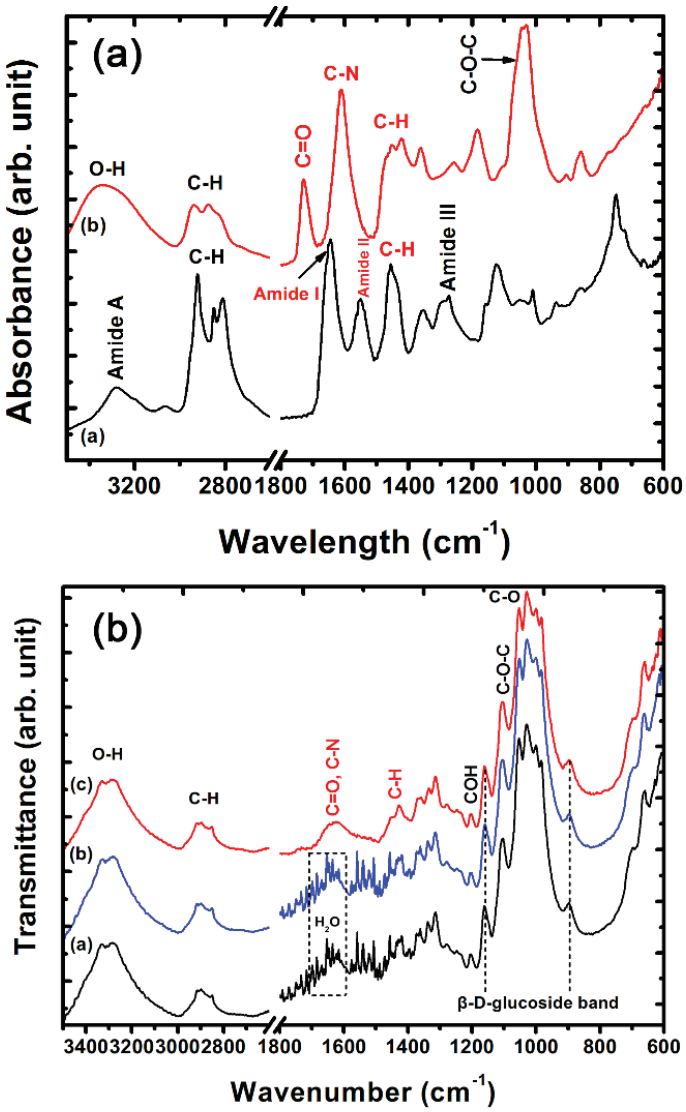

Figure 4.4 (a) FTIR spectra of HBPAA (black) and HBPAE (red). (b) FTIR spectra of pristine CFs (black) and 3 mg/g (blue) and 15 mg/g (red) of heterostructured AgNP-coated CFs.

4.3.4 Morphological characterizations of functional CFs

The morphologies and distribution states of AgNPs assembled on the CF surface significantly affect the function of the final nano-coating as observed by FESEM and SEM. As shown in Figure 4.5, the pristine CFs exhibited unique morphological characteristics, including nature-formed convolution and parallel-arranged macrofibrils

with a certain degree of orientation [Figure 4.5(a)-4.5(c)]. After coating with HBPAA/AgNPs and HBPAE/AgNPs, an obvious distinction presented between the uncoated and AgNP-coated CFs. Numerous monodispersed AgNPs and few of AgNP clusters were uniformly scattered on the cotton surface when Ag content was only 3 mg/g. Unlike monodispersed AgNPs on a fiber surface, Ag cluster formation was attributed to the chemical interactions between HBPAA and HBPAE [Figure 4.5(d)-4.5(f)]. Even so, the diameter of the constituent AgNPs in nanoclusters remained unchanged relative to the determined sizes of the HBPAA/AgNPs and HBPAE/AgNPs as observed under FESEM when the NPs transferred from water to the solid cotton surface. Hence, no crystallization growth of AgNPs occurred during the self-assembly process, as shown in Figure 4.5(f). Furthermore, the assembled AgNPs may have inherited their intrinsic nano-properties after the spatial transformation. By further increasing the concentration of heterostructured AgNPs, we observed the coverage density of AgNPs on the cotton surface to proportionally increase as expected. Compared with that under low AgNP content and although monodispersed AgNPs remained as the dominant distribution mode, the proportion of the heterostructured AgNP clusters was slightly enlarged. Notably, this coating remained well distributed through a fraction of large aggregates, suggesting that heterostructured AgNPs tend to attach interfaces between the cotton and AgNPs rather than self-stacking during the self-assembly process. This effect was probably caused by the combined intermolecular forces among the HBPAA/AgNPs, HBPAE/AgNPs, and cotton cellulose, making AgNPs preferentially anchored to the negative charged cotton interfaces. The chemical characteristics of the nanocoating were further confirmed by the energy dispersive spectroscopy (EDS) mapping analysis of elements N and Ag. As displayed in Figure

4.5(j)-4.5(*l*), additional N and Ag elements were found in the heterostructured AgNP-coated CFs compared with the pristine CFs, which should be ascribed to the attachment of HBPAA, HBPAE, and metallic AgNPs to the CFs. Notably, the N and Ag distributed evenly on the CF surfaces, which is in good agreement with FESEM measurements. This effect was mainly attributed to the ordered self-assembly of the heterostructured AgNPs on the CF surfaces.

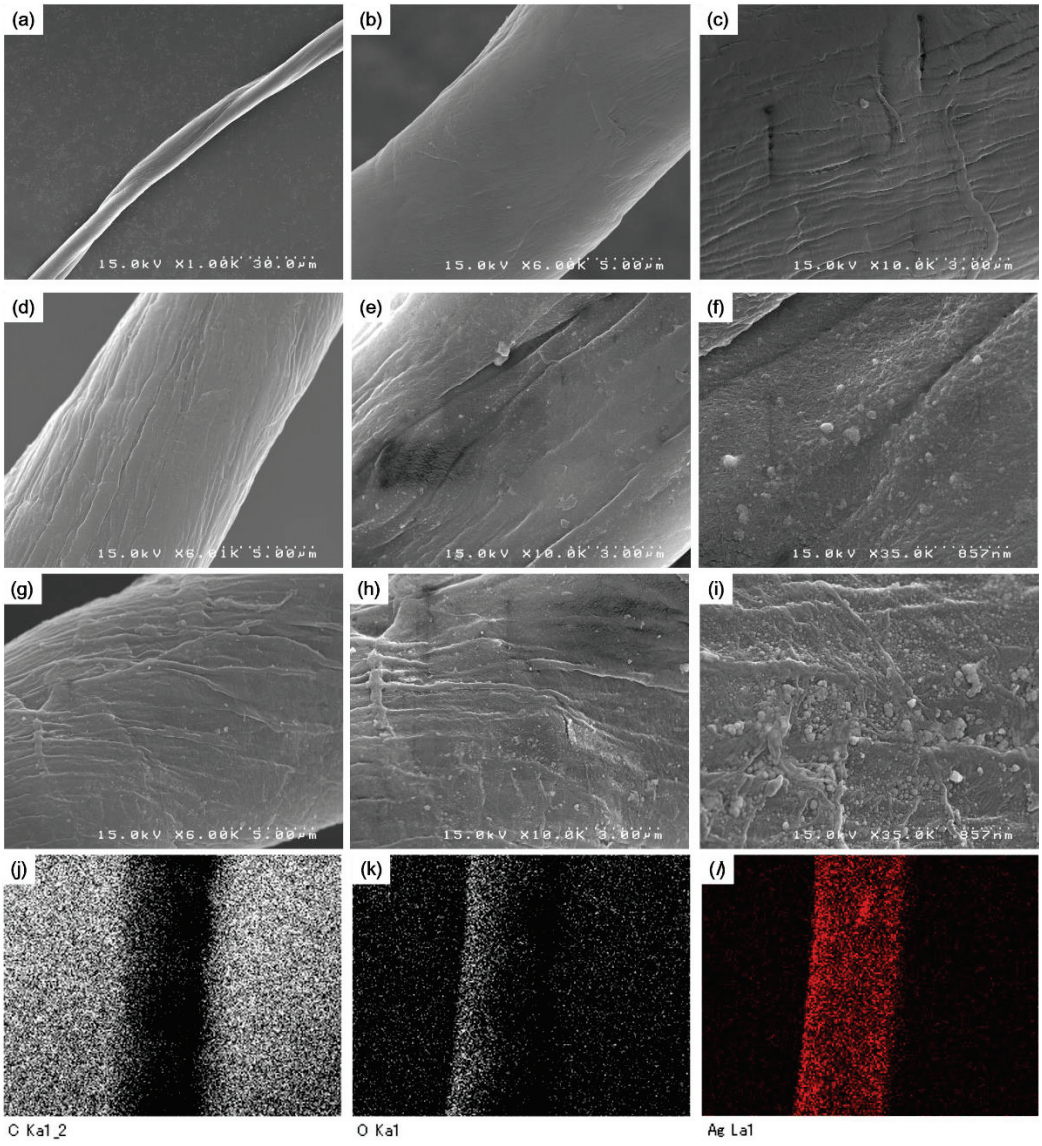

Figure 4.5 FESEM images of (a-c) pure cotton and (d-f) 3 mg/g and (g-i) 15 mg/g of

heterostructured AgNP-coated CFs. (j-l) Corresponding EDS element mapping images showing the distribution of C, O, and Ag elements obtained from SEM (Ag content: 15 mg/g).

4.3.5 XPS and XRD analysis

Metallic NPs are prone to corrosion when transferred from water to oxygen (O_2)-rich air environment. Therefore, the capping of 3D-structured HBPAA and HBPAE serves another important purpose, i.e., the isolation of the NPs from O_2, with final improvement of the NPs' chemical stability. To verify the protective ability of the capping molecules, we conducted XPS spectra of pure cotton fibers and 3 mg/g and 15 mg/g of the heterostructured AgNP-coated CFs. Figure 4.6(a) shows the wide-scan XPS spectra of pure CFs and 3 mg/g and 15 mg/g of heterostructured AgNP-coated CFs. The pure CFs showed only C1s and O1s peaks whereas N1s peaks at around 400 eV and Ag3d at around 374 and 368 eV were found in coated CFs, indicative of the attachment of heterostructured AgNPs. The intensities of N and Ag elements increase synchronously with increasing Ag content, suggesting their close integration. Moreover, the attachment of HBPAA and HBPAE could be further verified by analyzing the C1s XPS spectra of cotton and the 3 mg/g and 15 mg/g samples of heterostructured AgNPs as shown Figure 4.6(b). The C1s peaks of CFs could be classified into four categories as follows: C-C (284.5 eV), C-O (286.4 eV), C=O (287.8 eV), and O-C=O (289.0 eV). These peaks were attributed by cellulose and impurities such as long chain fatty acids. Notably, with rising Ag content of the coated CFs, the intensities of C-O and C=O augment, attributing to the increased content of HBPAA and HBPAE. The Ag3d deconvolution shown in Figure 4.6(c) and 4.6(d) demonstrated that the heterostructured

AgNPs maintained their metallic character when AgNPs were transferred from water to the organic cotton surface.

To further examine the chemical stability, 15 mg/g of heterostructured AgNP-coated cotton fibers was stored in air for 1 month and then assessed by XRD. After the 1-month storage, the diffraction peaks at 38.1°, 44.2°, 64.4°, and 77.4° remained unchanged. All the peaks can be indexed to the (111), (200), (220), and (311) diffractions of the standard face-centered-cubic phase metallic Ag (JCPDS No. 04-0783) without any characteristic diffractions peaks of AgO, indicating chemical stability.

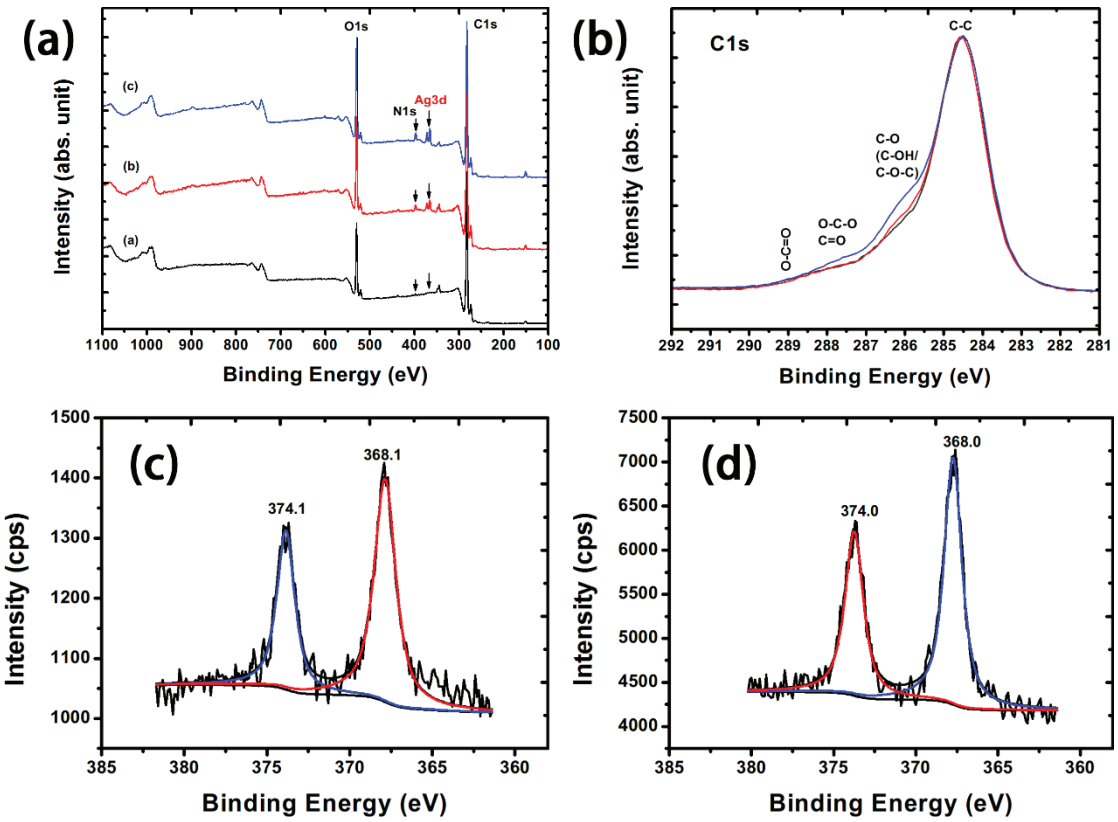

Figure 4.6 (a) Wide-scan and (b) C1s XPS spectra of pure CFs (black) and 3 mg/g (red)

and 15 mg/g (blue) of heterostructured AgNP-coated CFs and Ag3d XPS spectra of (c) 3 mg/g and (d) 15 mg/g of heterostructured AgNP-coated CFs

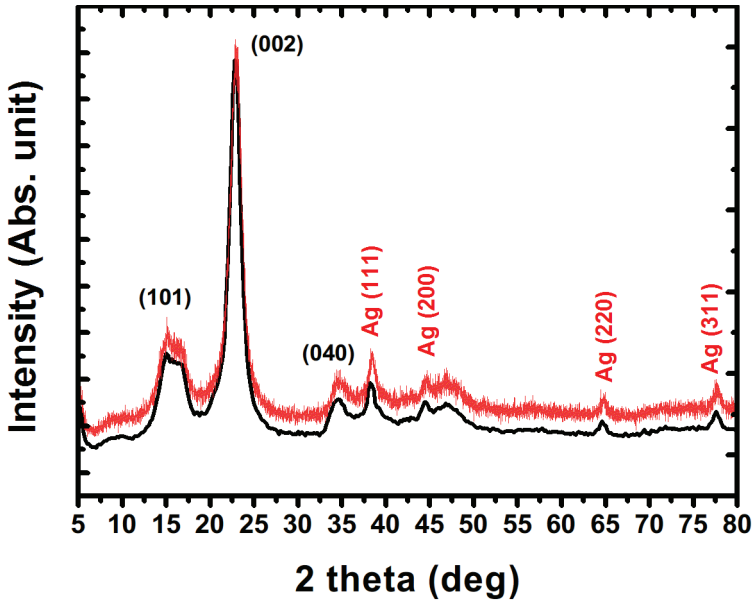

Figure 4.7 XRD of fresh prepared (black) heterostructured AgNP-coated CFs (15 mg/g) and (red) stored for one month.

4.3.6 Antimicrobial activity of heterostructured AgNP-coated CFs

The heterostructured AgNP-coated cotton fibers with Ag content from 1.5 mg/g to 15 mg/g were fabricated by the method described above, and their antibacterial activities against E. coli and S. aureus were quantitatively measured using the shake-flask method. Compared with biocompatible cotton fibers, the heterostructured AgNP-coated cotton fibers exhibited excellent antibacterial activities against E. coli and S. aureus (Table 1). The inhibition rates of E. coli and S. aureus both exceeded 99% when the Ag content was only 1.5 mg/g. As expected, the heterostructured AgNP-coated cotton fibers also showed Ag-content-dependent antimicrobial activity. The antibacterial rates against E. coli and S. aureus increased from 99.93% and 98.93% to 99.95 and 99.91%,

respectively, as Ag content increased from 1.5 mg/g to 3 mg/g. With further increase in Ag content to 6 and 15 mg/g, almost all of the E. coli and S. aureus were killed, indicating the materials' powerful antibacterial effects. Notably, the antibacterial function of the coated cotton was derived from the synergistic effects of the AgNPs and the capping molecules. The functionalization of NP surfaces with HBPAA and HBPAE endowed the NPs with molecular selectivity, affecting their surface binding to bacterial cells. Particularly, the HBPAA and HBPAE molecules on the AgNP surfaces can trap lipopolysaccharide- and peptidoglycan-containing E. coli and S. aureus onto the cotton fiber surface by electrostatic or hydrogen-bonding interactions because of their highly active amino and hydroxyl groups. Consequently, the NPs exhibited efficient antibacterial activities.

Table 4.1 The antibacterial activities of CFs and coated CFs against E. coli and S. aureus.

Cotton samples	Ag content (mg/g)	Antibacterial activities			
		E. coli		*S. aureus*	
		Surviving cells (cfu/mL)	% Reduction	Surviving cells (cfu/mL)	% Reduction
CFs	-	4.52×10^{6}	-	1.37×10^{7}	-
Coated CFs	1.5	1.89×10^{2}	99.93	3.64×10^{3}	98.93
	3	1.35×10^{2}	99.95	3.06×10^{2}	99.91
	4.5	56	99.98	1.36×10^{2}	99.96

	6	31	99.99	37	99.99
	15	0	100	0	100

4.4 Conclusions

Heterostructured AgNP-coated cotton fibers with tunable Ag content were fabricated by an eco-friendly approach through supramolecular cooperative self-assembly of mutually recognized HBPAA/AgNPs and HBPAA/AgNPs. The as-synthesized HBPAA/AgNPs and HBPAE/AgNPs possessed opposite charges and high density of amino and hydroxyl groups, respectively, which were capable of forming strong electrostatic and intermolecular hydrogen-bonding interactions. The generation of a special heterostructured coating was dependent on two important characteristics. One is the good binding affinity of the HBPAA/AgNPs toward cotton cellulose derived from their dense functional amino groups. This attribute rendered the initial self-assembly between the HBPAA/AgNPs and cotton fibers possible. The other attribute is the ability of the HBPAA/AgNPs and HBPAE/AgNPs to mutually recognize and combine through ultra-strong supramolecular interactions. Therefore, the two distinct AgNPs could cooperatively self-assemble onto the cotton surface through a well-designed step-by-step assembly process. Specifically, heterostructured AgNP-coated cotton fibers were fabricated by the circular incubation of cotton fibers with HBPAA/AgNPs and HBPAE/AgNPs at room temperature. By carefully controlling the AgNP concentration and incubation time, the complete adsorption of heterostructured AgNPs on cotton fibers could be achieved. Further studies showed that the cooperative self-assembly maintained their high efficiency even after five cycle treatments. FESEM measurement suggested that the constructed heterostructured AgNP coating showed good uniformity, although a fraction of Ag nanoclusters exited. XPS and TEM analyses demonstrated the good chemical stability of AgNPs after spatial transfer from water to the organic solid surface, probably owing to the excellent protection afforded by HBPAA and HBPAE.

Our antibacterial tests showed that the fabricated heterostructured AgNP-coated cotton fibers exhibited Ag-content-dependent and tunable antibacterial ability because the Ag content in the cotton fibers could be precisely controlled. In summary, the advantages of cooperative self-assembly technology include environmental friendliness, precise control of Ag content, and high self-assembly capacity, indicating their potential application in antibacterial textiles.

References:

[1] Lu Y, Sathasivam S, Song J, Crick CR, Carmalt CJ, Parkin IP. Repellent materials. Robust self-cleaning surfaces that function when exposed to either air or oil. Science. 2015;347:1132-5.

[2] Hsu P-C, Liu X, Liu C, Xie X, Lee HR, Welch AJ, et al. Personal Thermal Management by Metallic Nanowire-Coated Textile. Nano Letters. 2015;15:365-71.

[3] Liu N, Ma W, Tao J, Zhang X, Su J, Li L, et al. Cable-Type Supercapacitors of Three-Dimensional Cotton Thread Based Multi-Grade Nanostructures for Wearable Energy Storage. Advanced materials. 2013;25:4925-31.

[4] Zeng W, Shu L, Li Q, Chen S, Wang F, Tao X-M. Fiber-Based Wearable Electronics: A Review of Materials, Fabrication, Devices, and Applications. Advanced materials. 2014;26:5310-36.

[5] Khan Y, Ostfeld AE, Lochner CM, Pierre A, Arias AC. Monitoring of Vital Signs with Flexible and Wearable Medical Devices. Advanced materials. 2016.

[6] Eckhardt S, Brunetto PS, Gagnon J, Priebe M, Giese B, Fromm KM. Nanobio silver: its interactions with peptides and bacteria, and its uses in medicine. Chemical reviews. 2013;113:4708-54.

[7] Schoen DT, Schoen AP, Hu L, Kim HS, Heilshorn SC, Cui Y. High Speed Water Sterilization Using One-Dimensional Nanostructures. Nano Letters. 2010;10:3628-32.

[8] Levard C, Hotze EM, Lowry GV, Brown GE. Environmental Transformations of Silver Nanoparticles: Impact on Stability and Toxicity. Environmental science & technology. 2012;46:6900-14.

[9] Xu S, Chen S, Zhang F, Jiao C, Song J, Chen Y, et al. Preparation and controlled coating of hydroxyl-modified silver nanoparticles on silk fibers through intermolecular

interaction-induced self-assembly. Materials & Design. 2016;95:107-18.

[10] Abidi N, Hequet E, Cabrales L, Gannaway J, Wilkins T, Wells LW. Evaluating cell wall structure and composition of developing cotton fibers using Fourier transform infrared spectroscopy and thermogravimetric analysis. J Appl Polym Sci. 2008;107:476-86.

Chapter 5
Fabrication of hierarchical structured Fe_3O_4 and Ag nanoparticles dual-coated silk and TiO_2 nanoparticle-coated cotton through self-assembly

Chapter 5 Fabrication of hierarchical structured Fe_3O_4 and Ag nanoparticles dual-coated silk and TiO_2 nanoparticle-coated cotton through self-assembly

5.1 Introduction

In Chapter 4, we demonstrated a cooperative self-assembly technology for fabrication of heterostructured silver nanoparticle (AgNP)-coated CFs through functionalization of surfaces of NPs with mutually recognized HBPAA and HBPAE molecules. Actually, this technology can be extended to coat various heterogeneous inorganic NPs on biological fibers. In the present work, we demonstrate a new preparation methodology for special hierarchical structured Fe_3O_4 nanoparticles (Fe_3O_4NPs)/Ag nanoparticles (AgNPs) dual-coated silk fibers (SFs) through a simple cooperative self-assembly technology. The supramolecular self-assembly technology can also be used to coating other inorganic nanoparticles [here is Titanium dioxide nanocrystals (TiO_2 NCs)] onto biological fibers.

Here we prepared novel hierarchical structured Fe_3O_4NPs/AgNPs dual-coated SFs through a unique cooperative self-assembly technology using positively-charged HBPAA/AgNPs and negatively-charged citric acid-functionalised Fe_3O_4NPs (CA/Fe_3O_4NPs) as building blocks. Specifically, Fe_3O_4NPs/AgNPs dual-coated SFs were constructed by sequential impregnation with solutions of HBPAA/AgNPs and CA/Fe_3O_4NPs. The as-prepared hierarchical structured SFs were finally characterized by XRD, FESEM, and VSM.

We also prepared TiO_2 NC-coated cotton fabrics by supramolecular self-assembly. Water-soluble hydroxyl-terminated hyperbranched poly(amino-ester) (HBPAE)-capped titanium dioxide nanocrystals (TiO_2 NCs) were synthesized for coating a cotton fabric via a hyperbranched poly(amidoamine) (HBPAA)-mediated self-assembly strategy in order to produce a controllable and uniform TiO_2 coating on the cotton surface. As-prepared TiO_2 NCs were characterized by TEM, fFESEM, and XRD. It was demonstrated that hydroxyl-modified TiO_2 NCs were egg-shaped and had a narrow size distribution. A TiO_2 NC-coated cotton fabric was prepared by sequential impregnation with solutions of HBPAA and TiO_2 NCs. It was shown that HBPAA were chemically bound to the cotton surface. FESEM and XRD characterizations demonstrated that TiO_2 NCs could self-assemble on a cotton fabric efficiently and distributed uniformly on the cotton surface.

5.2 Experimental

5.2.1 Synthesis of HBPAA/AgNPs and CA/Fe_3O_4NPs

Positively charged HBPAA/AgNPs were synthesized by adding 48 mL of HBPAA solution (0.21 mM) to 2 mL of $AgNO_3$ (46.3 mM) at 35 °C using a well-described procedure as shown in Chapter 2. The reaction mixture was slowly heated to 90 °C and kept stirring at 90 °C for 3 h. This resulting solution was dialyzed against distilled water for 72 h.

Negatively charged CA/Fe_3O_4NPs were synthesized by adding 4 mL of 1M $FeCl_3$ solution, and 1 mL of 2 M $FeCl_2$ in 2 M HCl solution into 50 mL of water and temperature was increased to 70 °C. 0.8 M ammonia aqueous solution was instantaneously added to the mixture and kept this temperature for 20 min. Then 5 mL

of 2 mM CA was added to the reaction mixture and heated for 60 min at 90 °C. The as-prepared Fe_3O_4NPs were separated, purified, and redissolved in 200 mL of water [1].

5.2.2 Synthesis of HBPAE-capped TiO_2 NCs

HBPAE-capped TiO_2 NCs were synthesized using a modified hydrothermal method. Typically, 30 mL of ethanol solution containing titanium(IV) isopropoxide (35.2 mmol) and acetic acid (10 mmol) was dropwise added into 30 mL of water/ethanol mixed solution under vigorous stirring at 35 ^oC. The mixed solution was stirred for 1h and sequentially aged for 12 h to form a TiO_2 gel. After the formation of the three-dimensional network gel, 0.2 mol of HBPAE in 20 mL distilled water was added into the mixture, continuously stirring for 1 h, and finally transferred into a 100 mL Telfon-lined stainless-steel autoclave. The system was then heated at 200 °C for 10 h. The obtained yellow precipitates were centrifuged and repeatedly washed with deionized water. The resultant TiO_2 NCs were redispersed in deionized water.

5.2.3 Preparation of Fe_3O_4NPs/AgNPs dual-coated SFs by the cooperative self-assembly technology

SFs were added into 100 mL of AgNP solution (0.185 mM, pH=8.4) and kept at 95 °C with constant magnetic stirring for 30 min. The prepared HBPAA/AgNP-coated SFs were rinsed in deionized water several times and air-dried. Next, HBPAA/AgNP-coated SFs were added into 50 mL of Fe_3O_4 colloid solution (1.6mM, pH=6.3) and kept at 35 °C for 10 min. The resulting dual-coated sample was repetitively washed with water and ethanol, and dried under vacuum for 5 h at 50 °C.

5.2.4 Self-assembly of HBPAE-capped TiO_2 NCs on HBPAA-modified cotton fabric

The cotton fabric was first activated by alkaline treatment according the previous report [2]. Next, 2 g of activated cotton fabric was added into 100 mL of 10 g/L HBPAA solution at 98 ^{o}C for 1 h. The obtained HBPAA-modified cotton fabric was rinsed with deionized water several times and air-dried, and then immersed subsequently in the solution of TiO_2 NCs (100-340 mg/L) and held at 60 ^{o}C in water bath for 1 h with constant stirring. The resulting TiO_2 NC-coated cotton fabric was washed with deionized water several times and oven- dried. The TiO_2 content on the cotton fabric was estimated by subtraction method, i.e., the difference in TiO_2 NC concentration in the solution before and after the assembly. The TiO_2 NC concentration in the solution was quantified by digesting the sample in HNO_3/HF mixture solution and then performing ICP-AES measurements (Vista MPX ICP-AES spectrometer) [3].

5.2.5 Sample characterization

Fe_3O_4NPs/AgNPs dual-coated SFs were analyzed by XRD (Bruker, Germany, D8 advance). FESEM (HITACH, Japan, S-5000), and vibrating sample magnetometer (VSM, USA, Lakeshore7307- 9309).

The morphology and size of the TiO_2 NC-coated cotton fabrics were observed using FEI Tecnai G220 TEM and FESEM (Hitachi S-4800 and S-5000) systems. UV-vis spectra were obtained using a Shimadzu UV-2700 spectrophotometer. FTIR spectra were recorded using a Perkinlmer Spectrum 100 FTIR spectrometer. Powder XRD patterns of the samples were obtained using a Shimadzu XRD-6100 X-ray diffractometer operated at 1320 W power (40 kV, 33 mA) and equipped with a Cu Kα radiation source.

5.3 Results and discussion

5.3.1 Fabrication of hierarchical structured Fe_3O_4 and Ag nanoparticles

Hierarchical structured Fe_3O_4NPs/AgNPs dual-coated SFs were constructed using a cooperative self-assembly technique to sequentially coat positively charged AgNPs and negatively charged Fe_3O_4NPs on the surface of SFs. The potential mechanism is presented in Scheme 5.1. The positively charged HBPAA/AgNPs played a significant role in the assembly. Due to the cationic character of HBPAA, HBPAA/AgNPs were endow with positive charges with zeta potential of +38 mV, which can be assembled on the surface of negatively charged SFs through electrostatic attraction in alkaline medium. In addition, the surface of AgNPs was capped by HBPAA molecules, which could introduce positively charges to the surface of the fibers. Thus negatively charged Fe_3O_4NPs could be adsorbed on the AgNP surface through intermolecular electrostatic interactions.

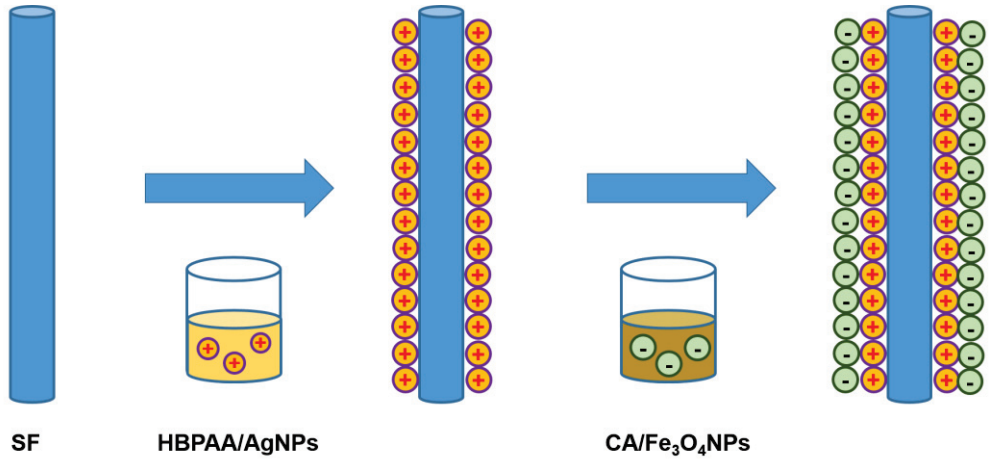

Scheme 5.1 Procedures of sequent assembly of HBPAA/AgNPs and CA/Fe_3O_4NPs on the surface of SFs.

The crystalline structures of SFs, HBPAA/AgNP-coated SFs, and Fe_3O_4NPs/AgNPs dual-coated SFs were firstly studied using XRD (Figure 5.1). All

XRD patterns display typical diffraction peaks at around 9.4°, 20.5°, and 24.3°, which can be attributed to the β-sheet crystalline structure of silk fibroin [4]. In the cases of the XRD patterns of HBPAA/AgNP-coated SFs and Fe_3O_4NPs/AgNPs dual-coated SFs, expect for the diffraction peak of silk fibroin, the diffraction peaks at 38.1°, 44.2°, 64.4°, and 77.4° can be respectively indexed to (111), (200), (220), and (311) diffractions of the face-centered-cubic phase metallic Ag (JCPDSNo.04-0783), indicating the attachment of metallic AgNPs. However, Fe_3O_4NPs/AgNPs dual-coated samples exhibited additional diffraction peaks located at 30.2°, 35.5°, 57°,and 62.7°, which suggests face centered cubic structured Fe_3O_4NPs (JCPDSNo.65-3107) were adsorbed on the Ag surface. These findings indicate that both AgNPs and Fe_3O_4NPs have assembled on the SFs.

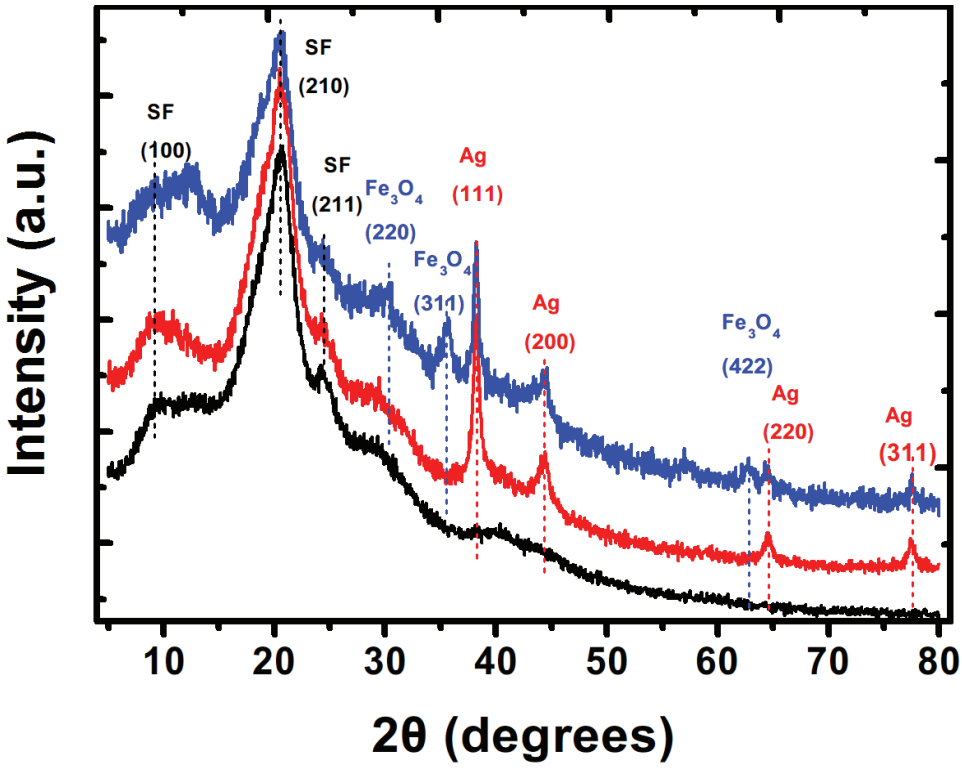

Figure 5.1 Representative XRD patterns of blank SFs (black), HBPAA/AgNP-coated SFs (red), and Fe_3O_4NPs/AgNPs dual-coated SFs (blue).

The surface morphology of SFs is imaged by FESEM, as depicted in Figure 5.2. The blank SF displayed a smooth surface with visible grooves aligned along the fiber axis [Figure 5.2(a) and 5.2(b))]. HBPAA/AgNP-coated SFs are displayed in Figure 5.2(c) and 5.2(d). Densely-wrapped spherical NPs with diameters in the range of 1–50 nm were observed on the surface of the SFs. It can therefore be concluded that the spherical NPs observed on the surface of SF [Figure 5.2(d)] should be easily contributed to the attachment of HBPAA/AgNPs. Notably, these assembled AgNPs were single-layered and monodispersed, which was due to the combined effects of both steric hindrance and electrostatic repulsion among HBPAA/AgNPs. Similar to the HBPAA/AgNP-coated SF, high dense NPs were also found on the surface of Fe_3O_4NPs/AgNPs dual-coated SF as shown in Figure 5.2(e) and 5.2(f). In order to confirm their hierarchical structure, HBPAA/AgNP-coated SFs were partially impregnated with Fe_3O_4NP solution in the experiment. The interface between impregnation area and non-impregnation area was investigated by FESEM. As displayed in the inset of Figure 5.2(f), an obvious hierarchical structure was observed. In comparison with HBPAA/AgNP-coated SF, a second NP coating was formed over the Ag coating after treatment with Fe_3O_4NPs solution, indicating Fe_3O_4NPs were successfully assembled onto the surface of HBPAA/AgNPs through intermolecular electrostatic attractions between the positively charged HBPAA/AgNPs and negatively charged CA/Fe_3O_4NPs.

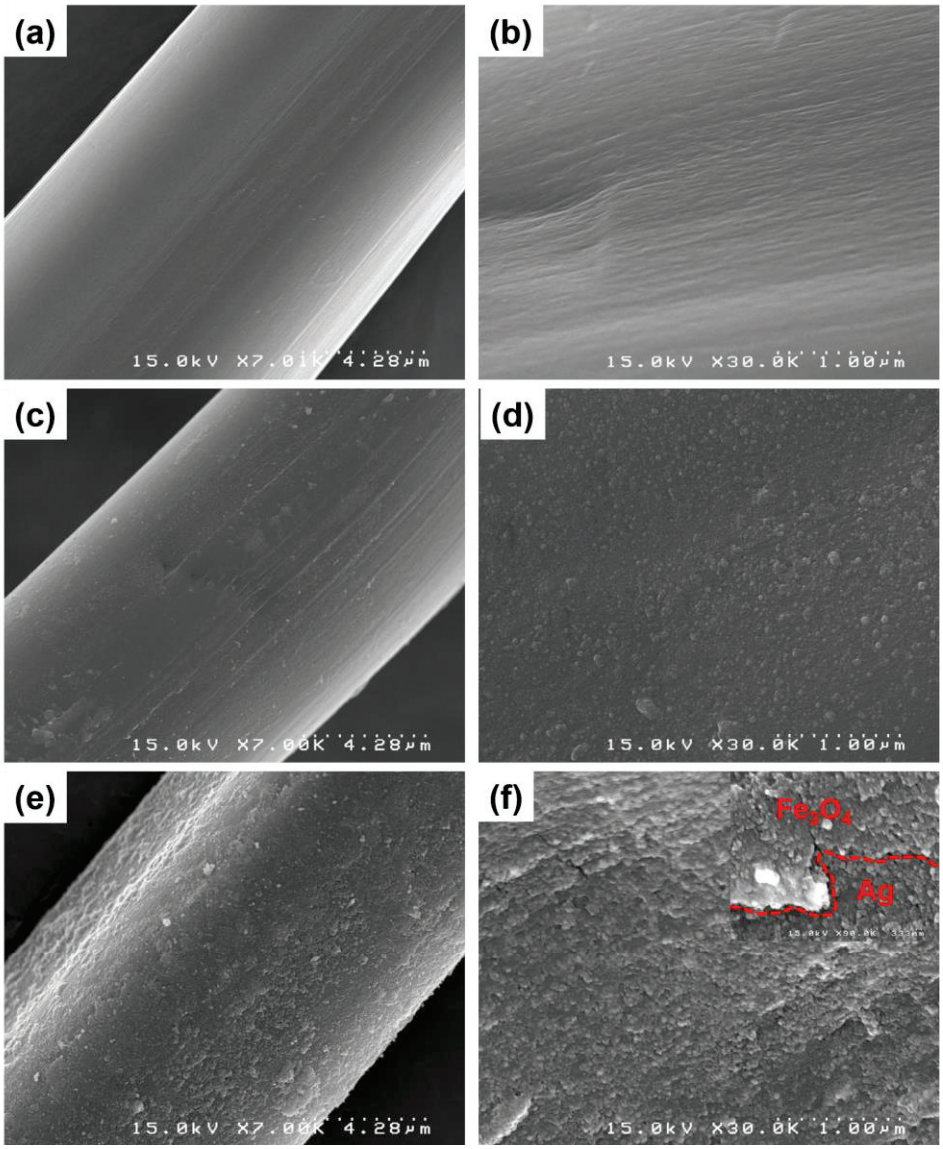

Figure 5.2 FESEM images of the (a × 7,000, b × 30,000) blank SF, (c × 7,000, d × 30,000) HBPAA/AgNP-coated SF and (e × 7,000, f × 30,000) Fe_3O_4NPs/AgNPs dual-coated SF. The inset of Figure 5.2(f) shows the interface between impregnation area (above the red line) and non-impregnation area (below the red line). The magnification of inset is 90,000.

The magnetic Fe_3O_4NPs/AgNPs dual-coated SFs were exhibited by the attraction to a magnet as shown in Figure 5.3(a). Dual-coated SFs could be attracted onto the magnet

and lifted against gravity, indicative of their excellent magnetic property. The magnetic property of the Fe_3O_4NPs/AgNPs dual-coated SFs was also quantitatively determined by VSM at room temperature, and the hysteresis loop was presented in Figure 5.3(b). It is noted that the Fe_3O_4NPs/AgNPs dual-coated SFs showed slightly ferromagnetic property revealed by the magnified plot in the inset, with the coercivity (Hc) of 8.44 Oe and a remanent magnetization of 0.024 emu/g. Their weak ferromagnetic behavior may be due to the slight agglomeration of a small portion of Fe_3O_4NPs during the assembly process. In addition, the as-prepared Fe_3O_4NPs/AgNPs dual-coated SFs exhibited good magnetic value with saturation magnetization (Ms) of nearly 3.21 emu/g in comparison with reported literature [5,6], which is due to the high dense Fe_3O_4NPs attached on the SF surface.

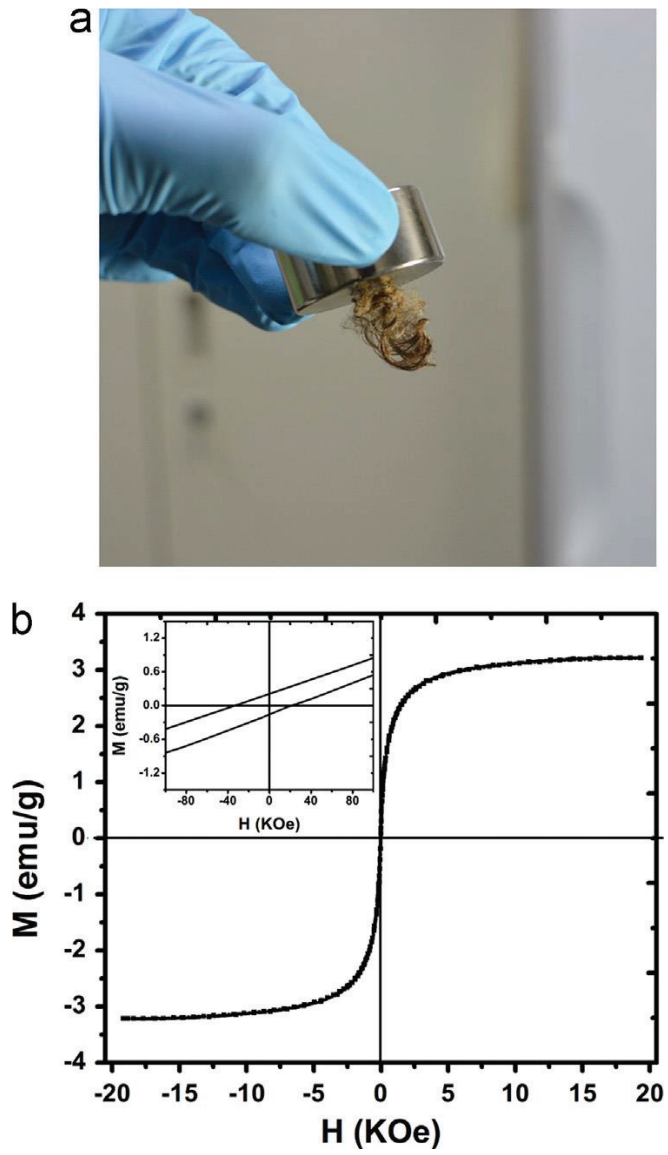

Figure 5.3 (a) Photo of the magnetic property of Fe_3O_4NPs/AgNPs dual-coated SFs under an external magnet, and (b) magnetic hysteresis loop of the Fe_3O_4NPs/AgNPs dual-coated SFs at room temperature.

5.3.2 HBPAA-mediated self-assembly of hydroxyl-modified anatase TiO_2 nanocrystals on cotton fabric

HBPAE-capped TiO_2 NCs were prepared by adding the desired amount of HBPAE solution to the TiO_2 gel made in an acidic medium followed by hydrothermal reaction.

The TiO_2 colloids prepared in acidic media are positively charged. They act as a support to adsorb HBPAE. Thus the negatively charged HBPAE can adsorb strongly onto the TiO_2 NC surface. Upon hydrothermal dissolution-recrystallization reaction, well-crystallized TiO_2 NCs are obtained in the liquid solution.

The light absorption property of HBPAE-capped TiO_2 NCs was first investigated by UV-vis spectroscopy. As shown in Figure 5.4(a), TiO_2 NCs exhibited a strong absorption band below 380 nm, corresponding to the band gap energy of TiO_2 NCs (3.2 eV). Moreover, the as-synthesized TiO_2 NCs in the presence of aqueous solution exhibited a transparent blue color [inset of Figure 5.4(a)], in accordance with the optical feature of TiO_2 NCs reported in the literature [7]. It is noted that blue coloration is the characteristic of free conduction band electrons in TiO_2, derived from oxygen vacancies or titanium interstitials that are formed during the synthetic process [8]. Furthermore, TiO_2 NCs exhibited good water solubility. This may be due to the electrostatic repulsion and steric hindrance among hydroxyl-functionalised nanoparticles.

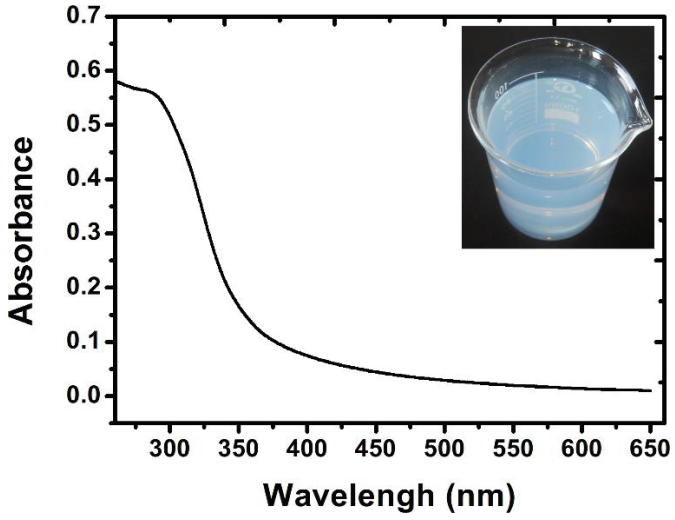

Figure 5.4 UV-vis adsorption spectra of TiO_2 colloidal solution. The inset of Figure 5.4 displays a typical photograph of the as-prepared TiO_2 solution.

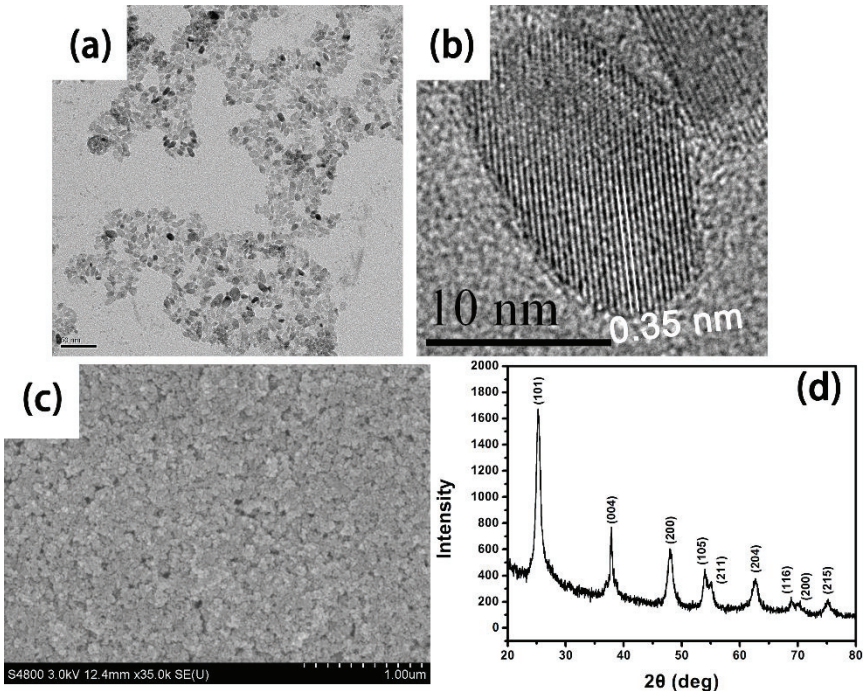

Figure 5.5 TEM, (b) HRTEM, and (c) FESEM images of TiO_2 NCs and the (d) XRD pattern of TiO_2 NCs.

Figure 5.5(a) and 5.5(b) show TEM and HRTEM images of the as-prepared TiO_2 NCs. It is clearly revealed that the TiO_2 NCs were monodisperse nanocrystals. Furthermore, the as-prepared TiO_2 NCs were egg-shaped and had a width of around 10 nm and a length of 17.6 nm. The small size was probably due to the volume restriction effect of HBPAE micelles [9]. The HRTEM image of TiO_2 NCs showed the unidirectional lattice fringes of the (101) plane with a lattice spacing of 0.35 nm (JCPDS No. 21-1272) [Figure 5.5(b)], affirming a preferential crystal growth along the (101) direction. Figure 5.5(c) displays the FESEM image of TiO_2 NCs. No large nanoparticles were observed, indicative of their uniform size.

The crystallinity of the as-synthesized TiO_2 NCs is further verified by XRD. As shown in Figure 5.5(d), broad reflection peaks were observed at 2θ values of

approximately 25.2, 37.9, 48, 53.9, 55.1, 62.8, 68.9, 70.4, and 75°, which can be indexed to diffraction peaks from the (101), (004), (200), (105), (211), (204), (116), (220), and (215) planes of anatase (JCPDS No. 21-1272). Note that there are no additional diffraction peaks corresponding to rutile or brookite phases, indicating their pure anatase phase.

The modification of the surface chemistry of cotton fibers is necessary prior to the assembly of TiO_2 NCs on a cotton surface. A cotton fiber is mainly composed of cellulose with repeating units of 1, 4-D-glucopyranose. Some side-chain OH groups of cellulose can be typically ionized in aqueous phase; thus, a cotton fiber carries certain negative surface charges, which exhibits electrostatic repulsion for negatively charged TiO_2 NCs. To improve the surface affinity of cotton, Amino-terminated HBPAA is employed as a surface modifier. As a three-dimensional cationic polymer with dense amino groups on the outer surface, the positively charged HBPAA can readily bind to a cotton surface through strong electrostatic and hydrogen-bonding interactions. The anchored HBPAA can further serve as the cationic template for attracting negatively charged hydroxyl-functionalised TiO_2 NCs through intermolecular interactions.

The modification of cotton with HBPAA was achieved by impregnating cotton fabrics with HBPAA solution at elevated temperatures. The HBPAA anchored on cotton surface was detected by FTIR. The FTIR spectra of a pure cotton fabric showed typical characteristic peaks of cellulose (the black curve of Figure 5.6). The broad band at 3150-3500 cm^{-1} was attributed to the O-H stretching vibration. Two weak peaks at 1918 and 2852 cm^{-1} resulted from the symmetric stretching vibrations of methylene groups. The characteristics of IR bands of the C-H, O-H, C-O, and C-O-C vibrations were observed in the range of 1500-900 cm^{-1}. The absorption peaks at 897 and 1159 cm^{-1}

correspond to the C-O-C stretching vibrations at β-d-glucoside linkage [10]. After modification, the overall spectra of the HBPAA-modified cotton showed the same pattern [the red curve in Figure 5.6(a)], suggesting that the surface modification had no effect on the chemical structure of cotton. Nevertheless, some clues of chemical interactions between the HBPAA and the cotton were found in the bands of the O-H stretching, CH_2 stretching, and C-O-C/C-O stretching vibrations. As shown in Figure 5.6(b), the broad band between 3700 and 3000 cm^{-1} was assigned to the O-H stretching vibration, which corresponds to intramolecular hydrogen bonds of O(2)H···O(6) and O(3)H···O(5) (3460-3410 cm^{-1} and 3375-3340 cm^{-1}), and intermolecular hydrogen bonding of O(6)H···O(3) (3310-3230 cm^{-1}) in the cellulose crystalline structure [11, 12]. The decrease in the intensity of the O-H stretching vibration in HBPAA-modified cotton (3330-3230 cm^{-1}) could be attributed to the disruption of intra- and intermolecular hydrogen bonds after the binding of HBPAA. The intensities of the CH_2 asymmetric and symmetric stretching vibration regions located at around 2982-2851 cm^{-1} as well as the absorption band in the range of 1600-1000 cm^{-1} slightly increased, probably resulting from the superposition of the adsorption of CH_2 asymmetric and symmetric stretching vibrations, amide I, amide II, and amide III from the HBPAA. Conversely, the intensities of the adsorption peaks of C(6)-O at around 1028 and 984 cm^{-1} decreased while the intensity of the adsorption peak of the C-O-C at 1053 cm^{-1} remained unchanged [Figure 5.6(c)] [11, 12]. This is probably attributed to the chemical interactions between amino groups in HBPAA and C(6)-OH groups in cotton. In summary, HBPAA chemically bound to the cotton fabric and had no effect on its chemical structure.

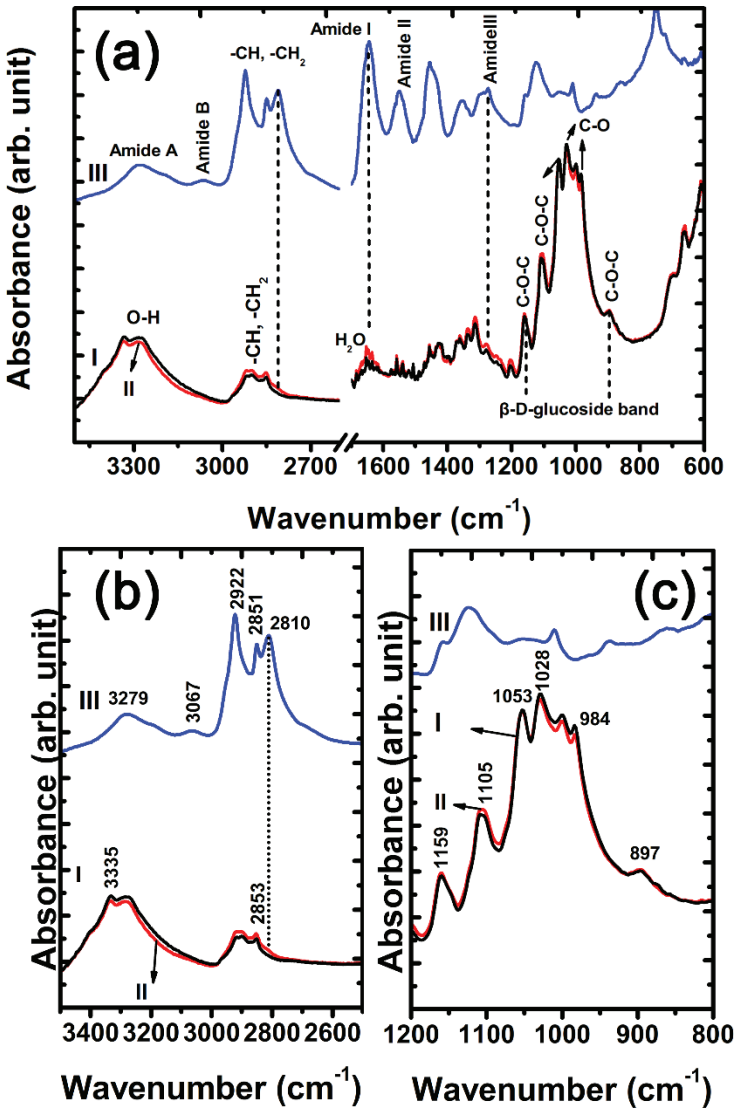

Figure 5.6 FTIR spectra of (I) cotton fabric, (II) HBPAA-modified cotton fabric, and (III) HBPAA.

TiO_2 NCs were self-assembled onto the cotton fabric by HBPAA-mediated self-assembly strategy. Contributed by strong electrostatic and hydrogen bonding interactions between HBPAA and HBPAE, the HBPAA-modified cotton fabric could trap HBPAE-capped TiO_2 NCs through intermolecular interactions. To evaluate the assembly ability of TiO_2 NCs, the adsorption ability of TiO_2 NCs on cotton as a function of the concentration of TiO_2 NC solution was investigated. As shown in Table

5.1, the TiO_2 content was TiO_2 NC concentration-dependent. By increasing the of TiO_2 NC concentration from 100 to 340 mg/L, the TiO_2 content increased from 5 to 11.2 mg/g. The adsorption efficiency of TiO_2 NCs decreased from nearly 100 to 65.9 %. Notably, the pure cotton fabric showed little TiO_2 adsorption (4.6% for 100 mg/L), indicative of poor chemical interactions. This probably results from the electrostatic repulsion between the cotton cellulose and the HBPAE.

Table 5.1 TiO_2 contents of cotton fabrics as a function of TiO_2 NC concentration.

Sample	Concentration of TiO_2 NCs (mg/L)	TiO_2 content of fabric (mg/g)	Loading efficiency (%)
Pure cotton	100	0.23	4.6
Modified cotton	100	~5	~100
	180	8.9	98.9
	260	10.8	83.1
	340	11.2	65.9

Cotton cellulose consists of repeated cellobiose units joined by β-(1,4) linkage into chains. The polymerization degree ranges from 1×10^4 to 1.5×10^4. Several cellulose chains are combined to form an elementary fibril with a diameter of 3.5 nm. Elementary fibrils are assembled into microfibrils with a diameter ranging from 10 to 30 nm. The microfibrils further form macrofibrils that range from 0.1 to 1.5 μm in diameter [13]. The characteristic microstructure of cotton fibers can be observed by FESEM. As displayed in Figure 5.7(a), the convolution of cotton fibers was clearly observed at a low magnification (1,000 times). The cotton fibers showed dense paralleled macrofibrils with diameters of around 0.4 μm and a clean and smooth surface at a magnification of

10,000 × [Figure 5.7(b)], in good agreement with the morphology characteristics of cotton fibers. On the contrary, HBPAA-modified cotton fibers exhibited a smoother surface [Figure 5.7(c)], probably due to the attachment of the HBPAA. After the assembly of TiO_2 NCs onto the cotton surface, numerous well-dispersed nanoparticles were found on the surface of cotton fibers compared with HBPAA-modified cotton fibers. The diameter of the spherical nanoparticles was found to vary from 10 to 100 nm, which was in line with the morphological features of TiO_2 NCs determined by TEM. Note that HBPAA was responsible for the attachment of TiO_2 NCs on the surface of cotton fibers.

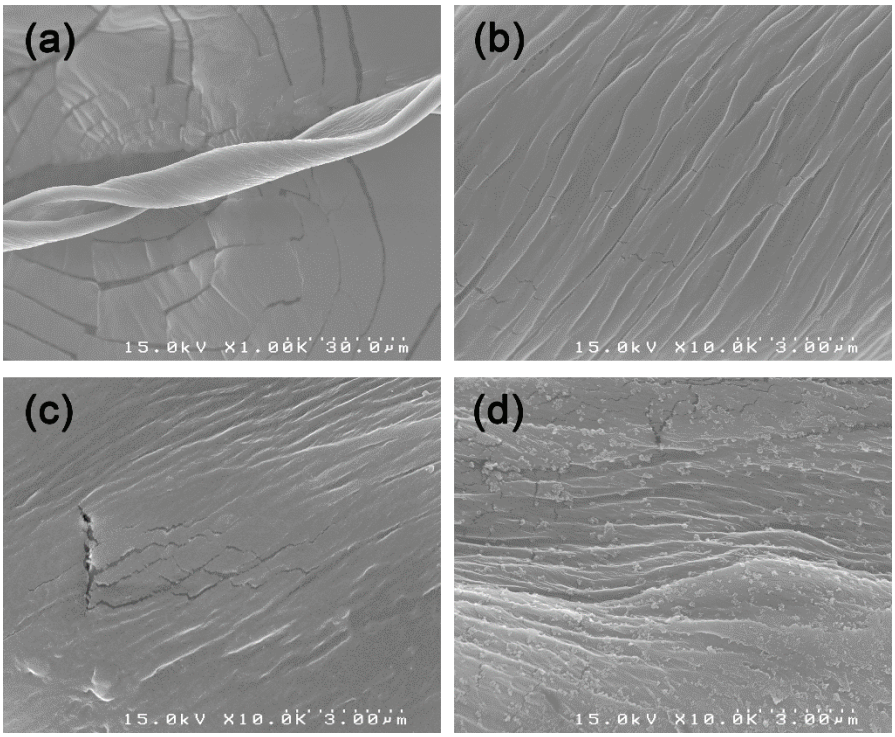

Figure 5.7 FESEM images of (a × 1000, b × 10000) pristine, (c × 10000) HBPAA-modified, and (d × 10000) TiO_2 NC-coated cotton fiber (5 mg/g).

The crystalline structure of the TiO_2 NC-coated cotton fabric was studied by X-ray diffraction analysis. Figure 5.8 shows representative XRD patterns of pristine,

HBPAA-modified, and TiO_2 NC-coated cotton fabrics. The peaks at 2θ values of around 15.2 , 16.7, 23, and 34.5° respectively correspond to the (101), ($10\bar{i}$), (002), and (040) planes of the diffractions of the cellulose I crystalline structure of cotton fibers (JCPDS. No. 03-0226). After coated with TiO_2 NCs, three reflection peaks centered at around 25.2, 38, and 48° appeared and all diffraction peaks could be indexed to the (101), (004), and (200) diffractions of the anatase phase of TiO_2, which were consistent with the values in the standard card (JCPDS No. 21-1272). This indicates the attachment of TiO_2 NCs on cotton fibers.

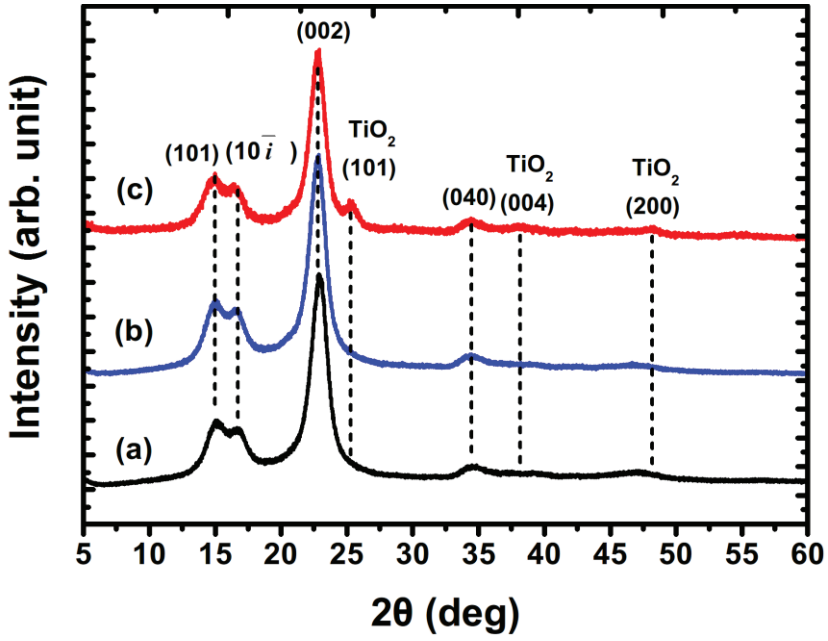

Figure 5.8 XRD patterns of (a) pristine, (b) HBPAA-modified, and (c) TiO_2 NC-coated cotton fabric (5 mg/g).

5.4 Conclusions

Fe_3O_4NPs/AgNPs dual-coated SFs were prepared through a special cooperative self-assembly technology using positively charged HBPAA/AgNPs and negatively charged CA/Fe_3O_4NPs as building blocks. Results from XRD showed that HBPAA/AgNPs and CA/Fe_3O_4NPs were anchored onto the surface of SFs. FESEM displayed that the high dense Fe_3O_4NPs and AgNPs hierarchically distributed on the fiber surface. The as-prepared dual-coated SFs exhibited excellent magnetic property, which can be attributed to the high dense Fe_3O_4NPs that were assembled on the surface of SFs.

Supramolecular self-assembly can be also used to fabricate TiO_2 NC-coated cotton. First, HBPAE-modified TiO_2 NCs were synthesized via hydrolyzation followed by hydrothermal reaction in liquid phase, employing HBPAE as the capping agent. As-prepared anatase TiO_2 NCs were egged-shaped and exhibited a uniform morphology. To improve the binding affinity between HBPAE and cotton cellulose, HBPAA was anchored to cotton by simply impregnation of cotton with HBPAA aqueous solution at 98 ^oC. The binding of HBPAA onto cotton endowed the cotton surface with cationic charges and huge numbers of amino end groups, allowing further self-assembly of hydroxyl-modified TiO_2 NCs. The FESEM and XRD characterizations confirmed that TiO_2 NCs were well dispersed on the cotton surface, which was probably due to electrostatic repulsions among HBPAE-capped TiO_2 NCs. The as-prepared TiO_2 NP-coated cotton fabric is expected to be used in various applications such as antimicrobial, anti-UV, and self-cleaning textiles.

References

[1] Nigam S, Barick KC, Bahadur D. Development of citrate-stabilized Fe_3O_4 nanoparticles: conjugation and release of doxorubicin for therapeutic applications. J Magn Magn Mater. 2011;323:237–243.

[2] Varesano A, Rombaldoni F, Tonetti C, Di Mauro S, Mazzuchetti G. Chemical treatments for improving adhesion between electrospun nanofibers and fabrics. J Appl Polym Sci. 2014;131:39766.

[3] Ates M, Daniels J, Arslan Z, Farah I. Effects of aqueous suspensions of titanium dioxide nanoparticles on Artemia salina: assessment of nanoparticle aggregation, accumulation, and toxicity. Environ Monit Assess. 2013;185:3339-48.

[4] Lin N, Meng Z, Toh GW, Zhen Y, Diao Y, Xu H, et al. Engineering of fluorescent emission of silk fibroin composite materials by material assembly. Small. 2015; 11:1205–14.

[5] Wang JT, Li LL, Feng L, Li JF, Jiang LH, Shen Q. Directly obtaining pristine magnetic silk fibers from silkworm. Int J Biol Macromol. 2014;63:205–209.

[6] Chang S, Dai Y, Kang B, Han W, Chen D. Fabrication of silk fibroin coated ZnSe: Mn^{2+} quantum dots under -radiation and their magnetic properties. Solid State Commun. 2009;149:1180–83.

[7] Ahn SH, Chi WS, Park JT, Koh JK, Roh DK, Kim JH. Direct Assembly of Preformed Nanoparticles and Graft Copolymer for the Fabrication of Micrometer-thick, Organized TiO_2 Films: High Efficiency Solid-state Dye-sensitized Solar Cells. Adv Mater. 2012;24:519-22.

[8] Gordon TR, Cargnello M, Paik T, Mangolini F, Weber RT, Fornasiero P, et al. Nonaqueous Synthesis of TiO_2 Nanocrystals Using TiF4 to Engineer Morphology,

Oxygen Vacancy Concentration, and Photocatalytic Activity. J Am Chem Soc. 2012;134:6751-61.

[9] Zhu B-K, Wei X-Z, Xiao L, Xu Y-Y, Geckeler KE. Preparation and properties of hyperbranched poly(amine-ester) films using acetal cross-linking units. Polym Int. 2006;55:63-70.

[10] Wei X, Lu Q, Sui X, Wang Z, Zhang Y. Characterization of the water-insoluble pyrolytic cellulose from cellulose pyrolysis oil. J Anal Appl Pyrol. 2012;97:49-54.

[11] Ciolacu D, Kovac J, Kokol V. The effect of the cellulose-binding domain from Clostridium cellulovorans on the supramolecular structure of cellulose fibers. Carbohyd Res. 2010;345:621-30.

[12] Oh SY, Yoo DI, Shin Y, Kim HC, Kim HY, Chung YS, et al. Crystalline structure analysis of cellulose treated with sodium hydroxide and carbon dioxide by means of X-ray diffraction and FTIR spectroscopy. Carbohyd Res. 2005;340:2376-91.

[13] Lee I, Evans BR, Woodward J. The mechanism of cellulase action on cotton fibers: evidence from atomic force microscopy. Ultramicroscopy. 2000;82:213-21.

Chapter 6
Conclusion

Chapter 6 Conclusion

Wastewater has been one of the most insurmountable problems in textile industry. Since the emerge and fast development of antimicrobial silver nanoparticle (AgNP)-coated textiles in recent several decades, AgNP-containing wastewater produced in the finishing process gradually poses a greater threat to the ecological environment than traditional organic dyes in textile industry because of their strong antimicrobial ability. Besides, although many nanocoating technologies have been developed to coat AgNPs on the surface of biological fibers, most of them are belong to top-down approaches. The precise control of Ag content and control of spatial arrangement of AgNPs on the fiber surface are still great challenges. To solve these problems, we developed three different supramolecular self-assembly technologies aiming to environmental-friendly coat AgNPs on biological fibers. The spontaneous arrangement of AgNPs on the fiber surface with good uniformity and mono-dispersity can achieve by controlling supramolecular forces including electrostatic attraction and hydrogen bonding interactions and electrostatic repulsion among NPs. The specific methodologies and related conclusion are as follows.

In Chapter 2, an environmental-friendly approach has been developed for preparation of AgNP-coated cotton, silk, and calcium alginate fibers by hyperbranched poly(amidoamine) (HBPAA)-guided assembly of AgNPs on the surface of biological fibers in aqueous solution. HBPAA-functionalized AgNPs (HBPAA/AgNPs) were synthesized in aqueous media using HBPAA as the reducing and capping agent. The self-assembly of HBPAA/AgNPs was realized by incubation of biological fibers in a colloidal solution of HBPAA/AgNPs. SEM and XPS characterizations demonstrated

that high density of metallic AgNPs were uniformly distributed on the fiber surface. The results of antibacterial tests indicated that the coated biological fibers exhibited high antibacterial activity against gram-positive and gram-negative bacteria.

In Chapter 3, we report an efficient and environmentally-friendly approach for the preparation of silver nanoparticle-coated silk fibers (SFs) through self-assembly of hyperbranched poly(amine-ester)s-modified AgNPs (HBPAE/AgNPs) on HBPAA-modified silk fibers (HBPAA/SFs) driven through intermolecular interactions between hydroxyl-terminated HBPAE and amino-terminated HBPAA. The HBPAE/AgNPs had a particle size of 11.8 nm and were slightly negatively charged. The self-assembly process was conducted by successively impregnating the SFs with HBPAA and HBPAE/AgNPs solutions. Up to 160 mg/L of HBPAE/AgNPs could completely self-assemble onto HBPAA/SFs (2 g) at room temperature within 10 min, allowing the Ag content of HBPAE/AgNP-coated HBPAA/SFs to be precisely controlled up to 8 mg/g by simply adjusting the concentration of the AgNPs. The antibacterial activity of HBPAE/AgNP-coated HBPAA/SFs was dose-dependent and the minimum Ag content was determined as 1.5 mg/g with an inhibitory rate of over 99%. Further characterization demonstrated that the as-prepared HBPAE/AgNP-coated HBPAA/SFs have unique structural features including well-dispersed NPs on the surface and good chemical stability. The developed self-assembly technology may provide a simple, efficient, and environmentally-friendly coating strategy for the precise control of Ag content on coated fibers, which is important for the quality control of antibacterial textiles.

In Chapter 4, we designed an environmentally-friendly and energy-efficient

bottom-up nanocoating strategy for cotton fibers by cooperated self-assembly of complementary AgNPs that are functionalised by amino-terminated HBPAA and hydroxyl-terminated HBPAE, respectively. HBPAA/AgNPs possess positively surface charges of + 40.8 mV and dense amino end groups while HBPAE/AgNPs own a slightly negatively surface charges (-15.8 mV) and abundant OH end groups. Therefore, owing to intermolecular recognition and interactions between HBPAA and HBPAE, heterostructured AgNPs could cooperatively self-assemble on the surface of biological fibers. Specifically, cotton fibers were alternately incubated with solutions of HBPAA/AgNPs and HBAPE/AgNPs and finally dried in an oven. Our SEM, FESEM, and XPS studies confirmed that heterostructured AgNPs were uniformly coated on the surface of cotton fibers, indicative of their excellent physical and good chemical stability. The coated cotton fibers show excellent antibacterial capability. At very low Ag content (3 mg/g), the coated cotton fibers showed satisfactory antibacterial effects with the antimicrobial rates of over 99 %. The developed cooperated self-assembly strategy showed nearly complete uptaking of AgNPs by natural fibers and precise control of Ag content, indicating its good potential for practical production.

In Chapter 5, we further used the cooperated self-assembly technology to coat HBPAA/AgNPs and citric acid-capped Fe_3O_4 NPs (CA/Fe_3O_4NPs) onto silk fibers. The hierarchical structured Fe_3O_4NPs/AgNPs dual-coated silk fibers were fabricated by sequential impregnation of silk fibers with solutions of HBPAA/AgNPs and CA/Fe_3O_4NPs. As-prepared hierarchical structured silk fibers were characterized by XRD, FESEM, and VSM. XRD and SEM characterizations demonstrated that silk fibers were hierarchically and uniformly coated by high dense AgNPs and Fe_3O_4NPs. VSM analysis indicated that the as-prepared ternary composite fibers showed excellent

magnetic property.

Besides, the supramolecular self-assembly technology can be used to design other inorganic nanoparticle coatings. As a demonstration, in chapter 5, water-soluble hydroxyl-terminated hyperbranched poly(amino-ester) (HBPAE)-capped titanium dioxide nanocrystals (TiO_2 NCs) were synthesized for coating a cotton fabric via an amino-terminated hyperbranched poly(amidoamine) (HBPAA)-mediated self-assembly strategy to produce a controllable and uniform TiO_2 coating on the cotton surface. It was demonstrated that hydroxyl-modified TiO_2 NCs were egg-shaped and had a narrow size distribution. A TiO_2 NC-coated cotton fabric was prepared by sequential impregnation with solutions of HBPAA and TiO_2 NCs. FESEM and XRD characterizations demonstrated that TiO_2 NCs could self-assemble on a cotton fabric efficiently and were distributed uniformly on the cotton surface.

Published papers

The dissertation based on following published papers:

1. Sijun Xu, Feng Zhang, Jiangchao Song, Yuki Kishimoto, & Hideaki Morikawa (2015). Preparation of silver nanoparticle-coated calcium alginate fibers by hyperbranched poly (amidoamine)-mediated assembly and their antibacterial activity. ***Textile Research Journal***, 86, 878-886.
2. Sijun Xu, Jiangchao Song, Hideaki Morikawa, Yuyue Chen, & Hong Lin (2016). Fabrication of hierarchical structured Fe_3O_4 and Ag nanoparticles dual-coated silk fibers through electrostatic self-assembly. ***Materials Letters***, 164, 274-277.
3. Sijun Xu, Siyu Chen, Feng Zhang, Chenlu Jiao, Jiangchao Song, Yuyue Chen, Hong Lin, Yasuo Gotoh & Hideaki Morikawa (2016). Preparation and controlled coating of hydroxyl-modified silver nanoparticles on silk fibers through intermolecular interaction-induced self-assembly. ***Materials & Design***, 95, 107-118.
4. Sijun Xu, Feng Zhang, Chenlu Jiao, Siyu Chen, Hideaki Morikawa, Yuyue Chen & Hong Lin (2016). Poly(amidoamine)-mediated self-assembly of hydroxyl-modified anatase TiO_2 nanocrystals on cotton fabric. ***Japanese Journal of Applied Physics***, 55, 06GH02.

Acknowledgments

First and foremost, I would like to express my deepest gratitude to my supervisor, Professor Hideaki Morikawa, for his valuable guidance, support, and encouragement in my academic research work. Special thanks are given to Professor Yasuo Gotoh and Limin Bao for their meticulous comments and advices.

I would like to thank my colleagues in Morikawa Laboratory for their generous assistance in every aspect in my life and warm encouragement during my study in Japan.

Finally, I dedicate my greatest thanks to my beloved family and my parents. They encourage me to move forward and make my life colorful and meaningful.